The Dissertation Committee for Hongxun Gao
certifies that this is the approved version of the following dissertation:

Investigation of a Railplug Ignition System for
Lean-Burn Large-Bore Natural Gas Engines

Committee:

_____

Matthew J. Hall, Supervisor

_____

Ronald D. Matthews

_____

Ofodike A. Ezekoye

_____

Janet L. Ellzey

_____

Laxminarayan L. Raja

Investigation of a Railplug Ignition System for Lean-Burn Large-Bore Natural Gas Engines

by

Hongxun Gao, B.E.; M.E.

Dissertation

Presented to the Faculty of the Graduate School of
The University of Texas at Austin
in Partial Fulfillment
of the Requirements
for the Degree of
Doctor of Philosophy

The University of Texas at Austin
December 2005

To my family

Acknowledgements

First I want to thank Dr. Matthews, Dr. Ezekoye and Dr. Hall from the bottom of my heart for their support and numerous discussions that helped me accomplished this work.

Thanks to Marcus who gave me some valuable suggestions about the engine set-up. Kim's helps was also appreciated with all the problems encountered with the DSP. I need to mention the others who made this work more pleasurable: Hari, Ozgur, Alok, Alex, Dr. Joo and other combustion group members. Thanks to Curtis Jonhson, Danny Jares, and Don Artieschoufsky in the machine shop who gave me a lot of assistance for the engine set-up and railplug fabrication.

Special thanks to Dongmei Zhou, Huijie Xu, and Daijiao Wang for their care and friendship. It is never easy for a student to both pursues a degree and raise a family, especially for a foreigner, so many nice people have helped me out and made Austin such an unforgettable city in my life.

Finally, I want to thank my wife, Jong Fang, who accepted to spend all this time with me and help me so much during the hard time. My lovely daughter, Erin Yiran Gao, and son, Jerry Gao, have given me so much pleasures. My family in China, they never stop encouraging me and praying for me. I want to dedicate this dissertation to my family.

Investigation of a Railplug Ignition System for Lean-Burn Large-Bore Natural Gas Engines

Publication No. _____

Hongxun Gao, Ph.D.
The University of Texas at Austin, 2005

Supervisor: Matthew J. Hall

The characteristics of three ignition systems, such as inductive ignition, capacitor discharge ignition, and railplug ignition system, are investigated. Based on the characteristics, the railplug is a very promising ignition system for lean burn natural gas engines with its high-energy deposition and high velocity plasma arc. Parallel railplugs are designed, fabricated and tested on an operating natural gas fueled engine. The engine tests shows that the lean-stability-limit (LSL) can be extended from a fuel/air equivalence ratio of $\varphi = 0.62$ for spark plugs down to $\varphi = 0.535$ using a railplug. Thus, engine-out NO_x emission is also reduced using railplugs. A heat transfer model is proposed to aid the railplug design. A parameter study is performed both in a constant volume bomb and in an operating natural gas engine to improve and optimize the railplug designs.

Table of contents

List of Figures

List of Tables

Chapter 1.0 Introduction and Background

As is demonstrated by the increase in fuel prices during the last three years, the coming decades will see an ever-increasing demand on dwindling petroleum supplies. The United States in particular is going to be in a difficult situation due to our heavy reliance on foreign oil supplies. An important part of creating a future in which we are less reliant on petroleum reserves is to improve the fuel efficiency of future vehicles, as well as increasing the use of non-petroleum-based fuels such as natural gas. This will be important for both mobile and stationary powerplants since 24% of primary energy in US is natural gas in 2001 [1].

An increase in environmental awareness has also prompted automotive engineers to find ways to reduce fuel consumption and harmful exhaust gases that contribute to smog and greenhouse effects. Natural gas is one of the most environmentally benign fuels, with the most potential for ozone reduction [2]. It also has the intrinsic benefits of super low Particulate matter (PM) and lower CO_2 emissions than gasoline because of its higher H/C ratio. One of the approaches to lowering the engine contribution to ozone formation is to change the character of the tailpipe emissions. This is the contribution that the alternative fuels can make. It is not the level of the tailpipe emission that is lower, it is the character and/or composition of the emission that is different. Hydrocarbon compounds have varying levels of reactivity in the atmosphere, as shown in Table 1 [2]. Fuels, such as natural gas, which produce less reactive exhaust emissions when burned

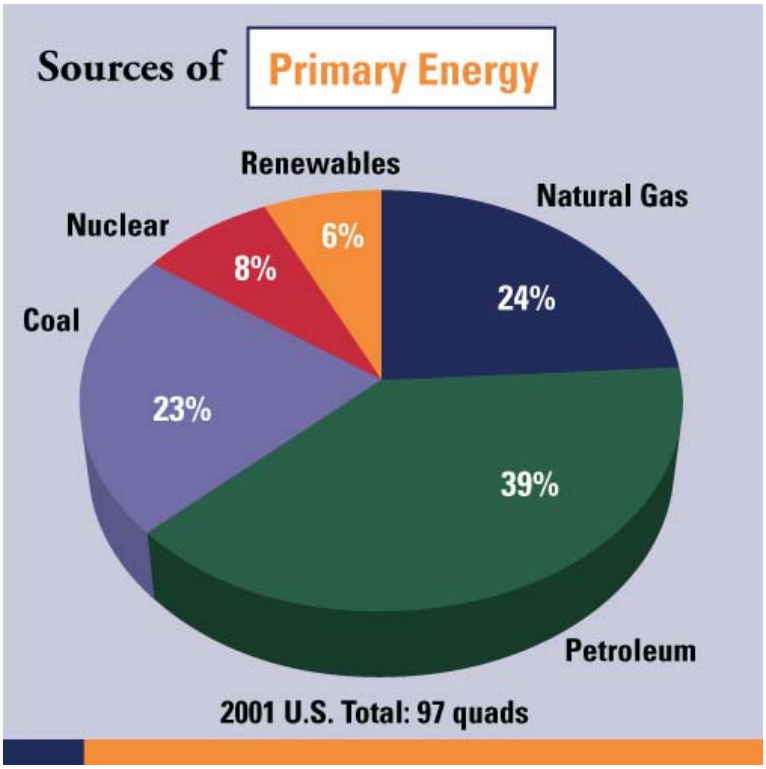

Figure 1.1. Sources of primary energy in US in 2001.

will generate less ozone. It is the way they react in the atmosphere after they leave the tailpipe that is important.

Driven by better fuel economy and tighter emission regulations, automotive engineers have been exploring I.C. engines operation with fuel-lean (ϕ<1) or highly dilute (e.g., with EGR) mixtures due to its higher brake thermal efficiency and lower engine-out NO_x emissions. Lean/dilute mixtures yield lower flame temperatures, which increases brake thermal efficiency (η_{BT}) because of lower heat losses, and reduces NO_x emissions due to the exponential temperature dependence of the NOx formation rate [3]. Brake thermal efficiency is also

Table 1. Photochemical reactivity of organic compounds: rate constants
For reaction with Hydroxyl (OH) radical.

Compound	K x 10^{-4} ($PPM^{-1}MIN^{-1}$)
Trans-2-Butene	10.5
1,2,4 Trimethyl Benzene	4.9
M-Xylene	3.4
Propionaldehyde	2.2
Acetaldehyde	2.2
Propene	2.1
Fomaldehyde	2.1
Ethylene	0.45
N-Butane	0.35
Propane	0.25
Methanol	0.148
Ethane	0.045
Acetylene	0.022
Carbon Monoxide	0.021
Methane	0.0012

increased by the more favorable (higher) ratio of specific heats (shown in Figure 1.2) and decreased pumping losses resulting from lean or dilute operation. However, the minimum ignition energy increases and the burning rate decreases as the mixture becomes more dilute, such that the slow burn, partial burn, and misfire limits are encountered when sufficiently lean or dilute mixtures are used. In turn, these result in decreased brake thermal efficiency and increased

hydrocarbon emissions. So it greatly demands on the ignition system in order to obtain the benefits of lean combustion.

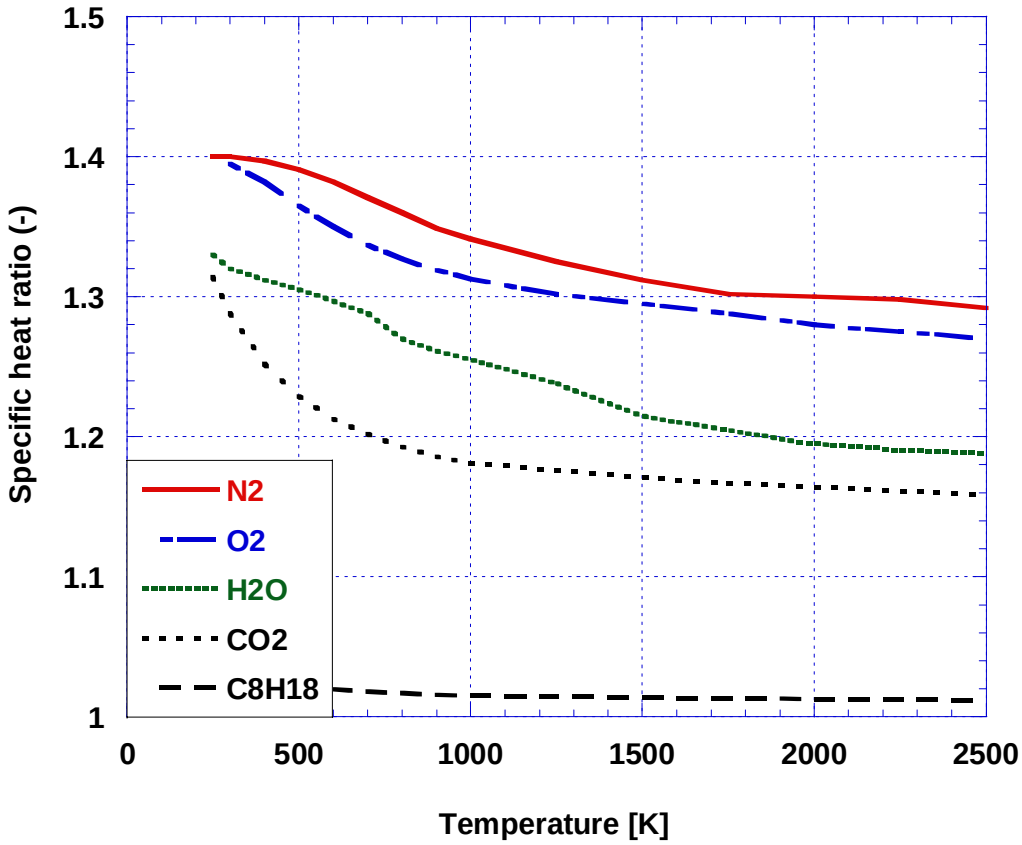

Figure 1.2. Specific heat ratio κ for different chemical components of engine combustion.

The main goal of this project is to develop a high energy ignition system for large-bore natural gas engines. For the past four years, government, industry and universities have joined together to develop high efficiency, low emissions, natural gas fueled reciprocating engines for power generation. The U.S.

Department of Energy has set an Advanced Reciprocating Engine Systems (ARES) program and has targeted 50% efficiency, 0.1 g/BHP-hr NO_x and 10% maintenance cost reduction by 2010 [4]. The engine manufacturers have determined that these goals cannot be met with current ignition system technology. The next generation ignition system needs to be developed to meet the engine cost, efficiency and emissions goals.

Increasing the efficiency requires increasing the compression ratio, but this in turn requires higher breakdown voltage for the ignition system and a more advanced knock control strategy. As described above, fuel lean combustion in natural gas engines is desirable in that it yields lower combustion temperatures which lead to lower NO_x emissions, and higher thermal efficiency due to lower heat losses and higher compression efficiency due to higher gamma ($\gamma=c_p/c_v$). However, there are several aspects of spark ignited lean burn engines that result in ignition and combustion challenges. Lean mixtures of natural gas and air are relatively difficult to ignite with the required minimum ignition energy increasing asymptotically near both the rich and lean ignition limits, whereas spark plug durability degrades rapidly with increasing spark energy. Spark plug durability is already of concern due to the associated maintenance costs.

Another approach to increase engine efficiency which natural gas engine manufacturers widely use is to increase Brake Mean Effective Pressure (BMEP). In terms of BMEP, the state-of-the-art for natural gas engines of all size is 20 bars [5]. High boost pressure is used to offset the power density loss due to the fuel lean operation and raise the BMEP of the engine. The higher BMEP levels have resulted in higher engine efficiency with improved mechanical efficiency as parasitic losses are a smaller portion of the engine power. Engine efficiency also

benefits from increased power density due to a greater specific power/heat loss ratio. Callahan [5] developed a simple regression analysis and found the following expression,

$$BTE \approx B_0 + 0.5(BMEP) - 0.003(rpm) \tag{1.1}$$

where, BMEP has units of bars.

The resulting increase in in-cylinder pressure at the time of ignition impedes the quality of the spark discharge. Pashchen, in 1889, outlined the electrical breakdown characteristics of gases which is now known as Pashchen's Law. He proposed that the breakdown voltage was a product of electrode gap and gas pressure (actually density), or V= f (*pd*), where *p* is the pressure and *d* is the gap distance. For breakdown in air with small gaps on the order of millimeters, an approximate estimate for the breakdown voltage is: V = 30*pd* + 1.35 kV, where *d* is in centimeters, and *p* is in atmospheres. It is seen from Pashchen's Law that high in-cylinder pressure requires high breakdown voltage. However, the high voltage demand puts additional stress on the secondary side of the ignition system, which delivers the coil voltage to the spark plug. High voltage is difficult to contain in the secondary system, and often, the secondary dielectric strength is not sufficient to deliver the voltage to the spark plug gap. This problem requires that small spark plug gaps be used to reduce the voltage demand.

Unfortunately, small spark gaps often do not deliver sufficient ignition energy to the lean natural gas and air mixture in the cylinder to consistently initiate a flame kernel, the beginning of combustion. Thus, the lean mixture ignitability limit is insufficient to meet the emissions and efficiency goals.

Raising the BMEP of the engine also increases the compression pressure and thermal loading on the spark plug. These factors reduce the useful life of the spark plug because as the electrodes erode, the gap size increases, the secondary voltage increases until the dielectric strength of the coil is exceeded and the spark plug quits firing.

Inductive ignition systems and Capacitor Discharge Ignition (CDI) systems are the two main types of ignition systems used today. From the literature, it is unclear which offers better performance. Inductive ignition systems store energy in the ignition coil and deliver longer duration sparks at lower peak power than CDI systems. The duration of the inductive system is usually between 1 and 2 milliseconds and it delivers total spark energy of around 20 to 100 mJ depending on the ignition system. CDI systems store energy in a capacitor and deliver shorter sparks at higher peak power levels. The spark duration of CDI systems is around 0.2 to 0.5 milliseconds and will deliver spark energies of around 100 mJ depending on the capacitor. CDI systems are most commonly used on large-bore natural gas engines. The ignition systems currently in use are derived from automotive applications and are not designed or optimized for the lower speed, higher load and leaner conditions of large-bore natural gas engines. Therefore, an acute need for a more robust ignition system for large-bore natural gas engines offering longer igniter life and better ignition characteristics.

With that motivation, engine researchers have been exploring a variety of new ignition systems, including but not limited to laser-induced ignition, pilot fuel ignition, and various types of plasma jet igniters, which will be discussed in

the later part of this chapter. The background of ignition will be described in the next section.

1.1 Background of ignition

1.1.1 Estimates of the minimum ignition energy

Classical combustion theory shows that two distinctly different modes of flame propagation exist, called deflagrations and detonations [6, 7]. Deflagrations are employed in virtually all practical combustion devises, while detonations are usually an undesirable mode of combustion. So only deflagrations are discussed in this section.

Lewis and von Elbe [6] describe ignition of deflagrations in premixed gases as follows: If a subcritical quantity of energy in the form of heat and/or radicals (chemically active atoms or molecules) is deposited in a combustible mixture, the resulting flame kernel decays rapidly because heat and radicals are conducted away from the surface of the kernel and dissociated species recombine faster than they are regenerated by chemical reaction in the volume of the kernel. The kernel extinguishes after consuming a small quantity of reactant. On the other hand, if the ignition energy exceeds a certain threshold called the minimum ignition energy (E_{min}), at the time when the peak temperature decays to the adiabatic flame temperature T_f, the temperature gradient in the kernel is sufficiently small that heat generated in the kernel is faster than it is lost due to conduction to the unburned mixture. This leads to the development of a steady

flame that consumes all of the available mixture. Thus, the simplest physical ignition criterion is that E_{min} must be sufficient to raise a sphere of gas of radius δ_{min} (minimum flame kernel radius) to temperature T_f. Of course, δ_{min} and E_{min} are functions of the properties of the combustible mixture and the characteristics of the ignition source.

Ronney [8] proposed a simple model of ignition of deflagrations based on the preceding (essentially thermal) hypothesis. According to Williams [7], the minimum radius of the developing flame kernel is related to δ_{min} by [7],

$$\delta_{\min} \approx \frac{\bar{k}}{\rho_0 C_p S_L} \approx \frac{\bar{k}}{k_0}\frac{\alpha_0}{S_L} \quad \text{and} \quad \alpha_0 = \frac{k_0}{\rho_0 C_p} \tag{1.1}$$

Where the over bar denotes temperature averaging. Then, the enthalpy contained in a volume of radius δ_{min}, which is presumed to be E_{min}, is

$$E_{\min} \approx \frac{4\pi}{3}\delta_{\min}^3 \rho_f Q \approx \frac{4\pi}{3}\left(\frac{\alpha_0}{S_L}\right)^3 \rho_f Q \left(\frac{\bar{k}}{k_0}\right)^3 \quad \text{and} \quad Q = C_p\left(T_f - T_0\right) \tag{1.2}$$

More accurate descriptions of flame ignition should consider the effects of the Lewis number (Le) [9], defined as the ratio of the thermal diffusivity of the gas mixture to the mass diffusivity of the scarce reactant into the gas mixture. However, for mixtures with Le close to unity (which is characteristic of many combustible mixtures), the critical ignition kernel radius is closed to δ_{min}.

1.1.2 Effects of experimental factors on ignition

Ignitability and flame propagation near the plug gap of an operating engine are significantly affected by the local chemistry of the mixture, the amount and duration of the spark energy, the gap size, the method of energy deposition and the local in-cylinder flow conditions. These effects are reviewed below.

Composition Many investigations have examined the effects of composition on the minimum ignition energy E_{min}, and in particular the effect of the equivalence ratio ϕ. As described in the previous section, Ronney [8] found that E_{min} is proportional to $S_L^{-1/3}$ where S_L is the unstretched laminar flame speed (generally < 1 m/s). E_{min} generally occurs slightly on the rich side of stoichiometric [10, 11]. Typical values of E_{min} are 0.4 mJ for stoichiometric CH_4 –air mixtures and 0.02 mJ for stoichiometric H_2 –air mixtures [6].

Spark plug gap The spark gap dimension is one of the most important plug parameters affecting lean ignitability [12-14]. Increasing spark gap size can increase the ignition power and deposited energy, which can be a benefit by forming a large initial flame kernel. There exists an optimum dimension, d_{opt}, which minimizes E_{min}. Generally, E_{min} increases slowly with d for $d > d_{opt}$, and more rapidly for $d < d_{opt}$ due to the rapidly increasing heat loss to the electrodes. However, the use of wider gaps is limited by erosion and breakdown voltage limitations.

Electrode diameter Larger electrodes increase heat losses from the initial flame kernel and thereby increase the minimum ignition energy requirement [14, 15]. The rate of initial flame kernel development is also adversely affected [14-

17]. Herweg and Ziegler [14] found that reducing the contact areas between the flame kernel and the spark plug leads to a faster kernel development, which can be achieved either by increasing the spark gap and/or decreasing electrode diameter. Using thin electrodes can extend engine lean stability limits [16, 17].

Spark duration This is a controversial issue. Numerous studies have been made of the effects of the rate and duration over which energy is delivered to the spark; in other words, attempting to determine the optimum spark power, energy, and duration [12, 13, 18-25]. The results from different researchers are not quite consistent. Generally, high power, short duration ignition systems, such as breakdown systems, can enhance the initial kernel growth under low turbulence conditions (e.g., low engine speeds). With very lean mixtures and high turbulence levels, long duration discharges may become more effective than a high power short discharge. The long duration system appears to provide a large enough ignition window to mask the effects of cycle-to-cycle mixture variations, which is more important for the operating engine when the mixtures become leaner. It should be noted that none of these engine studies used methane or natural gas as the test fuel. Because of the unique ignition characteristics of natural gas, such as, long ignition delay and slow laminar burning speed relative to gasoline [26] the effects of the duration of energy deposition on the ignitability are unknown.

Method of energy deposition The discharge energy can be deposited at one fixed point with a spark plug, or the energy can be deposited over a relatively large area, as with a railplug. Wagner [27] used rotating arc spark plugs to extend lean stability limits. The high-speed arc motion not only improves the igniter durability but also results in a fast burning rate and the ability to burn leaner mixtures than might ordinarily be possible. As the mixture becomes leaner, the

engine combustion can be limited either by ignition or by flame propagation. The deposited ignition energy is virtually an order of magnitude larger than the minimum ignition energy for all practical engine combustion. So misfire generally occurs in combustible mixtures that are too lean, leading to misfire or flame blowout conditions, which indicate that limitation on the flame propagation velocity, rather than intrinsic flammability, limit the performance of those engines [8].

In-cylinder flow conditions E_{min} generally increases with increasing flow velocity and increasing turbulence [8, 28, and 29]. This increase is attributed to the increase in flame kernel area caused by stretching the kernel. In turn, this results in increased heat loss and, thus, increased E_{min}. Increasing turbulence intensity increases the early kernel growth rate thereby decreasing its cyclic variability. However, there is a limit above which increased turbulence intensity causes excessive flame strain, leading to flame quenching. The minimum ignition energy decreases with increasing in-cylinder pressure [30]. However, the minimum ignition energy is a mild function of pressure.

1.2 New emerging ignition systems

Laser-induced spark ignition Laser ignition uses laser irradiance to generate a plasma either by the multi-photon ionization process or by an electron ionization process [8, 31-36]. There are generally three mechanisms by which laser radiation can ignite a combustible solid, liquid, or gaseous mixture: laser-induced thermal ignition, laser-induced photochemical ignition, and laser-induced spark ignition.

In laser-induced thermal ignition, laser radiation is used to heat and increase the target temperature. As a result, molecular bonds are broken and chemical reactions take place. This ignition mechanism can easily be used to ignite solids because of the absorption ability of the solids at infrared wavelengths. However, it is subject to some important limitations when it is used to ignite gaseous systems. First, a combustible mixture with strong absorption at the wavelength must be used. Second, complications associated with nonthermal components, such as photodissociation, hydrodynamic motion, and acoustic instabilities, might complicate the ignition process.

Laser-induced photochemical ignition can include resonant breakdown and resonant photochemical ignition. In resonant breakdown, a target molecule is dissociated by a nonresonant multiphoton dissociation process. The atom produced is then ionized by a resonant multiphoton ionization process. The electrons produced this way absorb more photons, leading to the formation of microplasmas. In resonant photochemical ignition, laser photons dissociate the target molecules into highly reactive radical species. If the rate of production of these radicals is greater than their recombination rate, they will initiate the usual chemical chain-branching reactions leading to ignition and full-scale combustion. The crucial factors that determine whether or not ignition occurs are the concentration of radicals produced by photon absorption, and the volume in which the radicals are contained – not the laser energy density. This might be a major difference from thermal ignition where minimum ignition energy and a minimum size are required. However, there are many disadvantages to the use of photochemical ignition for practical applications. First, a particular laser or a laser that is tunable might be required to provide the wavelength that matches with the target molecule's absorption wavelength in order for dissociation to occur.

Second, since the photon energy at visible and near-IR wavelengths is smaller than the dissociation energy of most gases, the photochemical ignition process is most effective at UV wavelengths. At present, such lasers are expensive, and compact, light-weight lasers for practical combustion applications are not yet available.

In laser-induced spark ignition, laser irradiance on the order of 10^{10} W/cm^2 is sufficient to generate spark plasma at the end of the laser pulse, either by the multiphoton ionization process or the electron cascade process. In the multiphoton ionization process, a gas molecule absorbs a sufficient number of photons. If the photon energy absorbed is higher than its ionization potential, the gas molecule is ionized. This process is important only at very short wavelengths (< 1 μm) or at very low pressure (< 0.1 atm), where collision effects are negligible. It becomes insignificant at visible and near-IR wavelengths because the photon energy at these wavelengths is much smaller than the ionization potentials of most gases. The electron cascade requires the existence of initial electrons to absorb more photons. If the electrons gain sufficient energy, they ionize other gas molecules on impact, leading to an electron cascade and breakdown of the gas. For ignition application, the creation of a laser spark is usually associated with this process. Laser-induced spark ignition is more favorable because it does not require a close match between the laser wavelength and the target molecule's absorption wavelength to create a spark. Although laser wavelength influence the threshold for breakdown, once breakdown is achieved, ignition depends only on the amount of energy absorbed in the plasma. Thus, the laser irradiance at the focal volume, not the laser wavelength, is the only crucial requirement.

According to Ronney [8], the potential benefits of laser ignition are that it is non-intrusive and is capable of providing multiple ignition sites that can be programmed to ignite a combustible mixture either sequentially or simultaneously. Problems such as wall effects, heat loss through the electrodes, partial burn, and misfire can be avoided. In addition, if a flame is initiated simultaneously at many points throughout the combustion chamber, the total burning time could be much smaller. This could be potentially important for fuel-lean engine combustion. Another possible means of exploiting the benefits of laser ignition is to make quite combustion chamber design possible. All practical combustion engines employ turbulence to accelerate mixing and/or burning; however, this turbulence also increases heat losses to walls. In typical automotive engines, the heat loss to the cylinder walls comprises 20% to 30% of the fuel energy input. Hence, if the need for acceleration of combustion by turbulence could be reduced by employing multiple-point laser ignition, it is possible that engine thermal efficiency could be increased.

Phuoc and White [6], using methane/air mixtures in a high pressure combustion vessel, found that laser ignition worked poorly under fuel-lean conditions while favoring fuel-rich conditions. This is different from spark ignition, which favors stoichiometric conditions. However, McMillian and coworkers [33-35] have successfully operated an engine leaner with laser ignition than with conventional spark plugs. Graf [36] studied the effects of contamination of optics in a Gasoline Direct Injection (GDI) engine. The engine was kept running over a test period of 200 hours by applying laser pulse energies of 50 mJ. The engine began to misfire after 31 hours for 45 mJ and 7 hours for 40 mJ. Considering other factors, such as cost, window fouling, and laser power

reliability, it appears that there are still barriers remaining before laser ignition become practical.

Pilot-fuel ignition Another promising ignition system is use of an auto-ignited pilot flame as the ignition source to ignite lean mixtures [37-39]. First, a micro pilot fuel (diesel fuel generally) is injected into premixed mixtures and auto-ignited; the ignition source can, thus, propagate throughout the entire combustion chamber. Saito [37] found that ignition of the pilot fuel occurs near the nozzle tip. The pilot flame, possessing 60-70 J more energy than a conventional spark, contributed to improved combustion stability in an ultra lean mixture with a lambda of approximately 2.0. The primary problem of such dual-fuel engines is misfire at idle and part load because the pilot flame intensity becomes weak as the engine load decreases [37]. Also, the pilot fuel ignition system has a high demand for injection stability. It was seen that the pilot flame had a cycle-to-cycle variation, which was larger than that of conventional diesel engines due to a small amounts of fuel injected, which can cause lean combustion fluctuations. Since the fuel spray does not penetrate very deep, the shape of the combustion chamber has to be designed for high swirl motion to promote propagation of the pilot flame.

Due to the limitations of these ignition systems, other types of advanced igniters are of interest.

1.3 Railplug ignition systems

The railplug, patented by researchers at The University of Texas [40], is a miniaturized railgun that has been developed as an igniter for internal combustion

engines [41-44]. Figure 1.3 is a schematic of the railplug circuit which consists of a breakdown circuit and a "follow-on" circuit. The conventional breakdown circuit is a standard inductive ignition circuit which provides the high voltage required for breakdown. Figure 1.4 is an illustration of a simplified railplug.

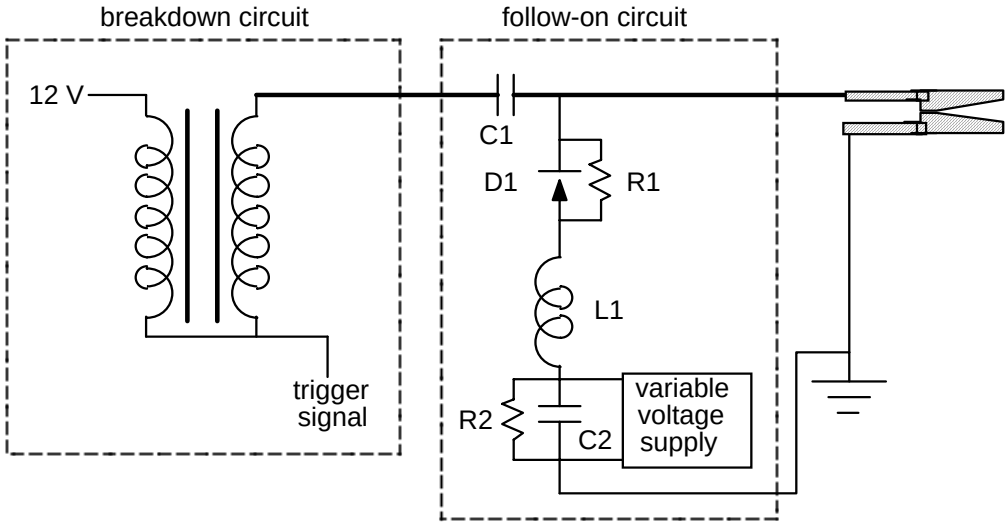

Figure 1.3. Schematic of the railplug electronics circuit.

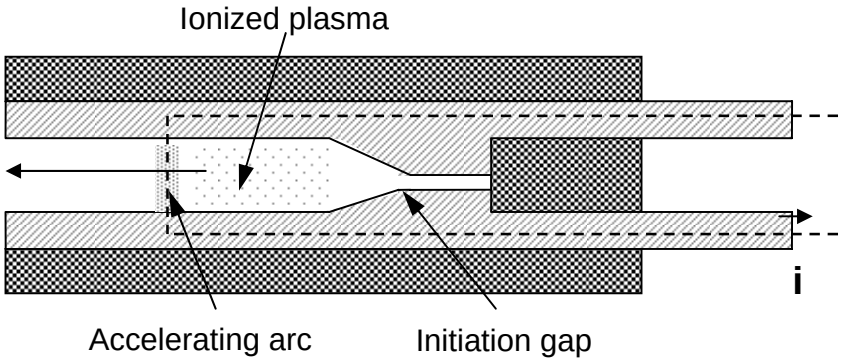

Figure 1.4. Schematic of a railplug.

When a sufficiently high voltage is applied across the rails to electrically breakdown the gap between them, an arc jumps across the rail. The capacitor in the follow-on circuit begins to discharge and provides a high current. The current loop that is attained by the electrical current flowing down one rail, across the arc, and back up the other rail produces an electromagnetic field. An electromagnetic force or Lorentz force is thereby created as a consequence of the interaction of the self induced magnetic field with the ions in the plasma arc. This Lorentz force accelerates the plasma moving along the electrodes. This process can be easily seen from the arc motion in Figure 1.5.

Compared to the laser ignition system and to the pilot fuel ignition system, a railplug has some similarities with a conventional electronic spark ignition system, such as using an electric discharge with breakdown and arc phases. However, Railplugs are fundamentally different from the most actively studied igniters derived from conventional spark plugs. Some of these igniters are briefly reviewed below.

High energy and surface discharge spark plugs are, at present, the igniters most commonly used in production lean burn engines. The basic approach is to modify the ignition circuit with higher energy input. Laboratory tests show that such spark plugs have been used to operate an engine at an air-fuel ratio of 23.5:1 ($\varphi = 0.62$, where φ is the equivalence ratio, which is the air-fuel ratio normalized by its stoichiometric value). It is not sufficiently lean to offer significant advantage. Although these plugs have the capability to ignite lean mixtures, they do nothing to solve the other problems of lean burn engines, such as slow combustion.

plasma jet igniters generally do not incorporate any electromagnetic effect and rely solely on thermal expansion of the product mixture through one or more orifices at the end of the igniter cavity. Thermal expansion dominates the physics of jet formation and penetration of the plasma jet igniter.

In contrast to plasma jet igniters, thermal expansion augments but does not dominate the jet ejection force of the railplug. Railplugs take full advantage of an electromagnetic force to accelerate the plasma. For the railplug, durability should not pose the same difficulty since the energy is deposited over a much larger surface area and the arc is not stationary as in the case of a plasma jet igniter. As described by Hall and coworkers [41], for railplugs, the arc sweeps down the rails, a large mass of plasma is generated In comparison to the plasma generated by a spark plug. Also, the high plasma velocity will result in a jet of hot plasma that penetrates across the combustion chamber, thereby, distributing the ignition source and causing turbulence due to the difference in the jet velocity and the bulk velocity in the combustion chamber. So the high velocity arc motion results in a faster pressure rise during combustion and the ability to burn leaner mixtures than might ordinarily be possible. It is seen that railplugs have many advantages compared to high energy spark plugs and plasma jet igniters, both in terms of their ability to ignite lean mixtures and for durability.

Though considerable progress was made during the previous railplug investigations, which showed that the railplug is a very promising high energy igniter for lean burn engines, a lot of work was required as part of this dissertation to optimize the railplug designs and make it more practical for large-bore natural gas engines.

During the previous projects, the railplug development focused on coaxial railplugs. As the name implies, one rail, generally the anode is placed in the center of a grounded metal cylindrical tube for a coaxial railplug. This design makes it much easier to fabricate because it does not require a complex insulation scheme and all of its parts are axisymmetric. However, this configuration suffers from a relatively low inductance gradient. Therefore, coaxial railplugs have lower Lorentz forces compared to parallel railplugs for the same delivered energy. So coaxial railplugs require relatively large ignition energies to accelerate the arc, generally, much larger than 1 J per shot. Zheng [44] demonstrated that railplug durability increases almost exponentially as the delivered energy decreases. So from the view point of railplug durability and performance, a parallel railplug should be better than a coaxial railplug.

There was a design flaw inherent to the previous railplug designs. In each design there was a sharp transition from the narrow ignition gap to the adjacent rail, which resulted in the arc being held at the sharp transition point and not traveling down the rails [50]. It was responsible for the main railplug failure mode: center rail erosion near the initiation gap. In this dissertation, new designs were created that eliminated the discontinuity.

There are two keys to railplug durability: spreading the energy over a large surface area (arc movement) and effective heat transfer away from the rails. Besides the geometric designs, making the arc move rapidly also depends on the electronics circuit optimization, such as spark duration, energy levels. A heat transfer model will be invaluable in aiding railplug designs and solving the durability issue.

1.4 Overview

This dissertation is devoted to the investigation of the characteristics of three ignition systems and the development of a high energy igniter, the railplug, for lean-burn large-bore natural gas engines. Railplugs were designed, fabricated and tested on a natural gas fueled engine. The engine performance and engine-out emissions using different igniters were measured. Railplug designs were improved and optimized based on the data obtained both using a high pressure combustion bomb and with the natural gas engine. The railplug electrode temperature was measured and a heat transfer model is proposed to aid railplug design.

Chapter 2 is devoted to the experimental investigation of the discharge and performance characteristics of three different ignition systems; an inductive ignition system, a capacitor discharge ignition system and a railplug ignition system. Discharge voltage and current were measured, and delivered energy was calculated based on the measured voltage and current data. The effects of experimental parameters on discharge characteristics are discussed. This paragraph was changed.

Chapter 3 introduces the railplug designs. A parametric study was done to improve plasma movement.

Chapter 4 describes the experimental setup along with the engine test conditions. The engine set-up included modifying the engine to run on natural

gas, ignition timing control, the dynamometer and its controller, a combustion analysis system for in-cylinder pressure measurement, ignition noise suppression, and engine-out emissions measurements.

Chapter 5 presents the experimental results. The performance of different igniters is compared. The effects of spark duration on engine Lean Stability Limit (LSL) is presented. The effects of railplug design parameters on engine COV of IMEP and mass fraction burning rate are discussed. Engine-out emissions, such as NO_x, HC and CO, were measured.

Chapter 6 presents the results of railplug temperature measurements. A railplug heat transfer model is proposed. The effects of engine operation and railplug design parameters on railplug heat load are discussed.

Chapter 7 summarizes this dissertation research, presents the corresponding conclusions and recommends future research in this area.

Chapter 2.0 Characteristics of Three Ignition Systems

As described in the prior chapter, the railplug is a very promising high energy igniter. The railplug ignition system has many similarities to conventional ignition systems, such as inductive ignition systems and capacitor discharge ignition systems. Studying and understanding the fundamental performance characteristics and the limitations of these existing ignition systems are quite helpful for railplug development.

The performance characteristics of three ignition systems were investigated experimentally outside of an engine. Those experiments and the results are discussed in this chapter. Those ignition systems are inductive ignition, capacitor discharge ignition (CDI), and railplug ignition. Inductive ignition systems are widely used on light duty vehicles. Conventionally, large-bore natural gas engines use CDI systems. CDI systems are also used on some racing cars because of their high ignition energy and the ability to keep an adequate reserve of secondary voltage and ignition energy over the wide operating speed range of the engine [3].

2.1 Ignition discharge measurement techniques

The spark ignition process is characterized by four distinct phases: pre-breakdown, breakdown, arc, and glow [51-61]. The ignition discharge is a very fast process, with breakdown occurring over a timescale of nanoseconds and both

arc and glow occurring over a few milliseconds. Measurement of these very fast signals requires care. Voltage, current, and luminous emissions data were recorded using a Tektronix 1012 digital oscilloscope. After transferring these data to a PC, the discharge energy was calculated by integrating the product of voltage and current over time. The spark luminous emissions were measured with a photodiode (Thorlabs DET110). The spark voltage was measured with a compensated 1000:1 differential voltage probe (Tektronix P6015A) at both the top (high voltage cable side) and the gap side of the spark plug's or railplug's positive electrode. A Pearson Model 101 current probe was placed on the high voltage railplug lead to measure the current flow to the railplug. For the conventional spark plug, a Pearson Model 410 current probe was used. Unfortunately, resolution of the voltage measurement during the arc phase was poor because of the range that is required to capture the entire event - from 20,000 V during breakdown to less than 50 V during arc. In order to decrease the measurement uncertainty, the voltage and current were initially measured with a high voltage setting, such as 1 or 2 kV/div, and then repeated with the voltage setting at 50 or 100 V/div to measure the arc and glow voltages. Since the voltage trend is quite repeatable and the breakdown phase is short, it is easy to find points near the end of the breakdown phase that correspond to points during the early stages of arc to align these two sets of measurements in time. Considering the total 2,000 sampling points, a mismatch in aligning the two curves by one or two points does not significantly affect the accuracy.

Unless otherwise noted, all spark plugs tested in this chapter are Champion Model D21 non-resistor plugs. For these spark plugs, both electrodes are nickel-coated. The high-tension cable used had a resistance of 10.5 kΩ. The ignition coil was a MSD Model PN 8207. The igniters were discharged into

ambient air, except for a few cases, as noted, where the igniters were mounted in a constant volume bomb and the discharge was into helium or a mixture of air and methane. In addition, one set of measurement was made in a firing engine. All of the open-air and bomb measurements were conducted at a pressure of 1 atm, except for those in the methane-air mixtures which were at a pressure of 2 atm.

Table 2. Current probe performance.

Type Pearson Model	410	101
Sensitivity (V/A)	0.1	0.01
Droop (%/ms)	0.06	0.1
"Un-seeable" rise time (ns)	20	100
Frequency Response Low (Hz) High (MHz)	 120 20	 0.25 4

Table 1 provides data regarding the current probes used in this study. The "un-seeable" rise time of the Model 410 is 20 ns, which means if the breakdown current rise time is less than 20 ns, it might have 10 percent overshoot. During the measurements, it was found that the current at the end of discharge became negative. The results should be compensated according to the droop rate that indicates the downward slope because of the slow change in input current.

2.2 Inductive ignition system

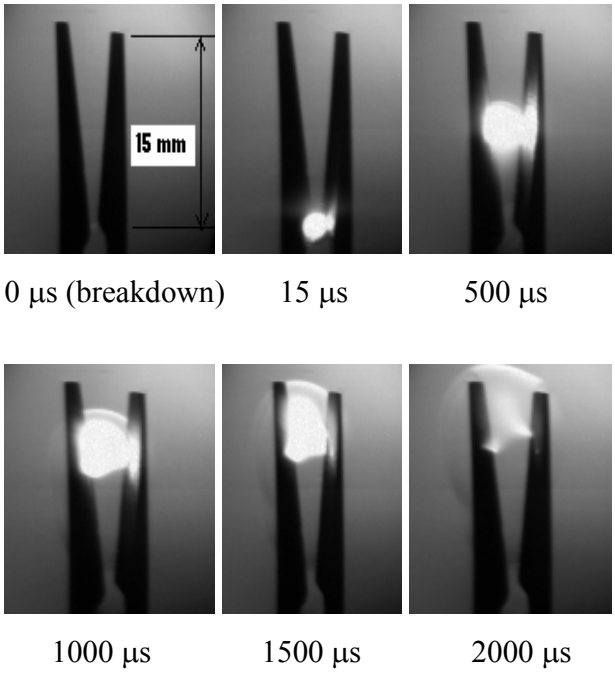

Figure 1.5. Images of arc moving down the rails of a "parallel" railplug. Rail length = 15 mm, initiation gap = 0.8 mm, capacitance = 600 μF, and capacitor charge voltage = 210 V. High-speed photography rate 70,000 f/s and shutter speed 2 μs.

The plasma jet igniter has a very small pre-chamber, or cavity, near the exit of the igniter. An orifice at the cavity exit is often used to pressurize the ionization and combustion products and cause a hot jet of reactive species to issue into the combustion chamber [45-49]. The engine tests show that the Lean Stability Limit (LSL, the equivalence ratio at which the COV of IMEP is 10%) is $\varphi \approx 0.6$. An ignition energy of 0.5-10 J is typically used. One of the primary difficulties with plasma jet igniters has been high electrode erosion rates due to the high electrical energies associated with these plugs. The designs of these

Figure 2.1 shows a typical inductive ignition spark discharge into air at a pressure of 1 atm. There are 4 phases of the spark ignition discharge. They are the pre-breakdown, the breakdown, the arc and the glow.

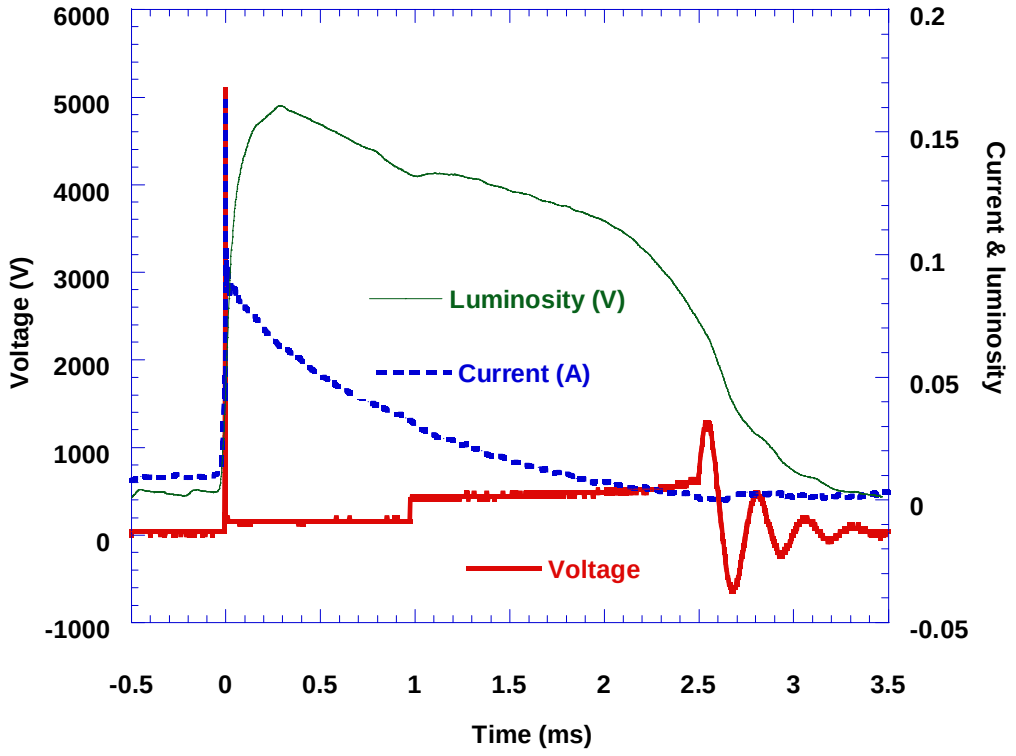

Figure 2.1. Characteristics of an inductive ignition spark discharge.

2.2.1 Phases of spark discharge

Pre-breakdown Initially, the gas between the electrodes acts as a perfect insulator. As the potential difference increases across the gap to a high enough value, the gas becomes a conductor. If the applied voltage is more than the minimum voltage for breakdown (3 $kV \cdot mm^{-1}$ for air at 1 atmosphere), then the streamer reaches the cathode with a current density of 100 – 300 $A \cdot cm^{-2}$ [61]. A

thin channel of electrons and highly ionized gases then closes the gap. The exact streamer diameter is a function of the voltage applied and gap distance.

Breakdown The pre-breakdown phase is then followed by the breakdown itself. Figure 2.2 shows the details of a breakdown phase. The breakdown phase is said to occur when the current begins to rise substantially. This occurs when enough feedback electrons are produced to facilitate an over exponential increase in current. In practical cases this occurs at currents in excess of 10 mA [51]. The current is limited only by the impedance of the discharge and the immediate external circuit close to the gap (i.e., the spark plug), and can rise to 10 – 100 A within a few nanoseconds. The voltage across the gap drops to around 100 V with a field strength of 1 kV/cm. The minimum energy needed to cause breakdown over a 1 mm gap at atmosphere is approximately 0.3 mJ [51].

It is seen from Figure 2.2 that the breakdown current measured by the author is much lower than the value presented by Maly [51]. One of the reasons might be the current probe the author used is not fast enough to capture the peak breakdown current. Recommended SAE Practice J973 (Ignition System Measurement Procedure) suggests using a sampling resistor between the spark plug shell and ground. The discharge current can be measured by measuring the voltage drop across the resistor. Note that J973 calls for a 100 Ω sampling resistor. In order to reduce the current error induced by the sampling resistor, the author used a 10 Ω metal oxide resistor because of its stability and negligible inductance. The results are shown in Figure 2.3. The peak breakdown current measured with a sampling resistor is higher than that with a current probe but it's

still lower than the value presented by Maly. Besides the peak current, the current traces measured by the two methods, however, are quite consistent.

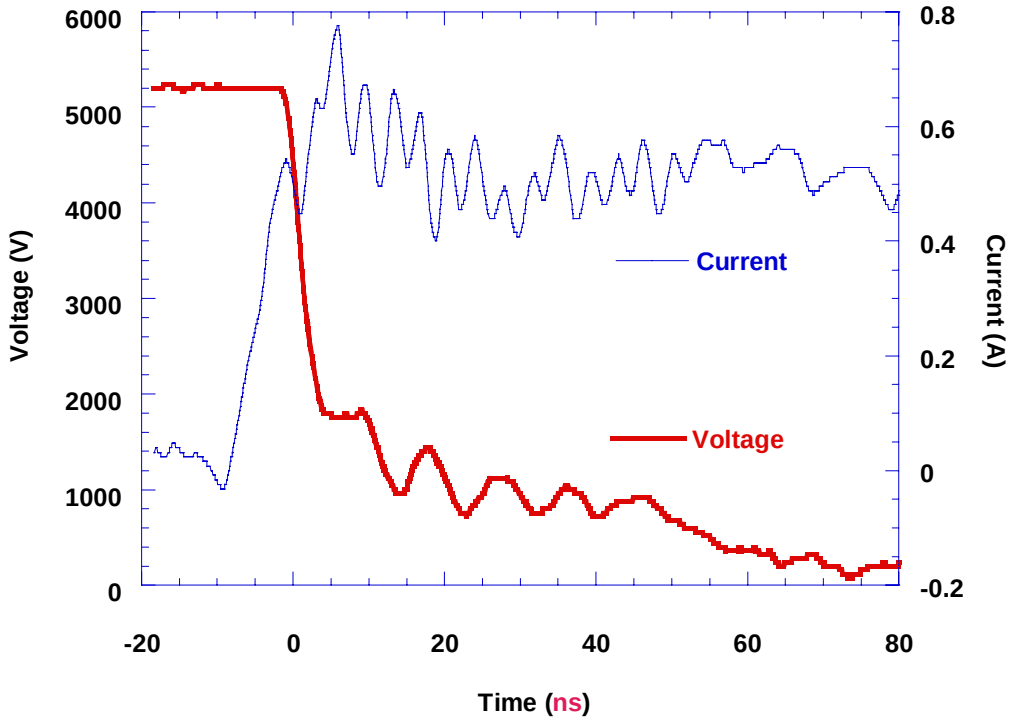

Figure 2.2. Details of a breakdown phase.

The breakdown voltage, in kV, for air can be approximated from the following empirical expressions as a function of temperature and pressure via Equations (2.1) and (2.2), here, the effect of temperature is considered [59],

$$V_b = 24.22 \cdot x + 6.08\sqrt{x} \qquad (2.1)$$

$$x = \left(\frac{293}{T}\right)\left(\frac{p_p}{1}\right)\left(\frac{d}{10}\right) \tag{2.2}$$

where, the pressure, p_p, is in atmospheres, d is the spark gap, in millimeters, and T is the temperature of the gas, in Kelvins. From the expressions, an increase in temperature, decreases the breakdown voltage, while an increase of pressure results in an increase of the breakdown voltage.

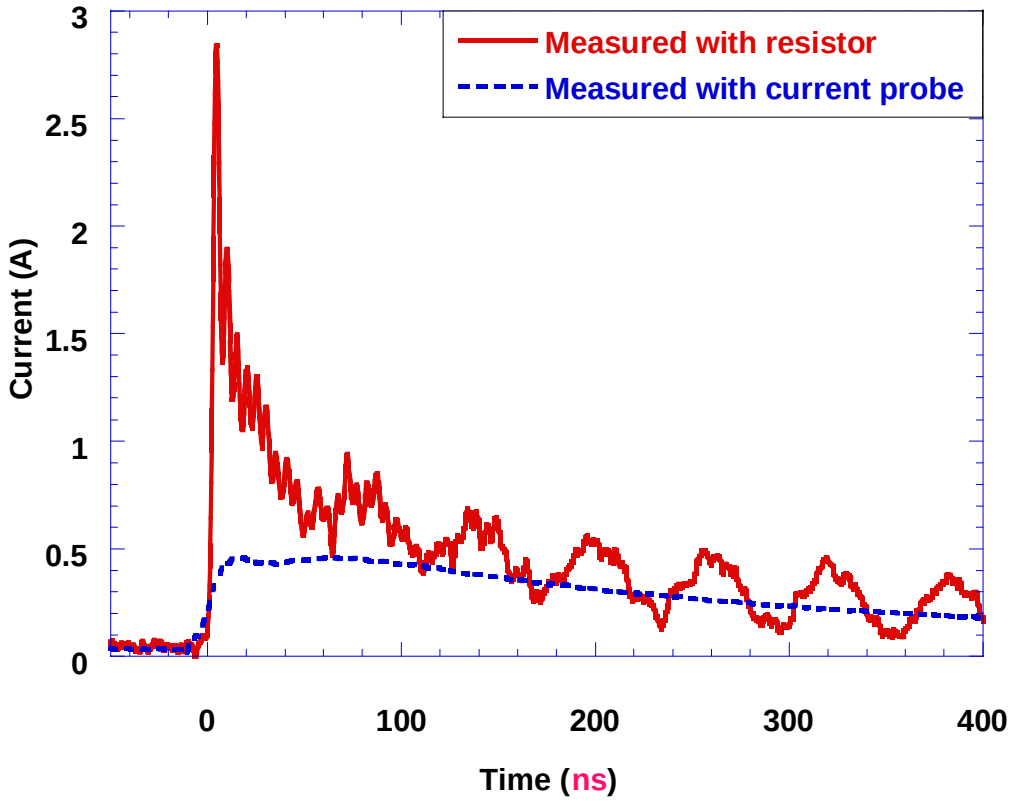

Figure 2.3. Comparison of breakdown current measured by different methods.

The breakdown voltage is affected by the gas mixture composition. Figures 4 shows the effect of the methane concentration in air, on breakdown voltage at a pressure of 2 bar. As the methane/air mixture gets richer, the breakdown voltage decreases. Figure 2.5 shows the measured breakdown voltage in helium. The breakdown voltage is as low as 600 V for Helium compared to 4,200 V for air at room temperature and ambient pressure.

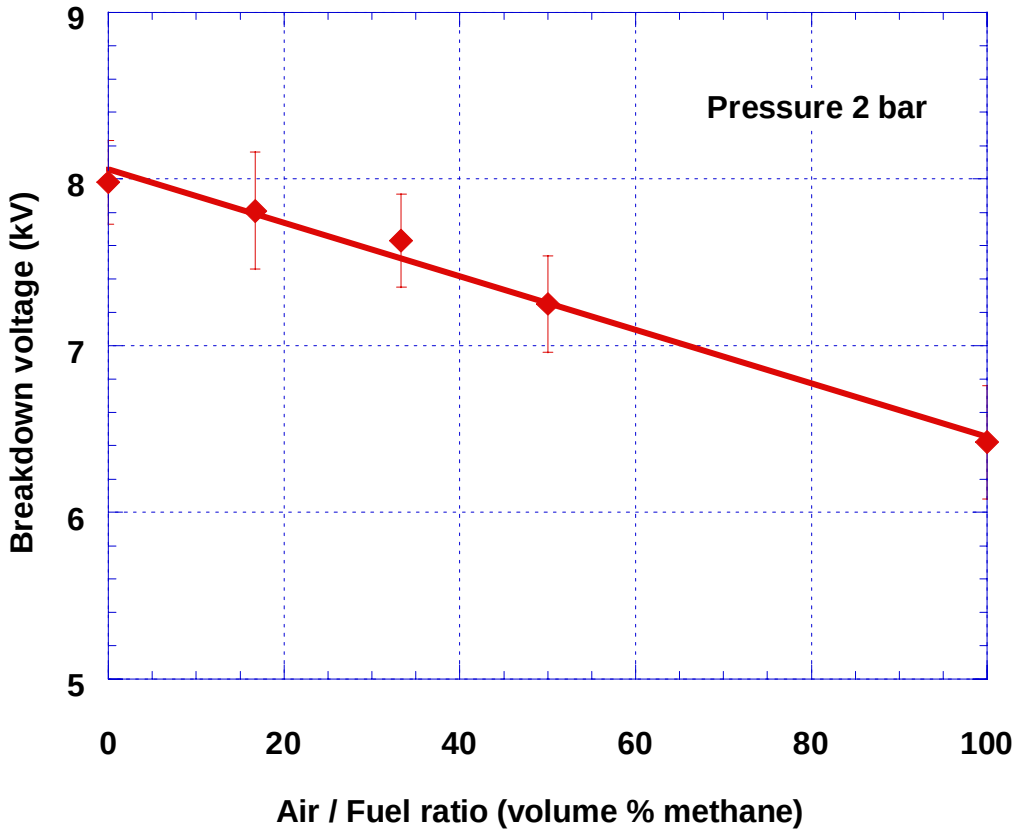

Figure 2.4. The effects of air/fuel ratio (as volume percent methane) for a methane/air mixture on breakdown voltage at 2 bar, the error bars show one standard deviation.

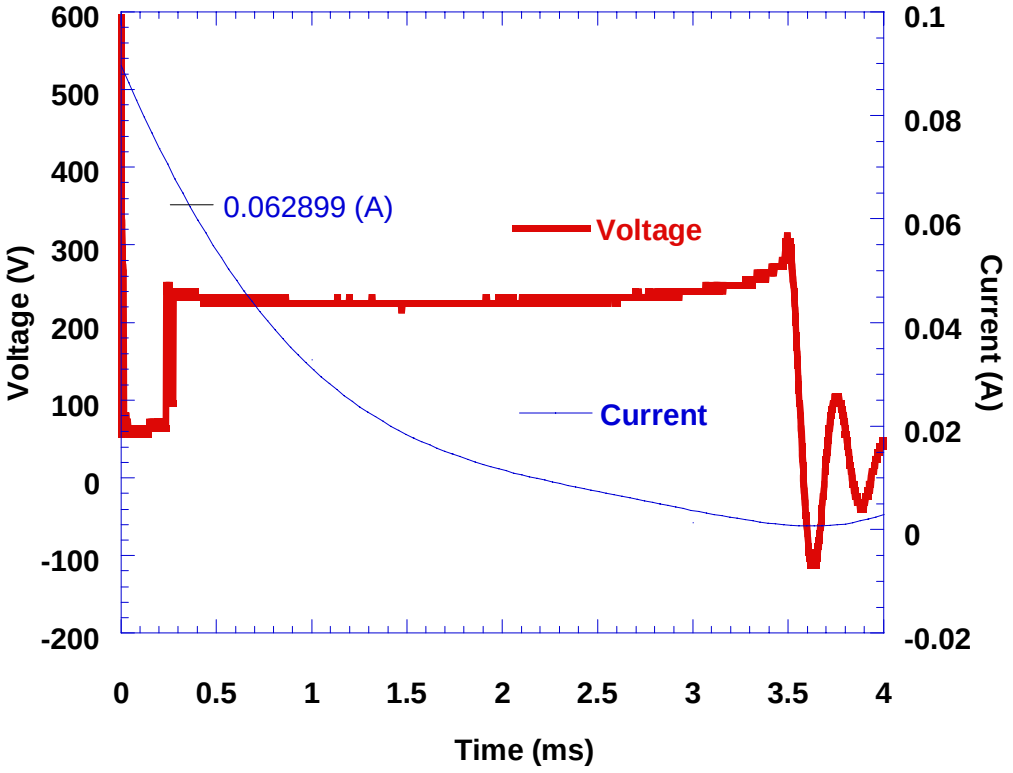

Figure 2.5. The effects of surrounding gas (Helium) on breakdown voltage at 1 bar and 298 K.

Arc Following a very short breakdown phase (about 20 ns), the arc phase is characterized by high, but falling, current and low voltage [51]. The arc is caused by the thermionic emission of electrons from a molten spot on the surface of the cathode [52]. Once the melting point of the metal has been reached, the cathode can then emit electrons. The arc cannot be sustained without these melted spots, which also lead to a loss of electrode material through evaporation. The voltage during arc is around 50 V at 1 bar in air with a 1 mm gap, split into 15 V in cathode fall, 25 V in anode fall, and 10 V in arc plasma [51]. The cathode fall voltage is a function of the cathode material.

Glow discharges are similar to arc discharges but exist with a cold cathode. That is, arc ends and glow begins when the cathode surface temperature falls below the melting point. During the glow phase, the bombardment of ions on the electrode surface becomes the dominant mechanism [53]. Since this mechanism has a very low efficiency, the current decays to a low value. The voltage, on the other hand, rises to a higher value (around 500 V). The glow phase is thus characterized by low currents and high voltages (relative to arc). The voltage splits into the following typical components: 400 V for the cathode fall, 25 V for the anode fall, and 100 V/mm for the positive column [51].

2.2.2 Arc to glow transition

Because breakdown is very short, most of the energy deposition occurs during arc and glow. Moreover, the arc phase is responsible for electrode erosion and therefore is a limiting factor for the durability of spark plugs. However, the characteristics of arc and glow, especially the transition from arc to glow, are not well known due to the complexity of the physics involved. Special effort was made in the present study to investigate the characteristics of arc and glow, especially the transition from arc to glow.

It is widely believed that the arc to glow transition occurs at a definite value of spark gap current. The current in the gap is due to electron emission from the cathode. This electron emission is governed by two basic mechanisms:

- Thermionic emission (arc phase)
- Bombardment of positive ions on the cathode (glow phase)

Most investigators put the transition at 0.1 A [51] or 60 mA (e.g. Kim and Anderson [54]) without any physical justification for this value. It has been assumed that by the time the current has dropped to 100 mA or 60 mA, the thermionic electron emission (which are characteristic of the arc phase) has ended. Once that mechanism ends, the mechanism of electron emission from the cathode changes to bombardment of the positive ions and the transition to the glow phase starts.

Figure 2.1 shows that the transition from arc to glow occurs at ~1 ms after the breakdown and at that moment the voltage suddenly increases from 160 V to ~500 V. The spark luminosity changes at the transition point, indicating some change in physical mechanism. The current at the transition, however, is much lower than the values Maly or Kim and Anderson proposed. Figure 2.6 shows that the transition point varies from shot to shot, possibly due to differences in cooling rate. For discharges in air at ambient pressure and room temperature with a 1 mm gap and a 10.5 kΩ cable, the average arc duration (transition point) was 1.4 ms with a 0.252 standard deviation. The transition current was as low as 20 mA.

The transition is also affected by the surrounding gas as shown in Figure 2.5. It can be seen that helium has much lower glow voltage compared to air.

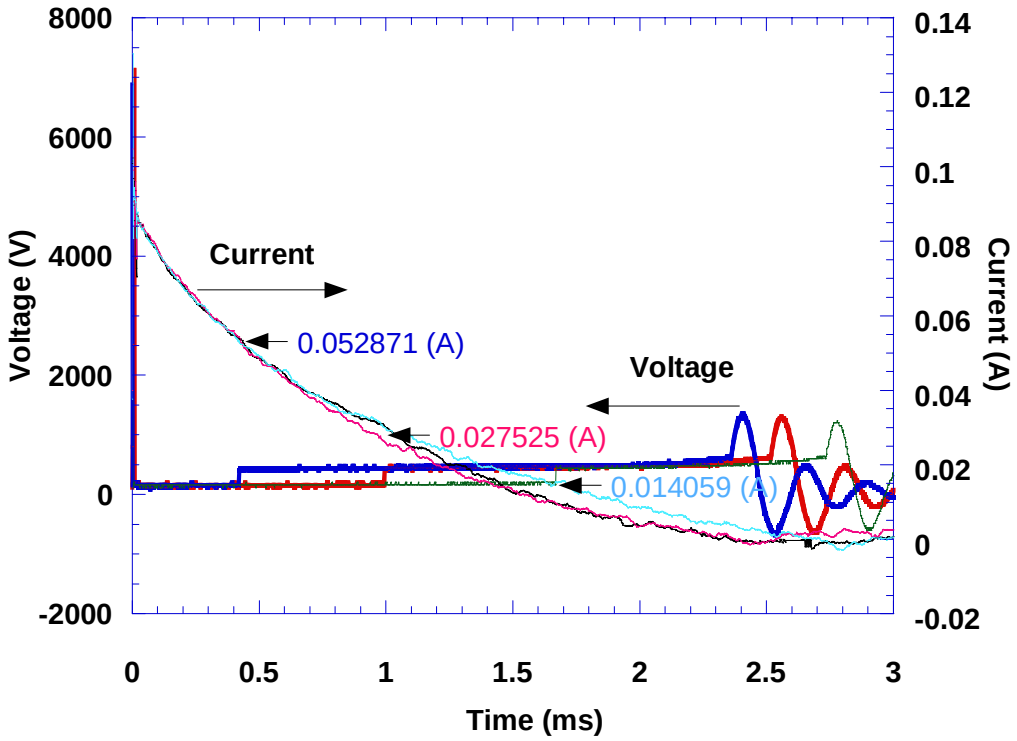

Figure 2.6. Shot-to-shot variation in arc-to-glow transition.

The electrode material can affect discharge characteristics. Discharge current and voltage behavior was measured and compared for electrodes made of copper versus tungsten. Each pair of cylindrical electrodes was positioned end-on with a 1 mm gap. Figure 2.7 shows the effects of electrode material on the arc-to-glow transition. Both tungsten and copper have very short arc phases. Comparing the two materials, copper has a higher arc voltage (about 300 V for copper and 100 V for tungsten). The arc-to glow takes place at about 100 mA for both materials, in agreement with one of the standard transition criteria [51].

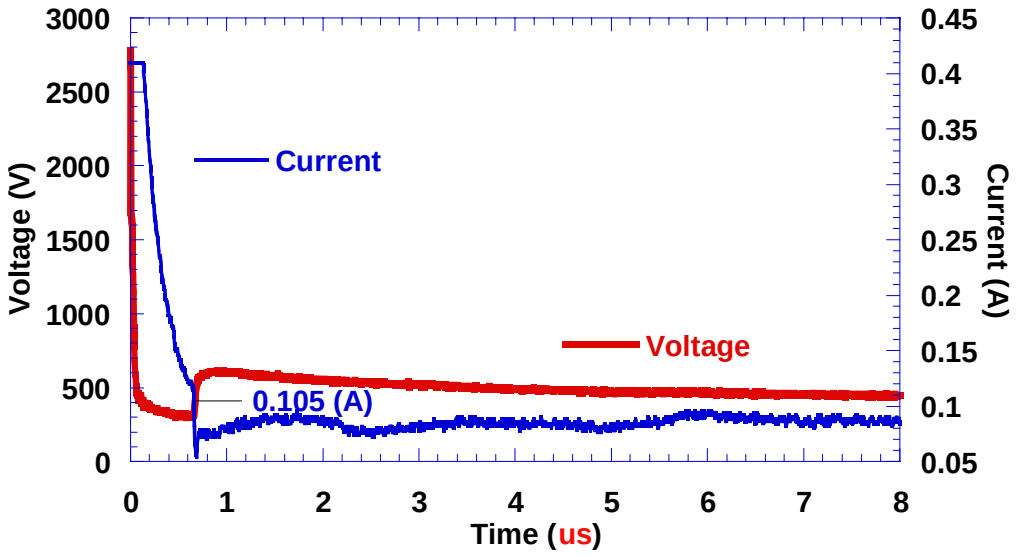

a: Copper

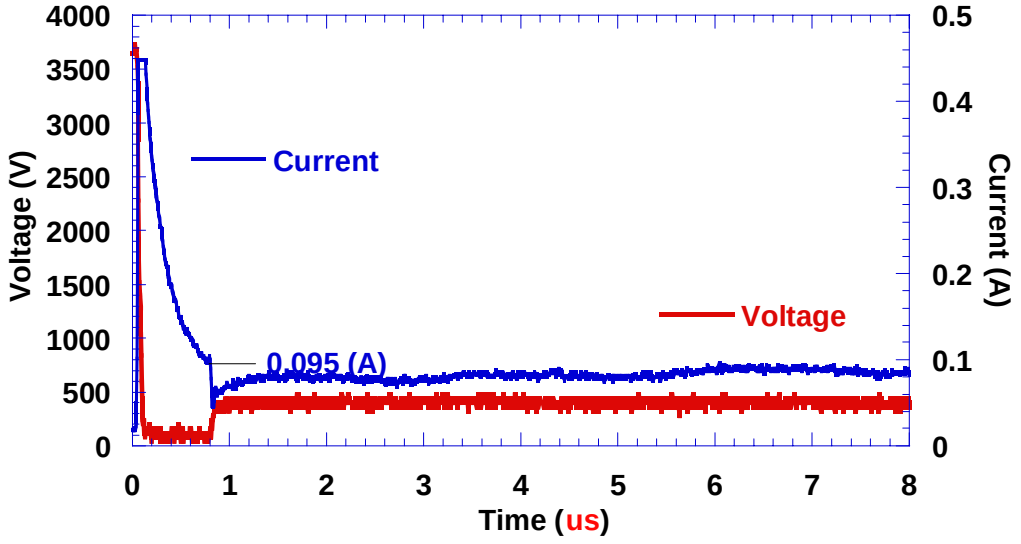

b: Tungsten

Figure 2.7. The effects of electrode material on discharge.

The flow field can have a significant effect on the discharge. A blower was used to create a flow across the gap of one of the spark plugs. The velocity was measured using a hot-wire anemometer. The results are shown in Fig. 2.8 and can be compared with the zero velocity case shown in Fig. 2.1. The spark duration decreases from 2.5 ms without flow (Figure 2.1) to about 1.8 ms when the flow velocity is 9.8 m/s (Figure 2.8). Arc and glow characteristics, especially the arc to glow transition, are also changed.

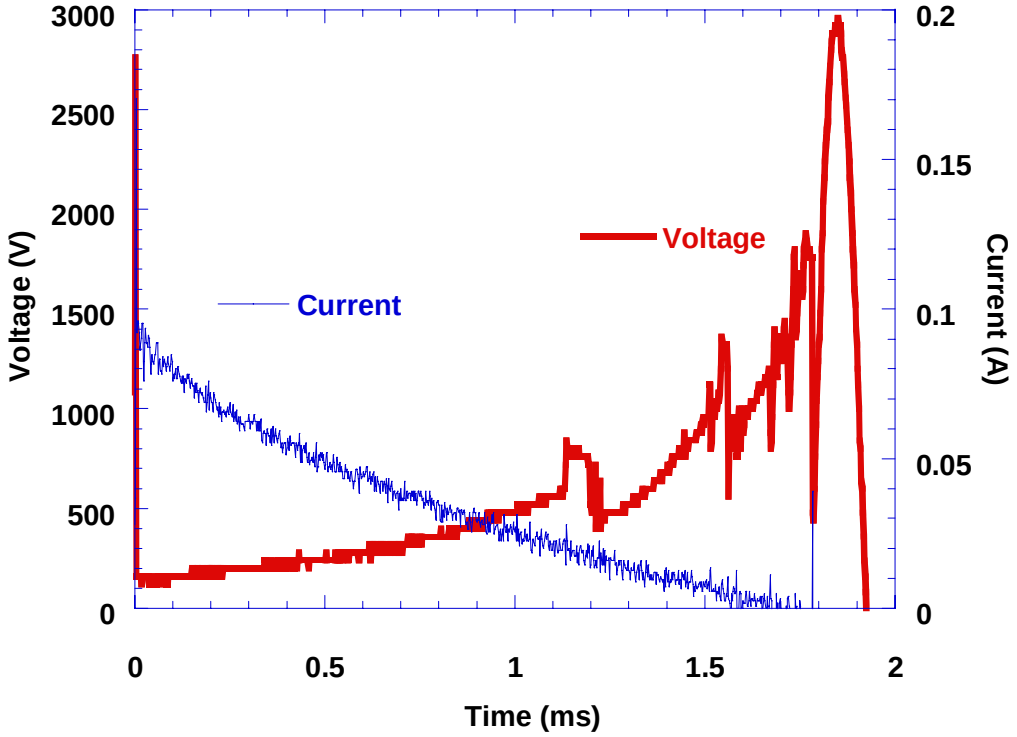

Figure 2.8. The effects of flow field on discharge, flow velocity of 9.8 m/s, room temperature.

Figure 2.9 shows results of a conventional inductive spark discharge in a SI engine run at idle and fueled with natural gas. It is hard to see the arc-to-glow transition. Lee at al [62] found that the fraction of the total discharge spent in the glow regime decreased while the fraction of time in the arc phase increased as pressure increased. At a pressure of 1 atm about one-half of the total discharge time is in the glow phase. The time spent in glow decreases as the pressure increases until the glow phase is absent above a pressure of about 7 atm.

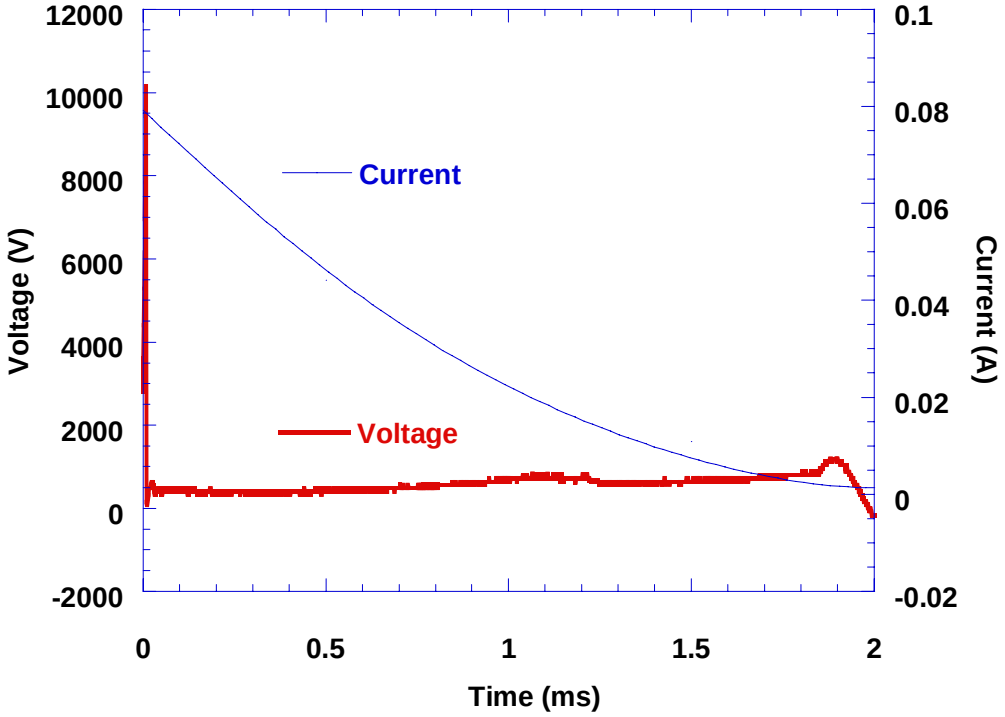

Figure 2.9. Discharge characteristics in an operating engine at idle conditions.

2.2.3 Discharge energy

The following terms are defined to aid discussion of the discharge characteristics: An energy balance yields:

$$E_t - I^2 R_{sp} = E_d \tag{2.3}$$

where E_t is the total energy provided to the igniter measured on the high tension cable end of the spark plug, I is the current, R_{sp} is the resistance of the spark plug, and E_d is the delivered energy, measured on the center electrode at the gap end. These two energies can be measured by integrating the product of the current and voltage with each measured either at the high tension end or the gap end of the center electrode:

$$E = \int IVdt \tag{2.4}$$

The discharge characteristics of a 16.5 kΩ internal resistance spark plug were examined with the voltage measured either at the top of the plug or at the gap. Figure 2.10 shows that the voltage characteristics are quite different when measured at different plug positions (top or gap end) for a resistant spark plug. Figure 2.11 shows that the total energy E_t is about 4 times the delivered energy E_d.

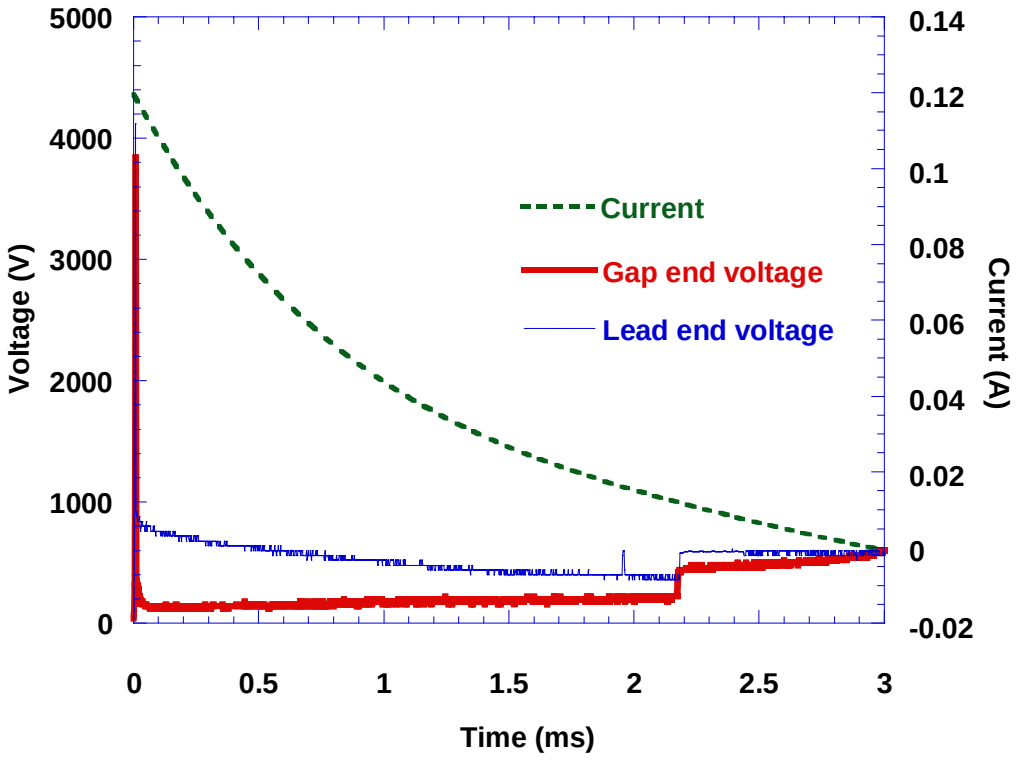

Figure 2.10. Discharge voltage and current of a resistant spark plug with 16.5 kΩ resistance.

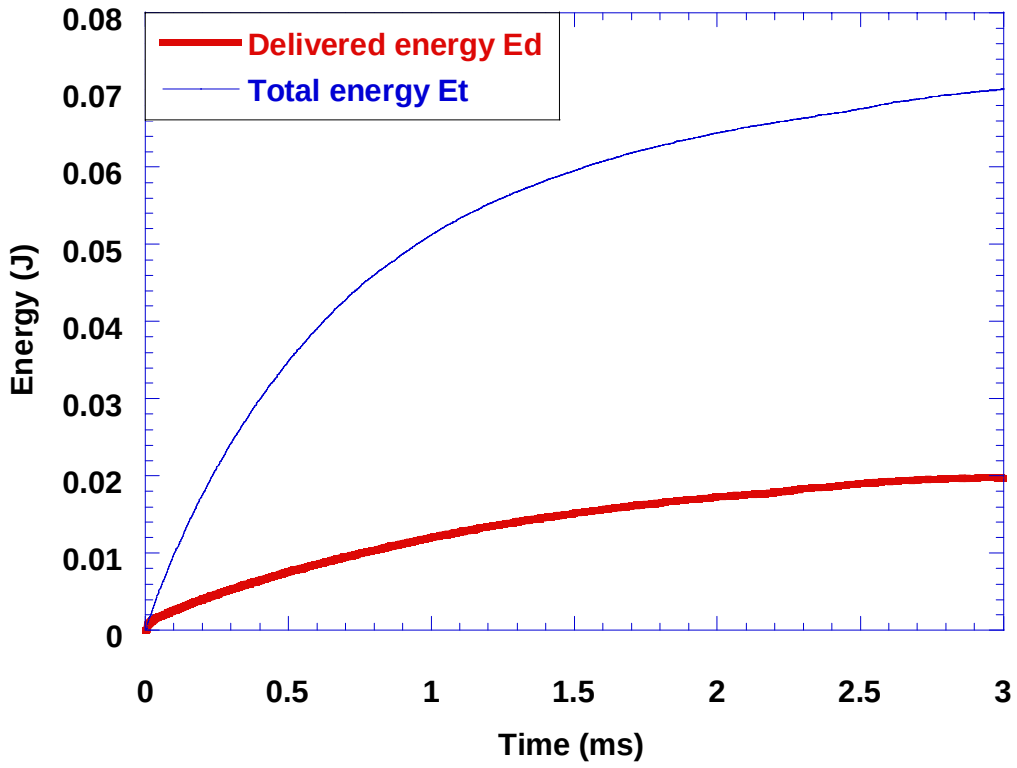

Figure 2.11. Comparison of discharge energies of a 16.5 kΩ resistant spark plug.

2.2.4 Effects of spark plug resistance on discharge

To isolate the effects of spark plug resistance, advantage was taken of the design of the Champion resistor-type spark plugs which have a cylindrical carbon resistor inside the ceramic. We removed the resistor and carefully reconnected it outside the ceramic on the high tension cable end. This allowed easy variation of this resistance with all other parameters held constant.

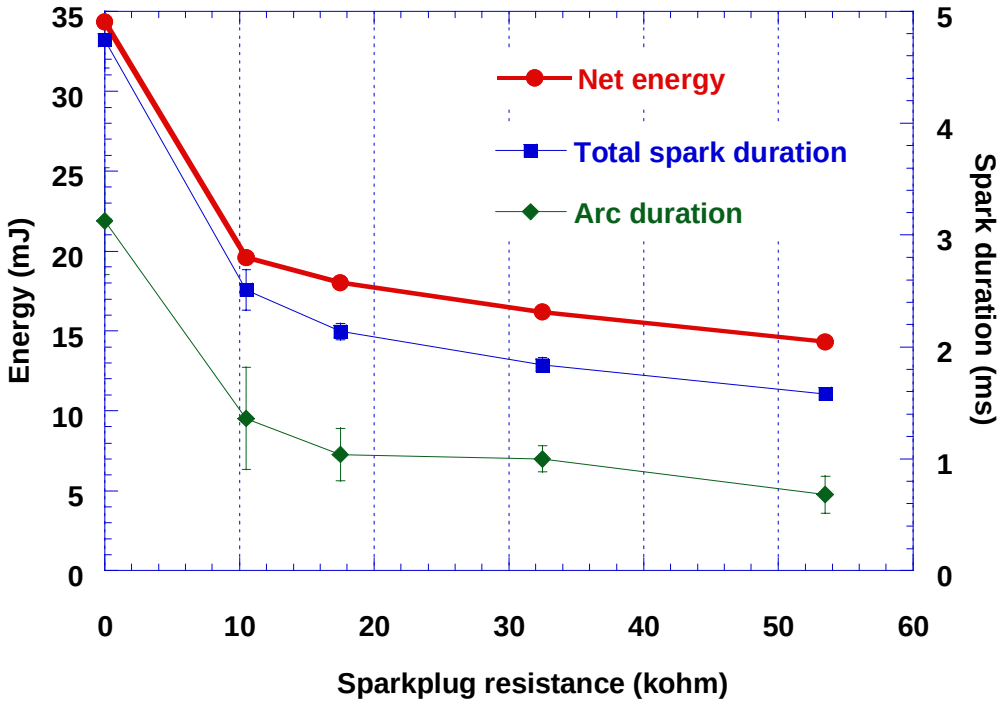

Figure 2.12. The effects of spark plug internal resistance on delivered energy and spark duration.

As shown in Figure 2.12, the "internal" resistance of a spark plug has a significant effect on both the spark duration and the net discharge energy. As the resistance increases, both the arc duration and the total spark duration decrease. The figure shows that spark duration decreases rapidly as the resistance increases from near zero. The spark duration then continues to decrease, but very slowly as the resistance increases to values above a few kilo Ω. Additionally, since the voltage at the gap during arc and glow doesn't change significantly as shown by Figure 2.13, the discharge energy decreases as the resistance increases. It should be noted that the voltage during arc and glow is not a constant for each spark discharge. However, the arc voltage remains relatively constant, but the glow

voltage increases steadily from the time of the arc-to-glow transition to the end of glow phase as shown by Figure 2.1 and 2.6. The voltages shown in Figure 2.13 are the average voltages of the arc and glow phases.

Figure 2.12 also shows that the total spark duration and the arc duration share the same trend, which implies that the glow duration, that is the difference between the total spark duration and the arc duration, does not change significantly as the spark resistance changes.

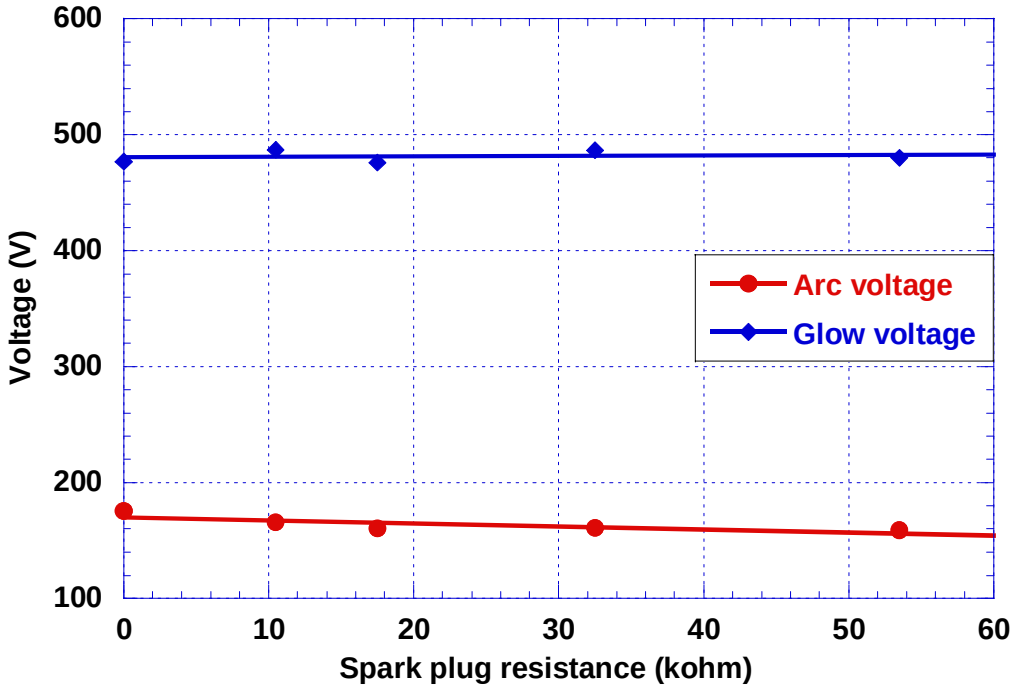

Figure 2.13. The effects of spark plug internal resistance on the average voltage of arc phase and glow phase.

2.2.5 Effects of spark gap on discharge

The gap size of the standard spark plug was changed to study the effect on discharge characteristics. The effects of the spark gap size on the discharge are shown in Figure 2.14. As the plug gap increases, both the average voltage of arc and glow increases whereas the spark duration does not change significantly as shown by Figure 2.15. Because the voltage increases while the duration is fixed, the discharge energy increases with increasing gap. However, since the voltage during the arc phase increases, electrode erosion should deteriorate with increasing gap.

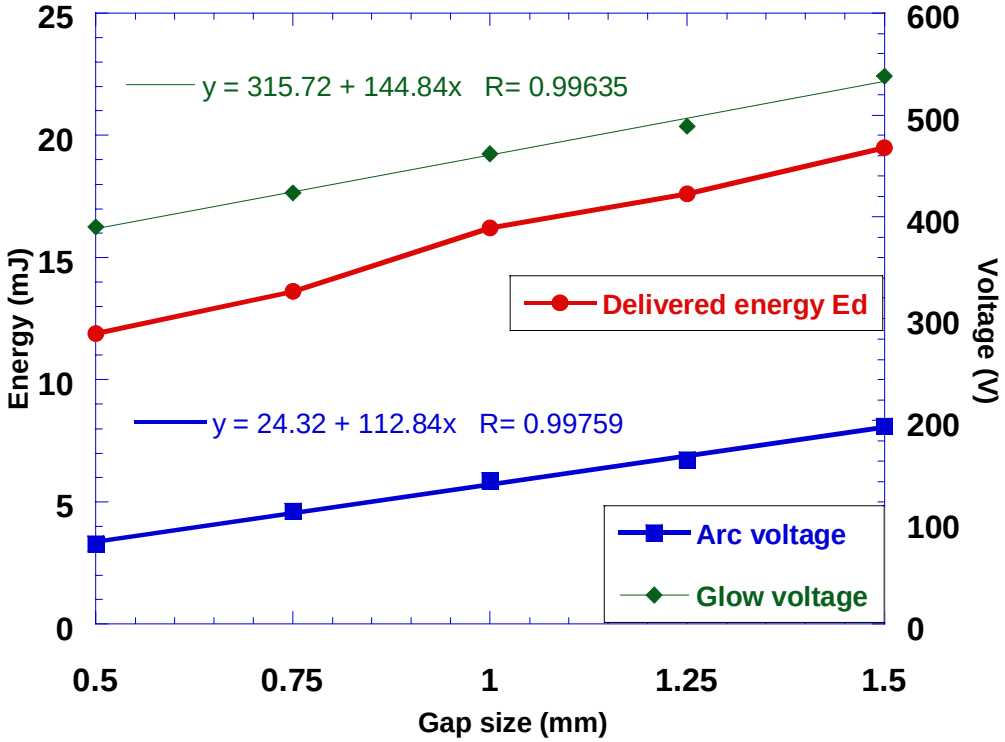

Figure 2.14. The effects of spark gap size on delivered energy, arc and glow voltage.

Figure 2.15 shows that as spark gap increases, the total spark duration decreases slightly whereas the arc duration increases slightly, which means that

the duration of glow phase becomes shorter. This is different from the effect of the spark resistance.

The following relationships can be drawn from the data in Figure 2.14:

$$V_{glow} = 144.84d + 315.72 \text{ (Volts)} \quad (2.5)$$

$$V_{arc} = 112.84d + 24.32 \text{ (Volts)} \quad (2.6)$$

where d is the gap size in mm.

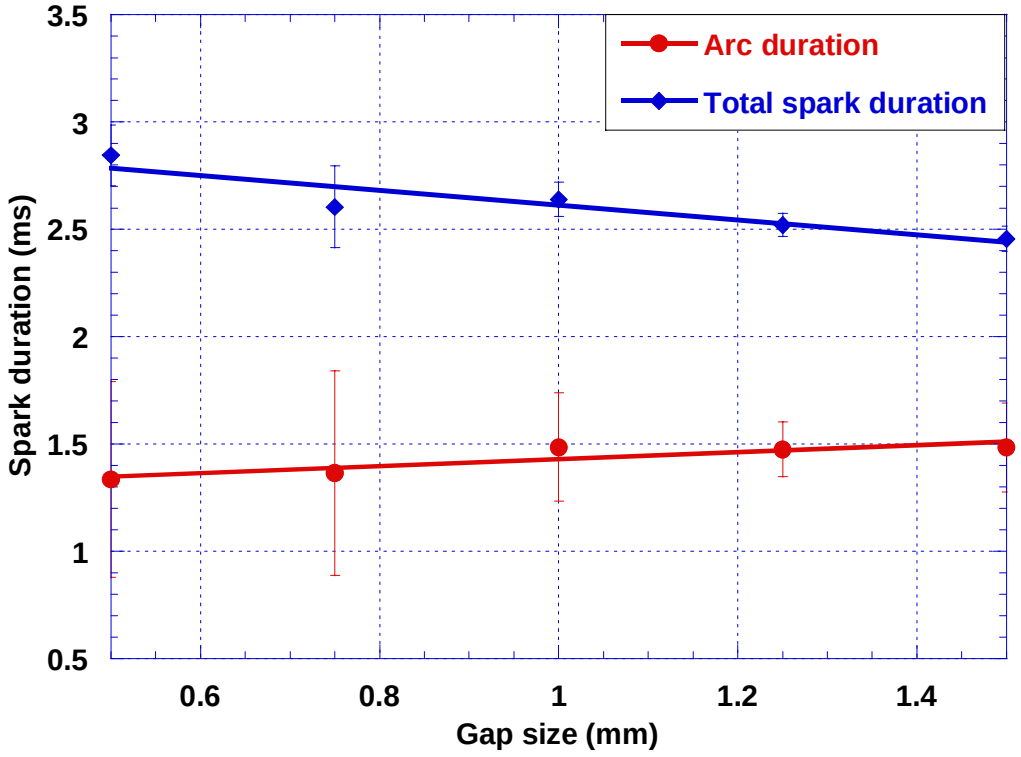

Figure 2.15. The effects of spark gap size on spark duration.

2.3 Capacitor discharge ignition systems

The capacitor discharge method of creating a high tension voltage spark across the spark plug electrodes is achieved by storing the electrical supply energy in a charging capacitor. When ignition is timed to occur, a thyristor power switch conducts and completes the capacitor primary winding circuit of the ignition coil. At that time, the capacitor will discharge through the primary winding. The sudden flow of current in the primary winding induces a very high voltage in the secondary winding and, since the spark plug forms part of the secondary winding circuit, this voltage pulse will be dissipated at the plug gap in the form of a spark.

The stored energy (E) in the capacitor is given by

$$E = \frac{1}{2} CV^2 \tag{2.7}$$

The CDI system that author tested was a MoteC CDI-1, where C=1 μF and V=450 V, so the stored energy E=101.25 mJ.

Figure 2.16 shows the discharge characteristics of the CDI system. Compared to the inductive ignition system shown in Figure 2.1, CDI systems have a relatively high current but have a spark duration about one-tenth as long. CDI ignition systems do not produce a glow phase. The delivered energy was about 37 mJ per shot, almost double the value of the inductive ignition system used. This value is much lower than the calculated stored energy because most of the stored energy was dissipated in the resistance cable.

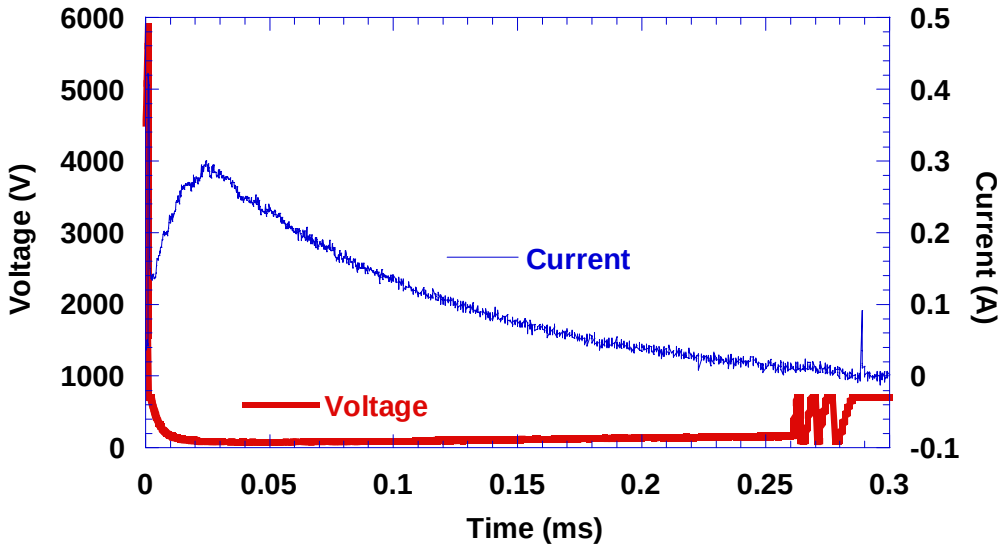

a: Discharge voltage and current

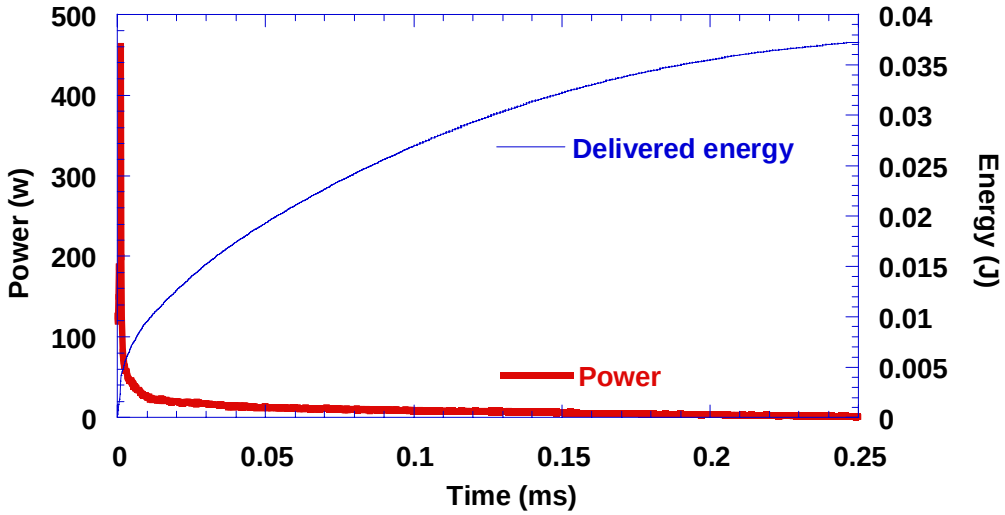

b: Discharge power and delivered energy

Figure 2.16. Characteristics of a capacitor discharge ignition discharge.

2.4 The Railplug ignition system

A novel electronics system was used to fire the railplug. As shown in Figure 1.3, this system consisted of a breakdown circuit and a "follow-on" circuit. The conventional breakdown circuit is a standard inductive ignition circuit which provides the high voltage required for breakdown and produces low currents (of the order of 100 mA). The follow-on circuit that is shown in Figure 2.17 consists of a capacitor which is charged, for the present experiments, using a Variac and bridge rectifier. This part of the circuit provides a high current (of the order of 100 A) after breakdown for accelerating the plasma down the rails. Isolation is necessary between the breakdown and follow-on segments. This isolation is achieved using a high-voltage diode D1 and a high-voltage blocking capacitor C1 between the ignition coil and follow-on circuit.

The stored energy in the follow-on capacitor can be calculated by expression 2.7. It should be noted that the capacitor voltage after its discharge, V_e, is not zero, which means a threshold of the charging voltage below which the follow-on circuit will not function. This threshold voltage is related to the voltage required to sustain the arc and is related to the characteristics of the circuit, such as the insulator diode. So the following expression was used to calculate the stored energy E_s,

$$E_s = \tfrac{1}{2} C\left(V_i^2 - V_e^2\right) \tag{2.8}$$

where, V_i is the initial charge voltage. The circuit discharge efficiency is defined as E_d / E_s. E_d is the discharge energy delivered to the spark plug or railplug

calculated via Equation 2.4 using the measured voltage and current. For the circuit that the author used, the discharge efficiency was about 40%.

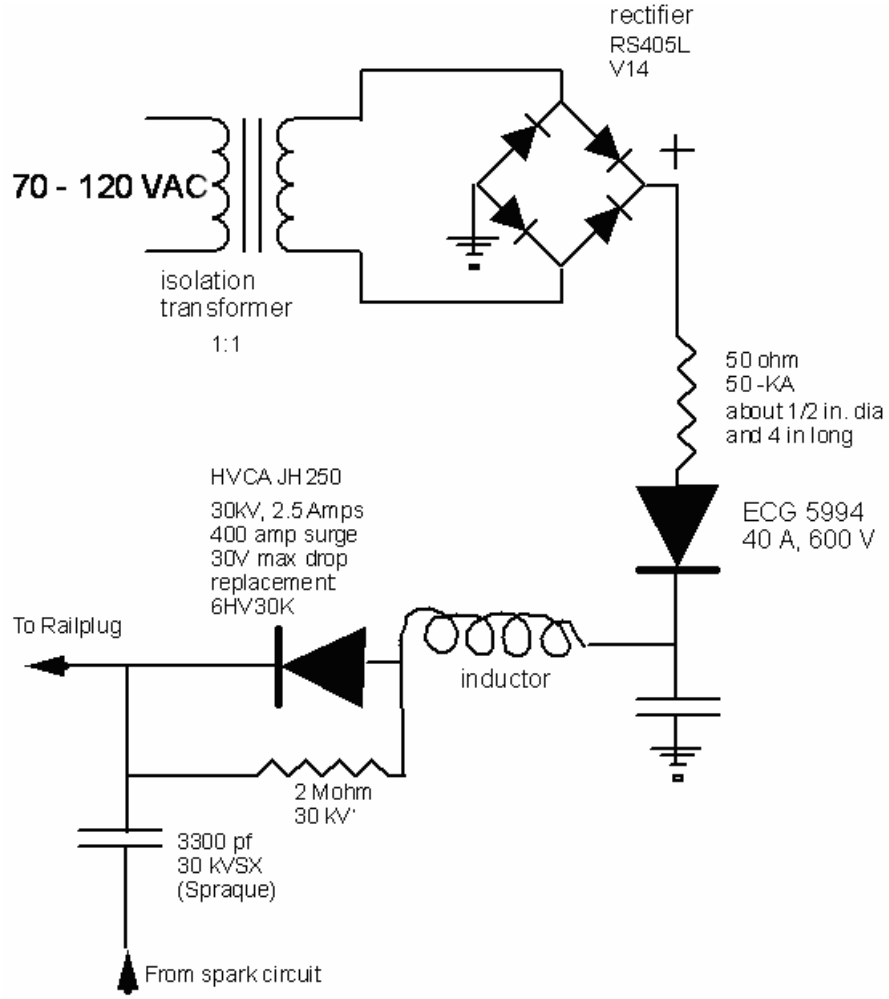

Figure 2.17. Railplug follow-on circuit.

Figure 2.18 shows the voltage, current, power, and delivered energy profiles of a typical railplug discharge ("firing" or "shot"). In this particular shot, the energy delivered was 0.47J with a peak current of 150 A and a spark duration

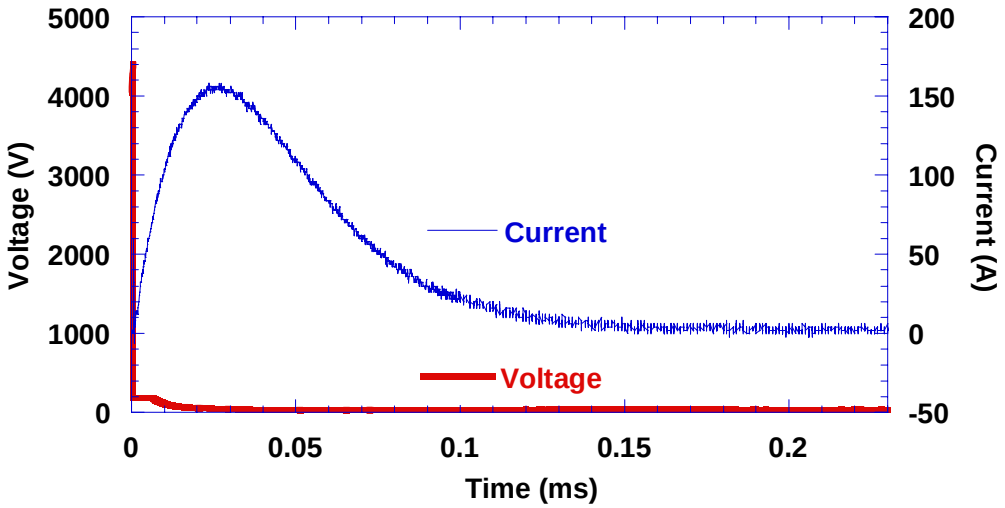

a: Railplug discharge voltage and current

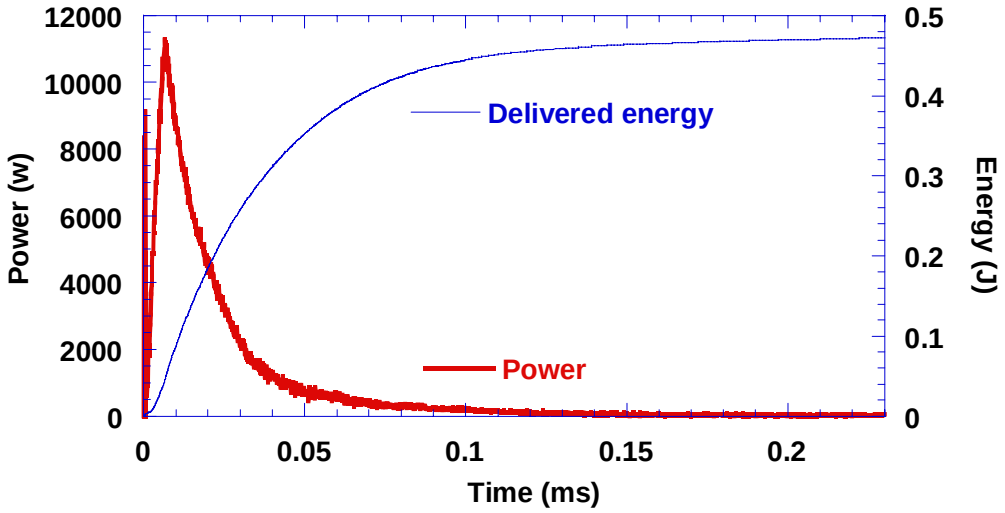

b: Discharge power and delivered energy

Figure 2.18. Characteristics of a typical railplug discharge with C=100 μF, charging V_i=180 V.

of ~0.2 ms. The stored energy in the capacitor was about 1.2 J so the efficiency was about 40%. Compared to the spark plug, the railplug has a very short spark duration (with this specific circuit).

Figures 2.19 and 2.20 show the effects of follow-on capacitance and initial charge voltage (V_i), respectively, on the current history. In these figures, it can be seen that increasing both capacitance and charge voltage increase the peak current. Of these two factors, the charging voltage affects the peak current more significantly. However, the voltage has only a very small effect on the spark duration whereas the capacitance has a relatively strong effect on the spark duration. In other words, a high charging voltage should be used if higher discharge power is preferred; but a high capacitance if longer spark duration is preferred.

The capacitance values used in this study were 22-220 μF and voltages were from 100-200 V. The capacitor discharge circuit in Figure 2.17 can be simplified to represent a simple RC circuit. To study the effects of discharge duration on railplug performance, we can change either capacitance C or resistance R to change the spark duration. For this purpose, an adjustable power resistor with full-scale resistance of 1 ohm was serially connected to the circuit just before the railplug to change the discharge time constant (not shown in Figure 2.17). It is, however, more effective and more convenient to change the discharge duration by changing the current shaping inductor L1. The effects of the inductance of the shaping inductor on discharge duration and plasma travel will be discussed in the next chapter.

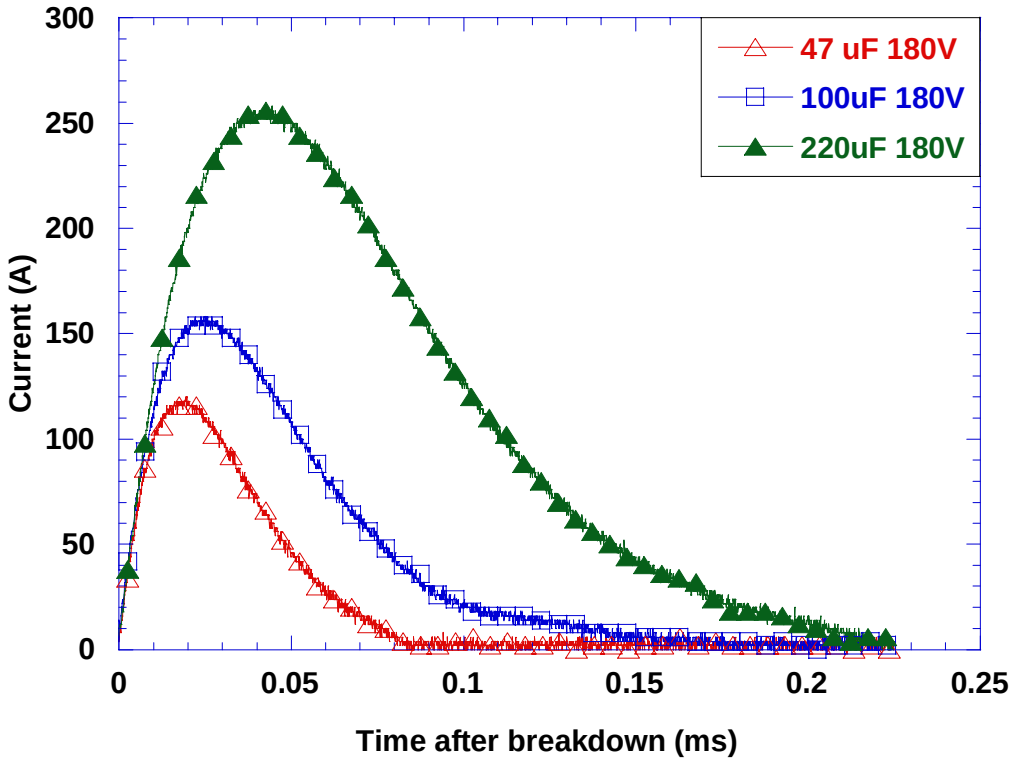

Figure 2.19. The effects of follow-on capacitance on discharge current.

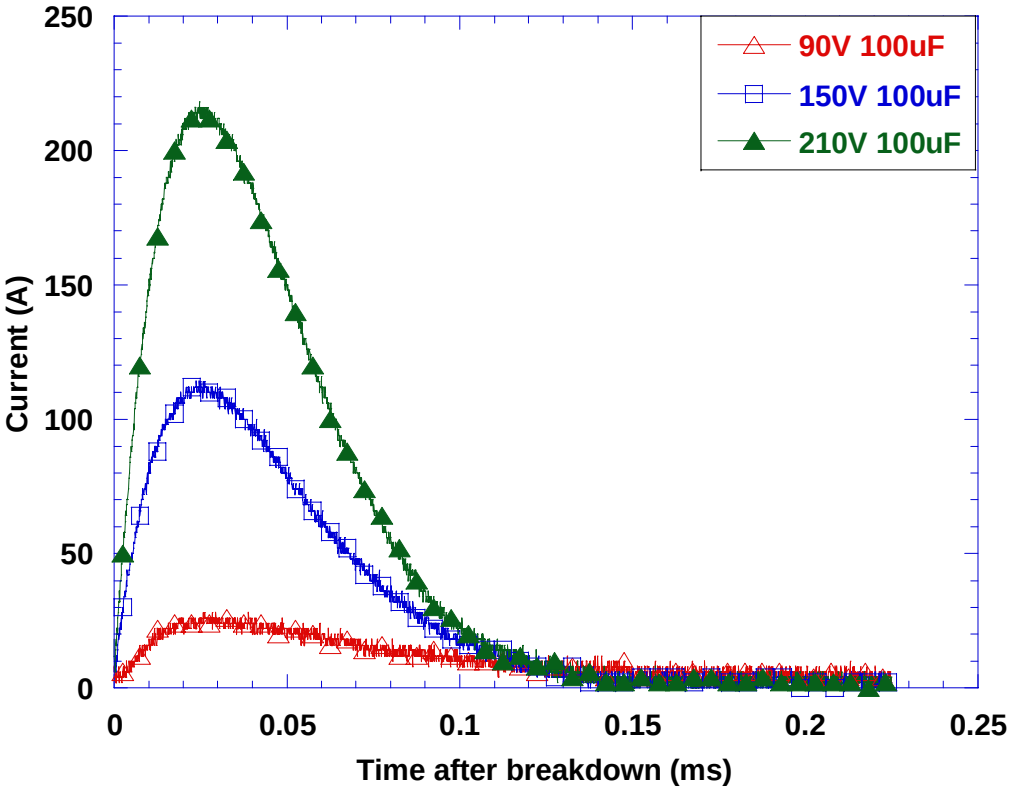

Figure 2.20. The effects of initial charge voltage on discharge current.

2.5 Chapter summary

Inductive ignition discharge has 4 phases: Pre-breakdown, breakdown, arc and glow. Since the breakdown phase is very short, most of the discharge energy is deposited during arc and glow. The arc phase has higher discharge efficiency compared to the glow phase. It is, however, responsible for electrode erosion and therefore is a limiting factor for the life of spark plugs.

The spark discharge can be affected by many factors. The time at which the arc to glow transitions occurs can vary greatly. It was also observed that this

transition does not occur at a fixed current level as many researchers assumed, rather, it can take place at different current values.

Spark plug internal resistance and gap size greatly affect delivered discharge energy. The delivered energy decreases as spark plug resistance increases because the spark duration decreases. The delivered energy increases as spark gap increases because both arc and glow voltage increase.

As shown in Table 3, compared to inductive ignition, both CDI and railplug ignition have shorter spark durations. They also don't have a glow phase. Their delivered energy, however, is higher than the inductive ignition because of the higher discharge current.

Table 3. Characteristics of the three ignition systems.

	Inductive	CDI	Railplug (variable)
Delivered energy (mJ)	19.5	37.5	470
Spark duration (ms)	2.5	0.25	0.2
Average power (W)	7.8	150	2350

Chapter 3.0 Railplug Design

The prototype railplugs discussed in this dissertation were designed, fabricated and tested by the author. The railplug development was a long procedure. First, a railplug was designed and fabricated based on the knowledge that we learned from the previous research. Secondly, it was tested in the open air and/or in a pressured constant-volume bomb. Once it passed the pressured bomb test, it would be tested in an operating engine. The railplug design was then improved based upon the engine test feedback. For simplicity, only a few of the more successful designs are discussed in this chapter.

Only 18 mm railplugs were developed because the objective of this research was to develop a new igniter for large-bore natural gas engines. Figure 3.1 shows some examples of railplugs tested in this dissertation. Several important issues need to be considered when designing and fabricating railplugs.

- It must be strong enough to hold in-cylinder high pressure and temperature gases.
- It must have high dielectric strength at high temperature because breakdown voltage increases as pressure increases and dielectric strength decreases as temperature increases for ceramics [63, 64].
- The components must be easy to machine.
- It must have good performance and durability.

Coaxial railplug

Open rails railplug

Partially enclosed railplug

Magnet enhanced railplug

Figure 3.1. Examples of railplugs.

In order to get good performance and durability for a railplug, it is necessary to take full advantage of the electromagnetic force to move the plasma faster. The high-speed arc motion results in a fast burning rate and the ability to burn leaner mixtures than might ordinarily be possible. The high-speed plasma movement also helps to improve the railplug durability since the energy is deposited over a much larger electrode surface area and the duration of the arc at any specific point decreases. So any method that helps arc motion improves both the ignitability and the durability of a railplug.

This chapter presents results of railplug discharge and performance measurements made outside of an engine. The measurements were performed in air at ambient conditions. The goal was to understand how various design and operating parameters affect railplug performance. Some of the parameters considered include railplug geometry, the diameter of the rails, and the amount of inductance in the railplug circuit, and the effect of using an external permanent magnet to enhance the Lorentz forces on the arc.

3.1 Railplug geometric design

As described in Chapter 1, the direction of the self-induced magnetic field is perpendicular to the plane of the paper and the electron flow is up one rail, across the arc, and down the other rail. This current loop results in the Lorentz force:

$$F = J \times B \tag{3.1}$$

where J is the current flow per unit area and B is the strength of the local magnetic field. If a constant current (I) is supplied to parallel rails, the Lorentz force is:

$$F = \frac{1}{2} L' I^2 \tag{3.2}$$

where L' is the inductance per unit length of the rails. For cylindrical conductors of radius r that are removed from an external conducting boundary, the inductance per unit length is:

$$L' = 0.4 \times 10^{-6} \left[\ln(d / r) + (1/4) - (1/R_a) \right] \tag{3.3}$$

in μH/m, where d is the separation distance between the centroids of each rail and R_a is the aspect ratio, which is the rail length divided by the rail separation.

Basically, there are two types of railplug designs: parallel electrodes and coaxial electrodes as shown in Figure 3.1. Coaxial railplugs are easy to manufacture since most of the components are the same as for conventional spark plugs. However, parallel railplugs have some advantages over coaxial railplugs. Parallel railplugs have a higher inductance gradient (L'). Typical L' values for the coaxial railplug range from about 0.18 to 0.25 μH/m while a typical value for the parallel railplug is about 0.30 μH/m. A higher inductance gradient produces a larger Lorentz force for the same current and, thereby, higher plasma velocity.

In a prior study of 14 mm coaxial railplugs, it was found that a discontinuity between the initiation gap and the remainder of the coaxial rails

tended to hold the arc, preventing motion past the discontinuity as shown in Figure 3.2. This had an adverse effect on durability since the energy was not spread over as large of an electrode surface area as would otherwise be possible. This discontinuity was eliminated for the design of the present 18 mm railplugs. For the parallel railplugs illustrated in Figure 3.3, this was accomplished by machining the rails to an angle of ~5^{o} downstream of the initiation gap as shown in Figure 3.3 [65].

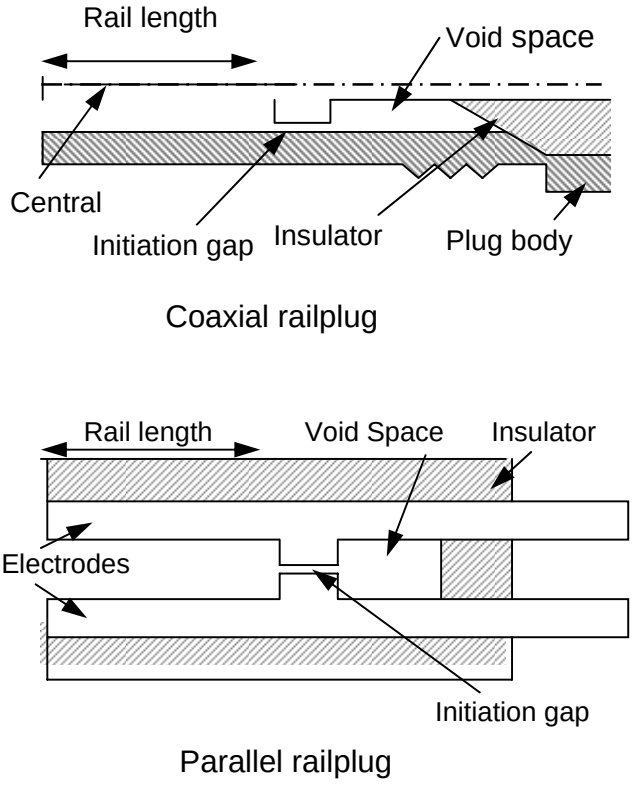

Figure 3.2. Schematic of old geometries of coaxial and parallel electrode railplugs.

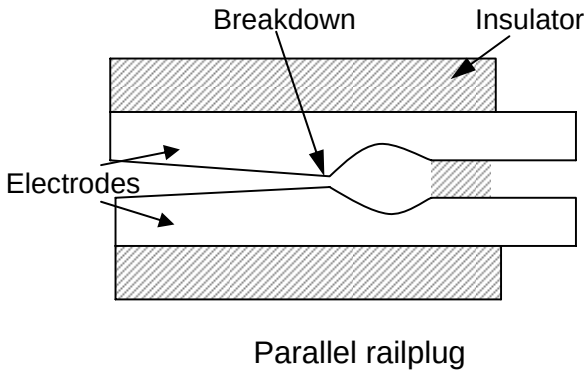

Figure 3.3. Schematic of a parallel electrode railplug having tapered rails.

Figure 3.5 shows the effects of railplug geometry on plasma motion. The rails in Figure 3.5-a were machined to have flat surfaces such that a muzzle end view of either rail has a shape similar to a D as shown in Figure 3.4. The rails in Figure 3.5-b were machined to form ridges along the center-plane such that a muzzle end view has a shape similar to a slice of pie. As noted above, for both designs the rails were tapered to remove the gap area discontinuity. Comparison of Figures 3.5-a and 3.5-b reveal that the plasma moves farther along the ridged rails. One of the reasons is that the plasma streamer along the ridged rails is thinner and more concentrated so it has higher density and less heat loss. Figures 3.5-b, 3.5-c and 3.5-d are all ridged rails; the only difference is how much the rails were enclosed. The arc moved farther for the partially enclosed rails (Figure 3.5- d) than for the open rails (3.5-b) for which the arc moved farther than for the fully enclosed rails (3.5-c). The fully enclosed rails may have excessive heat loss while thermal expansion aids arc motion for partially enclosed rails.

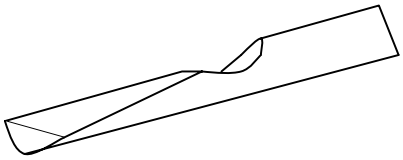

Flat electrode rail

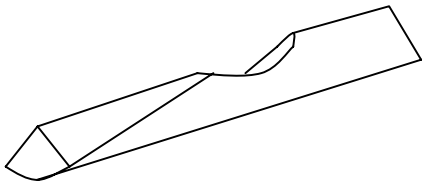

Ridged electrode rail

Figure 3.4. Views of the rail cross-sectional geometries.

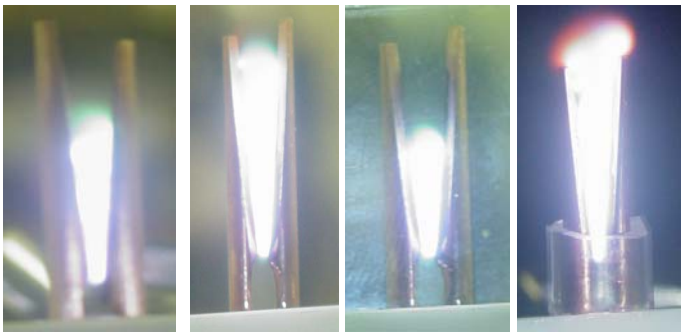

a b c d

Figure 3.5. Effects of railplug geometry on plasma motion. a: flat rails; b: ridged rails; c: ridged rails fully enclosed by transparent glass slides; d: ridged rails partially enclosed by a transparent tube. C=600 μF charged to 210 V.

Hari et al [50] investigated the effect of rail divergence angle on plasma movement. In general, arc propagation distance tends to decrease as the rail divergence angle is increased. For the ridged geometry railplug, however, a slight increase in rail propagation distance was observed with increasing angle for small angles and the arc travel distance was maximal with a 10^{o} divergence angle. So all the parallel railplugs shown in Figure 3.1 have a 10^{o} rail divergence angle. In order to prevent spark jumping at the rail tip as the initiation gap increases with erosion, a common railplug failure for the previous designs [43], the rail tips were tapered further as shown in Figure 3.6. The rails were machined to form ridges along the center-plane to enhance plasma movement. The ridged railed then were machined with small flat surfaces to form the tapered angle. So the final rail is the combination of a ridged rail and a flat rail as shown in Figure 3.6. This compromise approach was used due to its simplicity of machining. A double-bore ceramic tube was used to insulate the two rails. All the railplugs shown in Figure 3.1 have initiation gaps 1 mm.

For the magnet enhanced rail plug, a 15mm x 4mm x 3mm permanent magnet was located along one side of the railplug at a distance of 3 mm from one of the rails. The magnets were given by courtesy of The Arnold Engineering Co. as testing samples. At this distance, the magnet had a measured field strength of 4.5 Gauss. The type of the magnet used in this test is Alnico 8H. Alnico magnets offer excellent stability with respect to temperature changes: reversible change is 0.02% per degree Centigrade. Heating may produce an irreversible loss of magnet strength. In order to protect the magnet and prevent spark jumping to the magnet, a ceramic tube was used to cover the magnet as shown in Figure 3.1 for the magnet enhanced railplug.

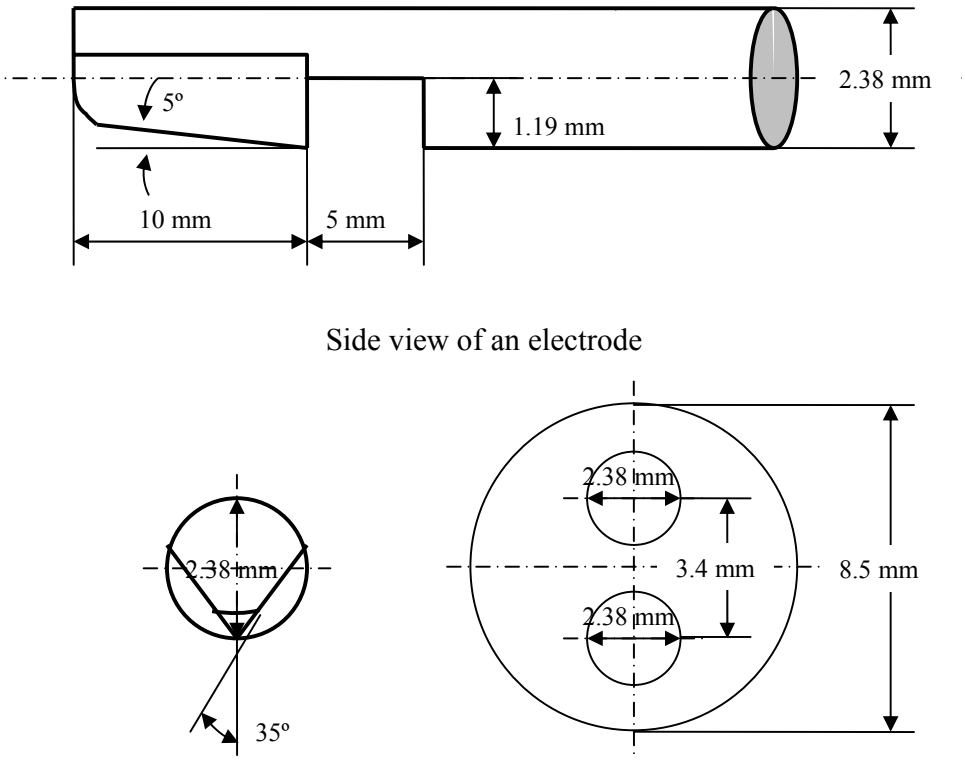

Figure 3.6. The dimensions of electrodes and insulating ceramic tube used for parallel railplugs.

3.2 Railplug design to prevent sparkover of insulating surfaces

It is very challenging to design parallel railplugs with effective and reliable insulation between the two rails. The parallel railplug requires a ceramic

sleeve or double bore ceramic tube as an insulator that is more complex in shape than the insulator used for the coaxial railplug. Much work has been done but it is still a weak point for parallel railplug design.

For coaxial railplugs, two failure modes were noted from previous research: blistering of the center electrode with > 1.0 J energy delivered, and center rail erosion near the initiation gap with 1.0 J or less energy delivered. The former failure is probably due to high arc current, the latter failure is probably due to the small arc movement.

For parallel railplugs, the most common failure mode is the sparkover of ceramic surfaces as shown by Figure 3.7. Once sparkover takes place, the engine begins to misfire and an oscilloscope showed that no follow-on occurred.

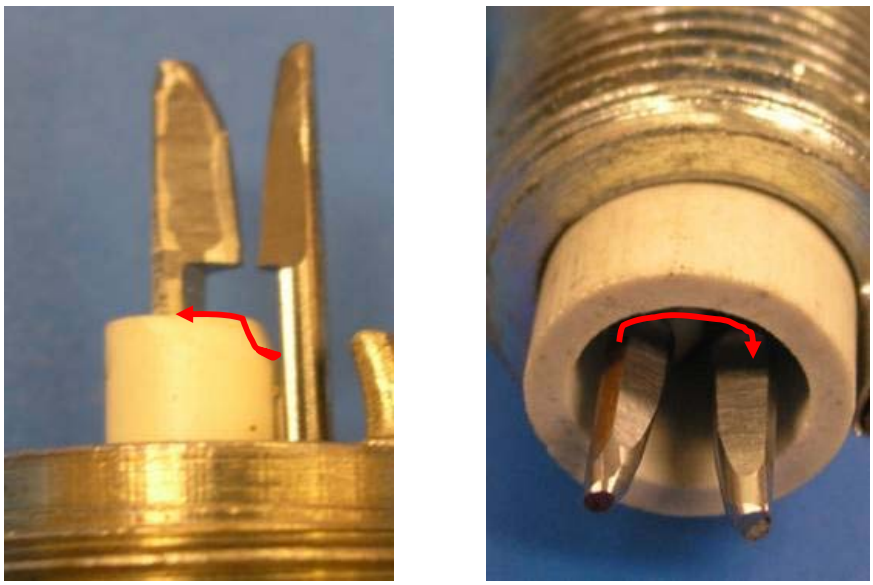

Figure 3.7. Sparkover ceramic surfaces.

Meek and Craggs [53] report that sparkover insulating surfaces significantly decreases breakdown voltage. The breakdown voltage for the sparkover across the surface of a 1 mm tall glass or porcelain cylinder between two metal plates in air and at atmospheric conditions is about 25 kV, whereas the breakdown voltage of a uniform field in the absence of the cylinder is about 45 kV. However, they didn't report the characteristics of arc and glow under these conditions. Moreover, an increase in humidity of the air is observed to cause a marked reduction in the sparkover breakdown voltage. For engine tests, once the railplugs become worn, the initiation gap becomes large due to erosion and the electrode surface becomes oxidized. This leads to an increase the normal breakdown voltage making sparkover across the ceramic more likely. Sparkover also occurs due to the high humidity inside the cylinder, especially for a natural gas engine which has high water production. So the discharge process is just a weak spark because there is no follow-on current. It is not yet clear why no follow-on discharge takes place. Because the breakdown voltage of the sparkover is low and probably the overall effective discharge energy is low, the engine, thus, begins to misfire, especially at very lean conditions.

Preventing sparkover requires a longer distance between the electrodes. It is more effective to insulate the electrodes partially by air as shown in the design examples of the railplugs shown. However, the crevice between the electrode and the insulating material makes electrode heat transfer poor. Good heat transfer is an important design parameter from a durability standpoint as electrode erosion rates increase at higher temperature. These trade-offs were not extensively investigated here.

3.3 Parameter study to improve arc movement

High-speed photography was used to study the effects of railplug parameters on arc movement. High speed images were taken with a Photron APX CMOS Camera. The high speed images were taken at 50,000 frames per second with a shutter speed of 1/87600 seconds/frame. The view area was 128 X 64 pixels on the computer which corresponds to around 68 mm X 17 mm actual scale. Neutral density filters were used to adjust the exposure of the images. The railplug performance parameters of primary interest were the plasma travel distance and velocity. Plasma travel distance was obtained by processing the high-speed images, from which the plasma velocity was derived using the central difference approximation. For this study, the magnet-enhanced railplug shown in Fig. 3.1 was used.

A study was performed to investigate the effect of the circuit inductance on plasma movement. Figure 3.8 shows that the peak discharge current decreases and discharge duration increases as the inductance of the shaping inductor increases (3.8-a). The discharge duration increases from 0.15 ms to 0.85 ms as the inductance increases from 0 to 788 μH, whereas the peak plasma velocity decreases from 70 m/s to 25 m/s (3.8-c). However, the plasma travel distance increases from 5 mm to 11 mm (3.8-b). From expression (3.2), high current means a high Lorentz force and high acceleration, leading to a high peak velocity. On the other hand, plasma movement suffers because of high viscous forces that occur as the velocity increases. So, a relatively longer discharge duration benefits the plasma travel with the same discharge energy.

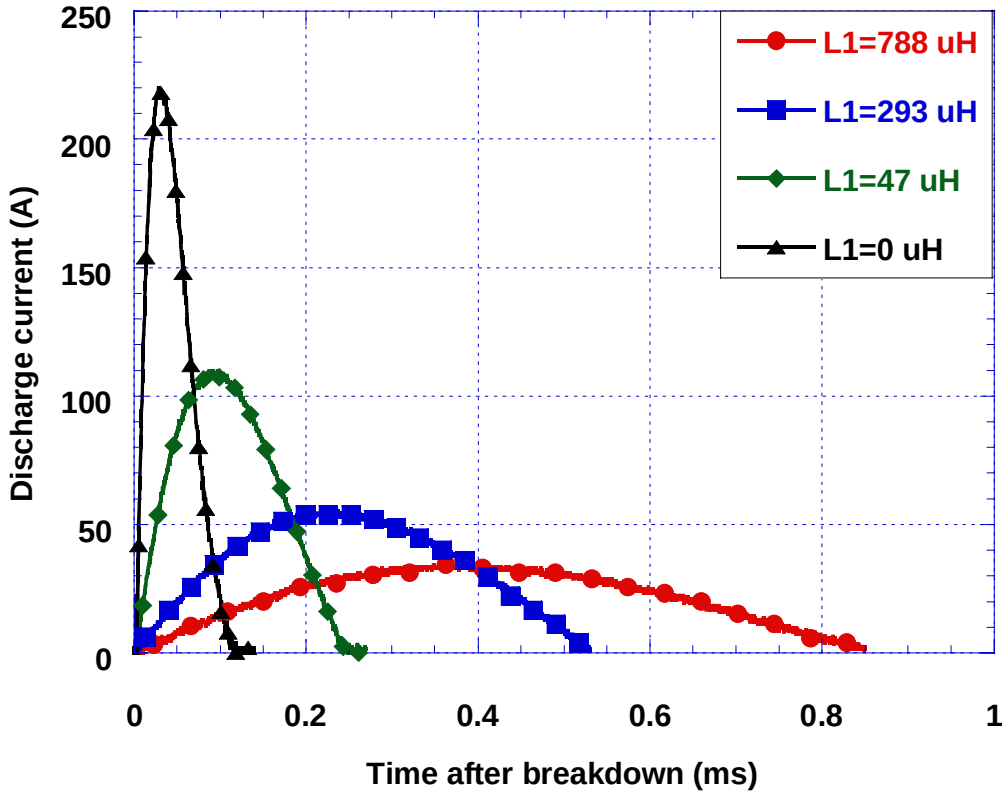

a: Discharge current

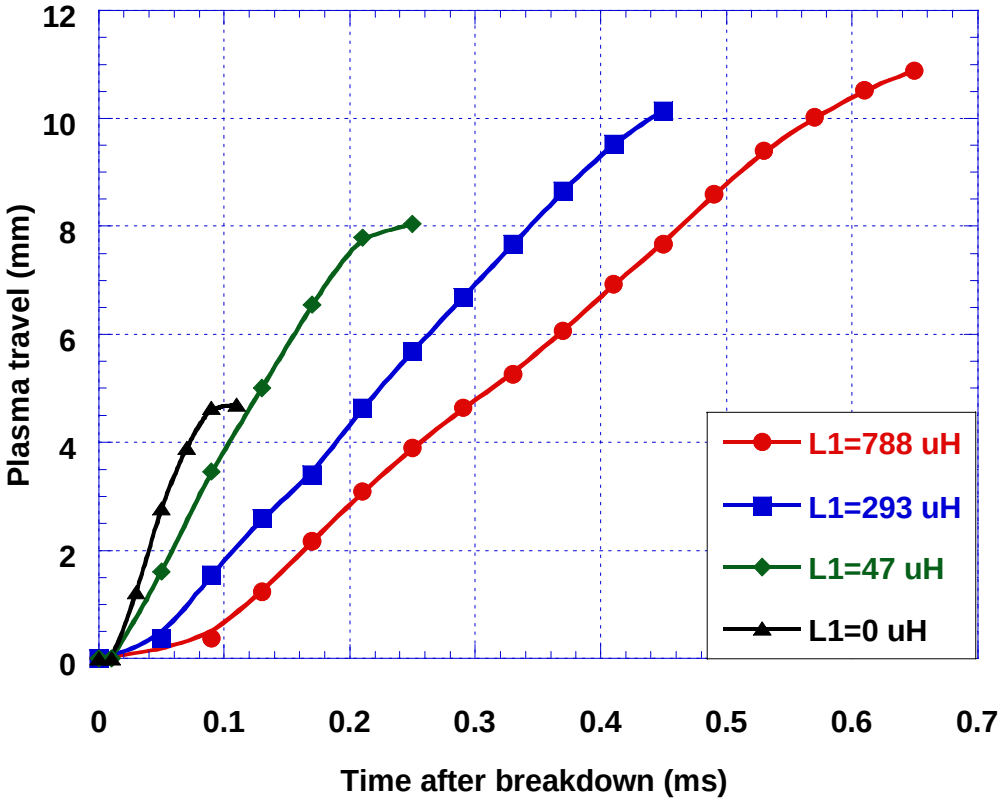

b: Plasma travel distance

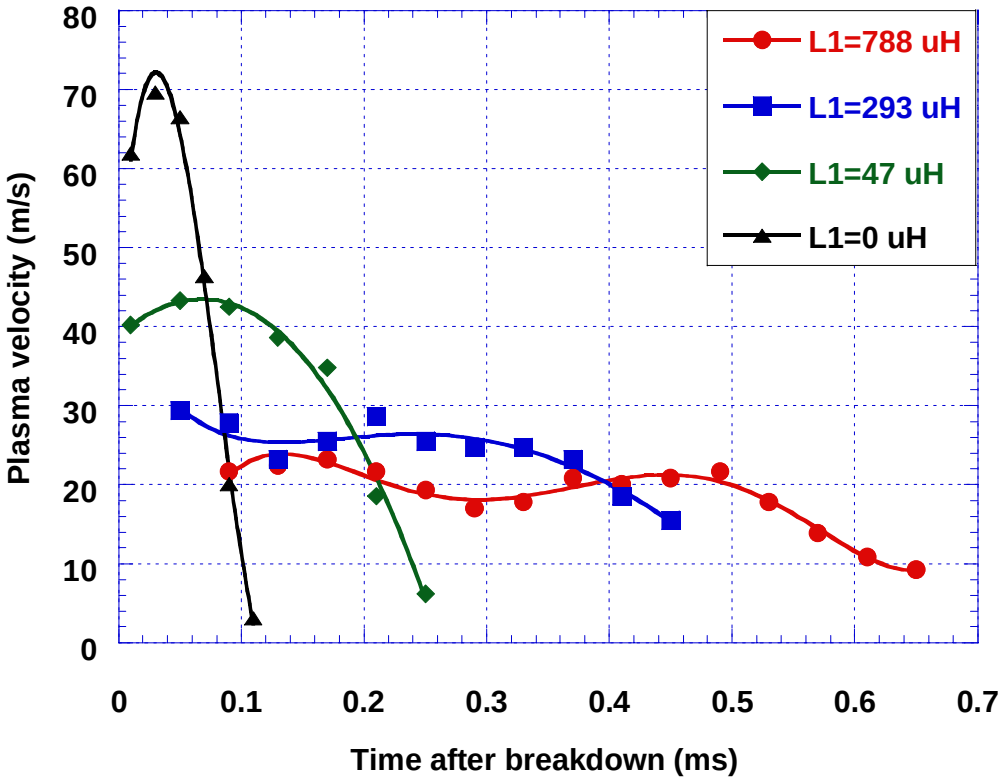

c: Plasma travel velocity

Figure 3.8. Effects of shaping inductor on discharge current, plasma travel distance and plasma travel velocity. Magnet enhanced railplug, delivered energy E_d = 0.7 J/shot.

Railplug theory predicts that as the diameter of the railplug rails decreases the inductance gradient increases, and should thus enhance railplug arc travel. Three different rail diameters were studied to investigate the effect. Figure 3.9 shows the effects of electrode cross-sectional size on plasma travel. As the electrode diameter decreases, plasma velocity increases and the arc moves further. It can be seen from expression (3.3) that the rail inductance is a function of electrode size. A simple calculation shows that the inductance L' increases about

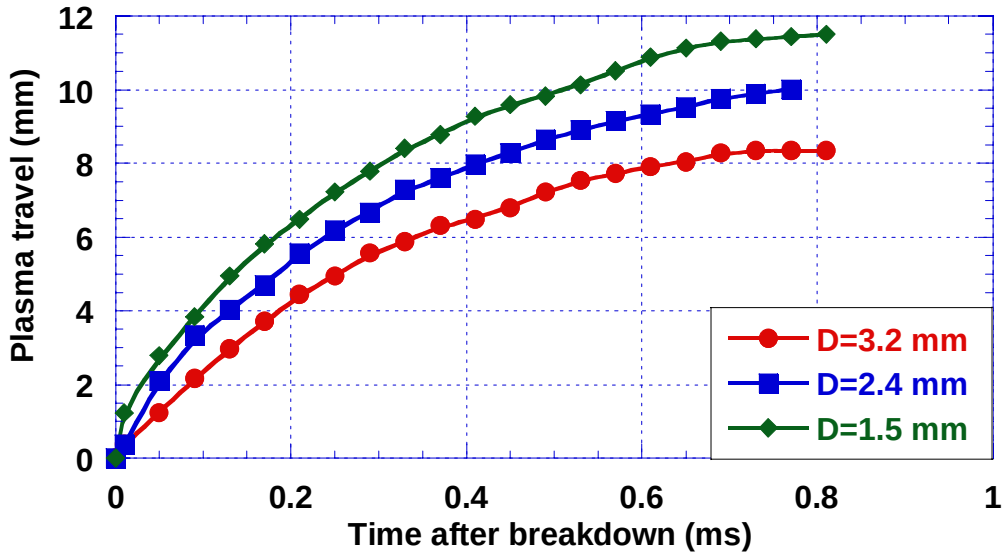

a: Plasma travel distance

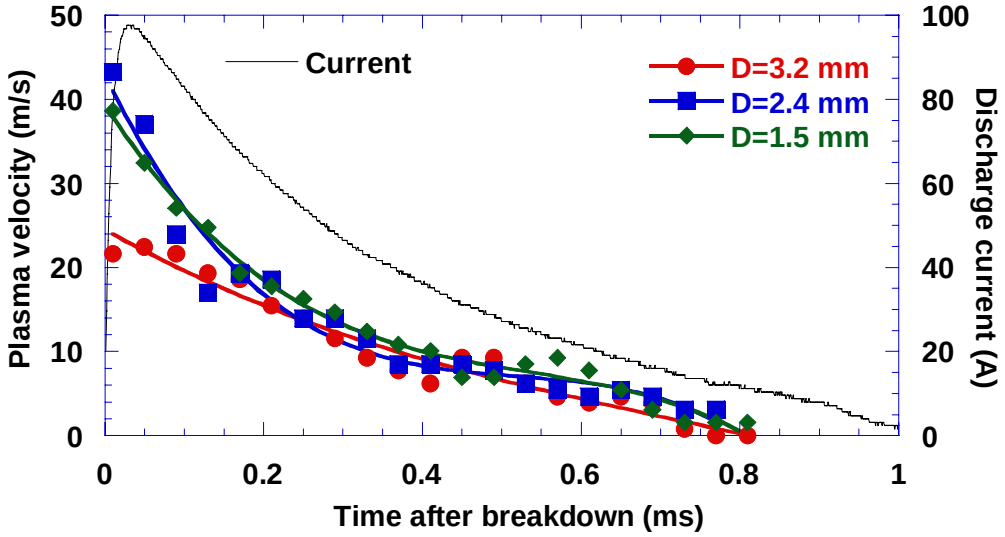

b: Plasma travel velocity and discharge current

Figure 3.9. The effects of electrode diameter on plasma travel distance and velocity. Non-magnet enhanced railplugs, delivered energy E_d = 1.5 J/shot, duration 1 ms.

20 percent as the electrode diameter decreases from 3.2 mm to 1.5 mm if other dimensions remain unchanged. Thinner electrodes also decrease the plasma heat losses, which benefits plasma motion.

As discussed in the prior sections, increasing the local magnetic field strength B can effectively increase the Lorentz force F, resulting in higher arc velocity and a longer plasma travel distance, which are showed in Figure 3.10. The figure compares the plasma travel distances and velocities of two railplugs each having a different strength permanent magnets. The railplugs had the configuration of the magnet-enhanced railplug shown in Fig. 3.1. They were fired with a delivered energy of 0.7 J/shot. The plasma traveled a longer distance for the railplug with the stronger magnet than that for the railplug with the weaker magnet. The railplug with the stronger magnet, had a higher plasma velocity during the early part of the discharge; the velocity, however, was lower after 2 ms. The reason, in this case, was that the plasma reached the electrode tip earlier because of its high velocity and the Lorentz force then decreased dramatically.

The results discussed in this section can be used to optimize railplug designs and improve railplug performance.

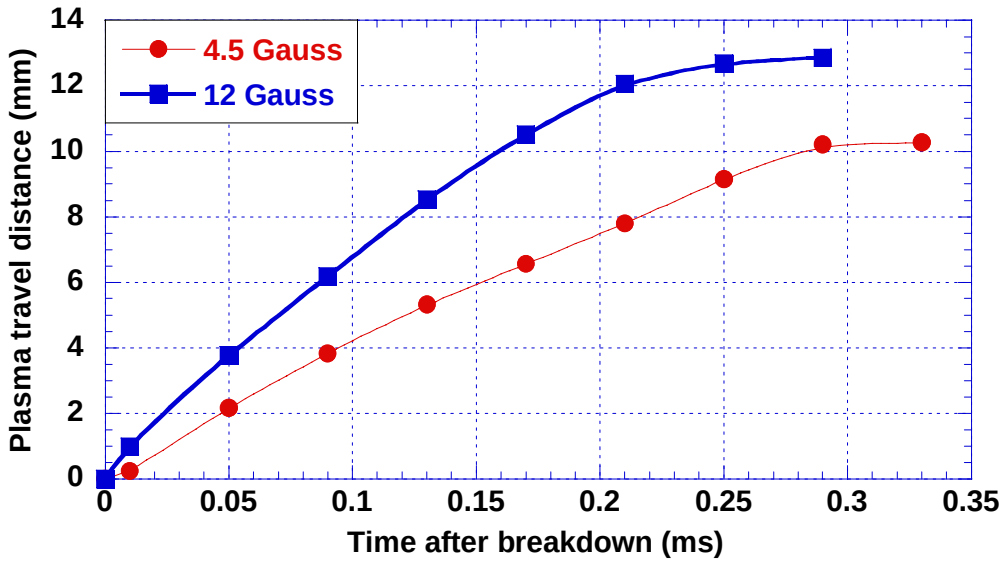

a: Plasma travel distance

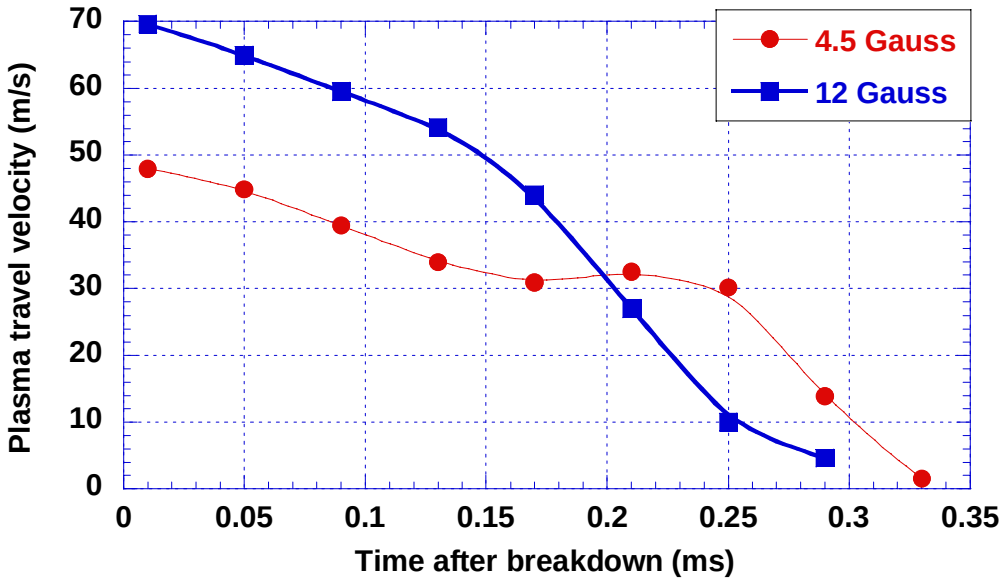

b: Plasma travel velocity

Figure 3.10. Effects of magnetic strength on plasma travel distance and velocity. Delivered energy E_d = 0.7 J/shot, duration 0.5 ms.

Chapter 4.0 Engine Experimental Set-up

This chapter describes the experimental set-up and the equipment that was utilized to perform the engine tests. The overall experimental set-up is represented schematically in Figure 4.1. A brief description is provided for each component in the following discussion, which includes:

- Engine modification to run natural gas;
- Ignition timing control;
- The dynamometer and its controller;
- A combustion analysis system for in-cylinder pressure measurement;
- Ignition noise suppression;
- Engine-out emission measurements.

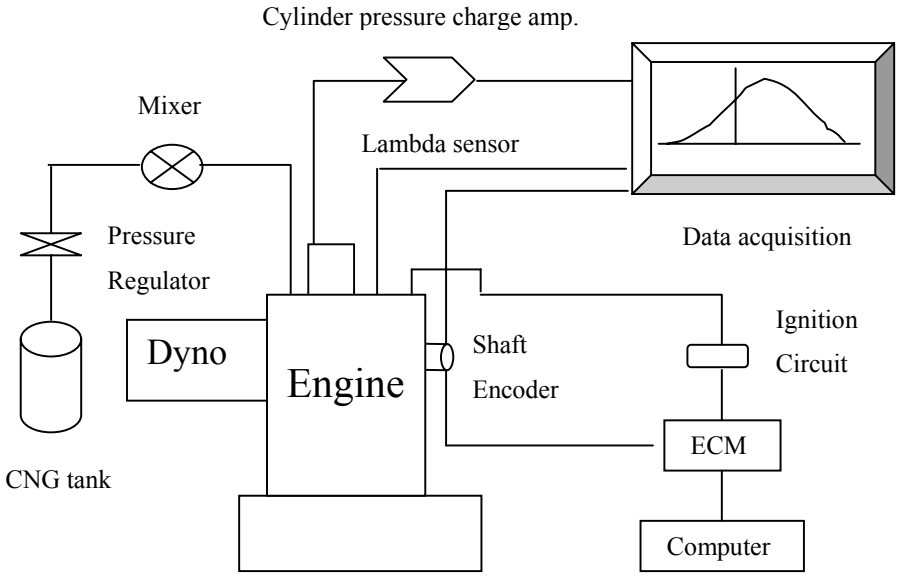

Figure 4.1. Schematic of the engine experimental set-up.

4.1 Engine modification to run natural gas

Table 4 provides the important engine parameters. The engine was a 4-cylinder, 2.2-liter and 2-valve gasoline engine that was modified to operate on natural gas. Natural gas was provided from a 20.6 MPa (3,000 psig) pressure tank (shown in Figure 4.2) through a high-pressure regulator, a low-pressure regulator, and a mixer as shown in Figure 4.3. Cylinder 4 was instrumented to assess the performance of railplugs and spark plugs (shown in Figure 4.4). The original engine used 14 mm spark plugs, so the spark plug hole for this cylinder was machined to accept 18 mm igniters due to the present interest in large bore engines.

Table 4. Engine parameters.

No. of cylinders	4
Displacement	2.2 liter
Bore	89 mm
Stroke	88 mm
Compression ratio	8.85
Test speed	1200 rpm

Only cylinder 4 was run by railplug and other 3 cylinders were still run by conventional spark plugs. In order to test the lean stability limit of the railplug cylinder, it was necessary to provide more fuel for the 3 cylinders run by spark plugs at very lean mixtures. A needle valve was used to manually control the propane flow rate to the 3 cylinders. For this purpose, two Horiba Universal Exhaust Gas Oxygen (UEGO) sensors were used. One was connected to the

manifold of cylinder 4 to measure the air/fuel ratio of cylinder 4. The other one was used to monitor the overall air/fuel ratio as a feedback for the needle valve control.

Figure 4.2. High pressure natural gas tank.

Large-bore natural gas engines use a 24 V power supply to charge the ignition coils. So two 12 V batteries were connected in series in this set-up to provide power for the spark discharge.

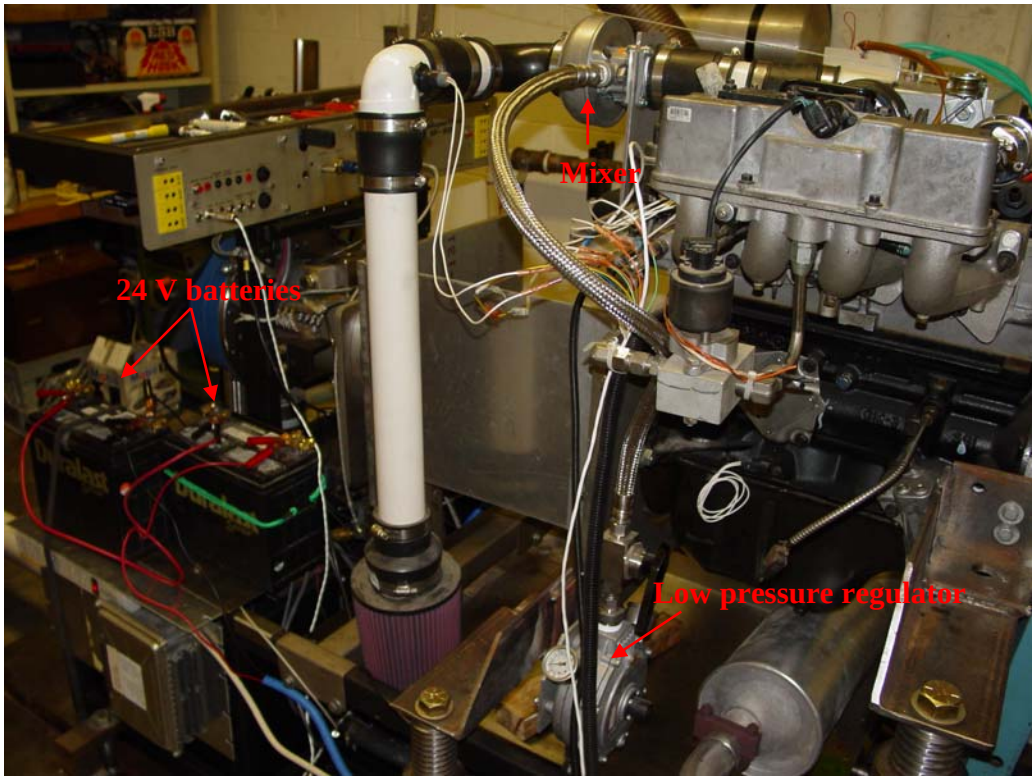

Figure 4.3. The modified engine with natural gas fueling system.

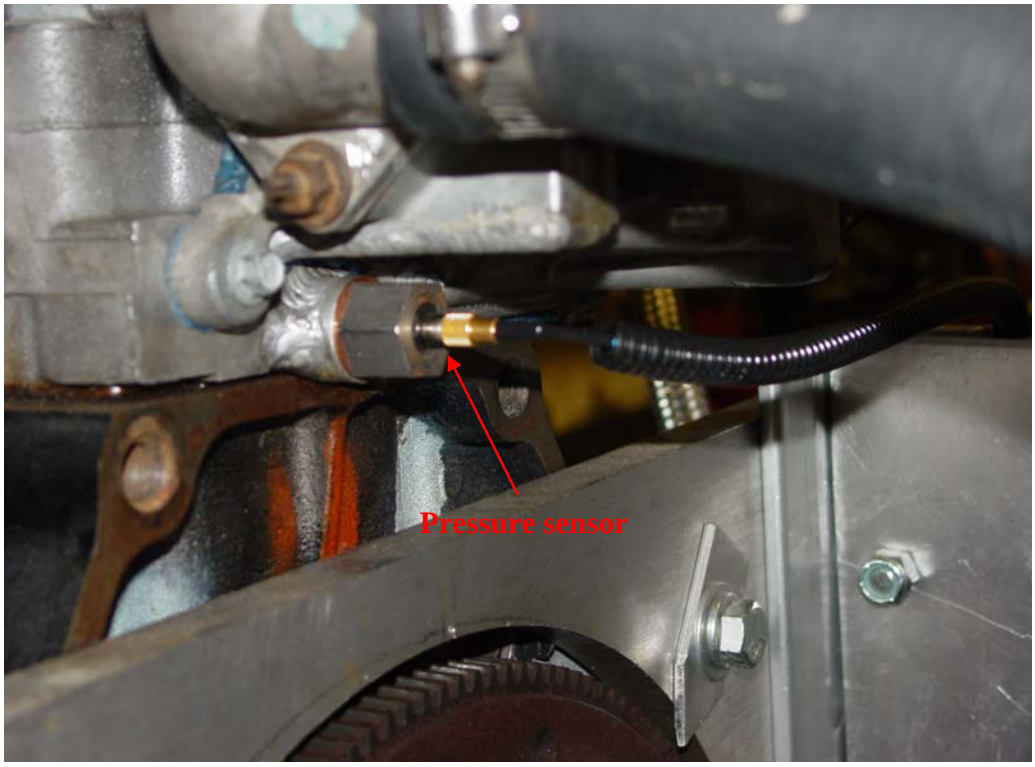

Figure 4.4. Pressure sensor installed on cylinder 4.

4.2 Ignition timing control

The ignition timing was controlled via a MoTeC M4 programmable engine controller shown in Figure 4.5. The MoTeC ECU is a programmable engine controller and can control ignition timing, fuel injection timing and injection pulse width. The main inputs are the necessary timing information such as engine crank angle and cam shaft position captured by encoder signals. A computer was connected to the ECU to adjust the ignition timing via the ignition main table adjustment. The engine load can be derived from either the throttle position sensor or MAP (Manifold Air Pressure) sensor. The throttle position

sensor was used to indicate the engine load and the MAP sensor as a reference in this dissertation. The air temperature sensor was mainly used to correct for air density change due to air temperature variation. The engine temperature sensor was used for cold start enrichment. The Motec ECU automatically adjusted the ignition dwell time depending on the battery voltage, e.g., lower battery voltage resulted in a longer dwell time, to fully charge the ignition coils. The output of the ECU is the ignition signal to the ignition modules. Four Denso ignition coils were used. The Denso coil has a built-in ignition module.

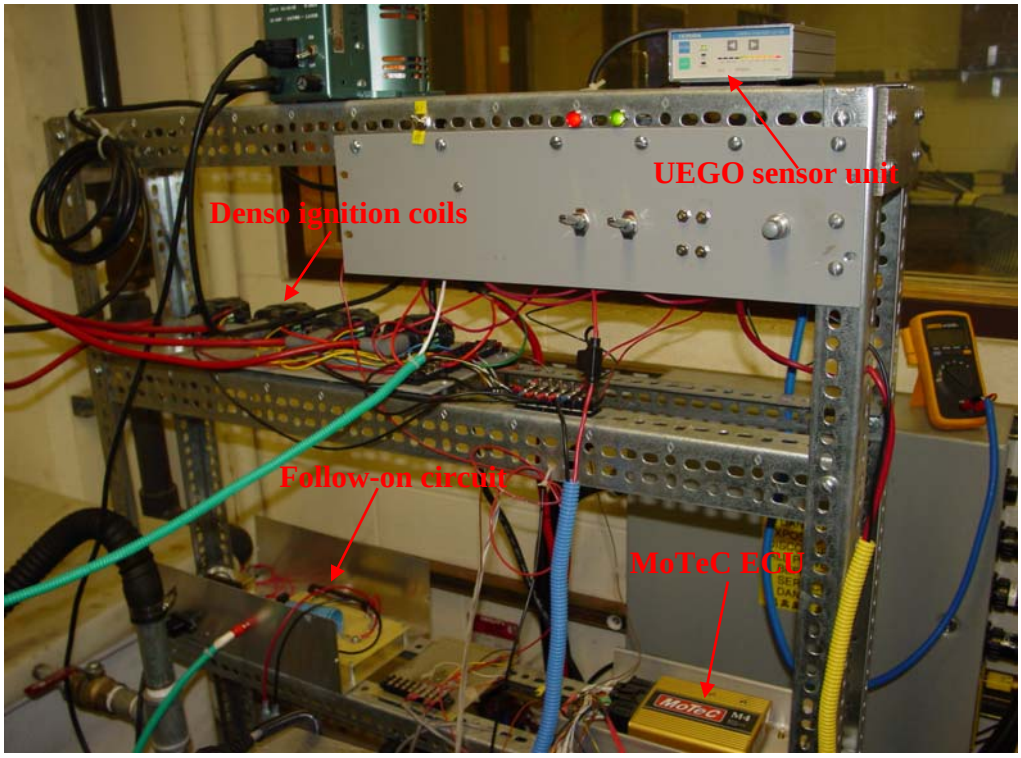

Figure 4.5. ECU and ignition circuit.

4.3 The dynamometer and its controller

The engine was connected to a Super Flow SF-901 water-brake dynamometer as shown in Figure 4.6. It is a relatively small dynamometer and it is hard to effectively absorb the engine power at Wide Open Throttle (WOT) if the engine speed is below 1000 rpm. Figure 4.7 shows the dynamometer controller. During tests, after the engine had warmed up, the Super Flow "load control" switch was changed from Manual to Servo. Then the rotary dial knob to its right was turned to select and set the engine speed (i.e., 1200 rpm). This maintained the engine at the set speed. Water brake dynos, however, cannot hold the speed precisely constant, so this knob required fine-tuning occasionally to maintain the set speed.

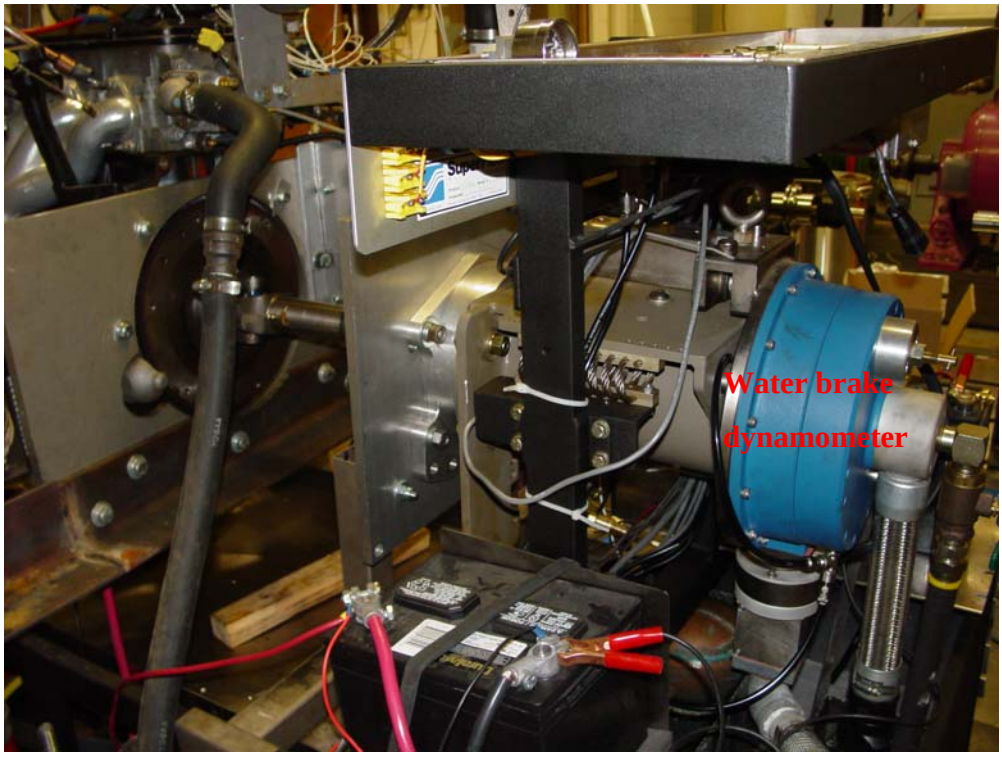

Figure 4.6. Water brake dynamometer.

4.4 In-cylinder pressure measurement and data acquisition

A Kistler quartz piezoelectric pressure transducer (model 603B1) was installed in cylinder 4 to acquire cylinder pressure data. A Kistler model 5010 charge amplifier was used to condition and amplify the pressure signal. Pressure transducer signal drift was compensated for in software by referencing ("pegging") to the known intake manifold pressure at BDC near the end of the intake process.

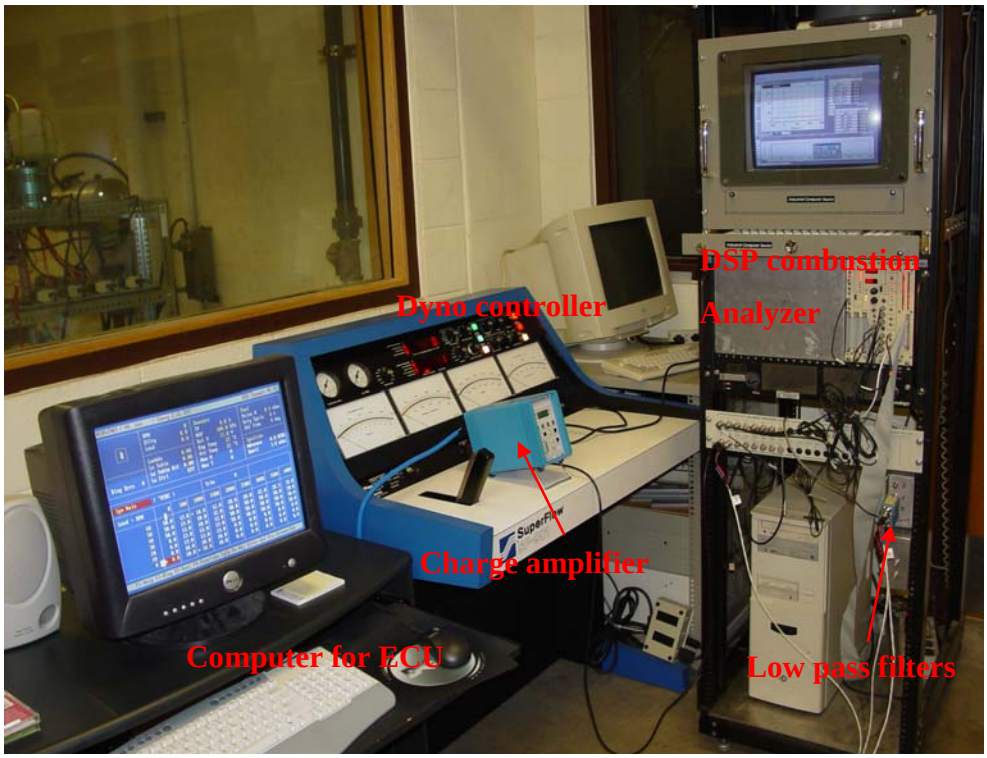

Figure 4.7. Dynamometer controller and DSP combustion analyzer.

The cylinder pressure data were acquired using a DSP Technology combustion event analyzer with DSPT model 4325 real time processor. The ACAP software needed the in-cylinder pressure signal from the charge amplifier, the encoder signals for crank angle degree and top dead center position and finally the intake manifold pressure, which was used as a reference pressure. The in-cylinder pressure was set, at bottom dead center of intake, to be equal to the intake manifold pressure at that instant. This data acquisition system allowed automatic determination of the indicated mean effective pressure (IMEP), location (crank angle) of peak pressure (LPP), mass burned fraction profiles, percent misfiring cycles, and coefficient of variability (the standard deviation normalized by the mean) of the IMEP (COV of IMEP). The COV of IMEP is routinely used as a measure of cyclic variability or combustion stability. All results were averaged over 500 cycles. The COV of IMEP was calculated as the ratio of the standard deviation of the IMEP divided by the mean IMEP as represented by Equation 4.1

$$COV(IMEP) = \frac{\sigma(IMEP)}{\overline{IMEP}} \times 100 \tag{4.1}$$

For each experiment, the air/fuel ratio was determined from the exhaust gas using a Horiba wide-range lambda sensor (Model LD-700). The analog reading was corrected to natural gas because the instrument is calibrated for gasoline with C/H=1.85 and O/C=0. The output from this instrument was automatically logged by the DSP data acquisition system and averages were taken over the same 500 cycles as were the other data.

4.5 Ignition noise suppression

It is well known that ignition can produce radio frequency noise because of the super fast rising voltage and current. A strong electromagnetic field is derived from the big current gradient. RF noise causes engine ECUs to run erratically if they are not shielded, and it causes interference with radio equipment and other communications gear. An effective way to lower RF noise is to use resistive spark plug wires and resistive spark plugs. Unfortunately, a railplug ignition system cannot use either resistive wires or resistive railplugs because of the high current needed to cause plasma movement. In addition, RF noise can prevent the data acquisition systems, such as the DSP and charge amplifier used in this study, from working normally. So approaches have to be found to effectively reduce RF induced ignition noise.

Most unwanted signals can be suppressed by shielding the actual source [66-68]. Ignition noise appears as high frequency spikes (~100 MHz). The high frequency signals can be dissipated by keeping reflections on the inside surface of the shielding materials. The shielding material does not need to be thick because high frequency signals cannot have weak penetration. However, care must be taken to eliminate gaps in the shielding because ignition noise has a very short wave length.

Railplug wire was shielded with wire braid as shown by Figure 4.8. The end closest to the spark plug end was grounded to the metal plug cover. Actually, both wire braid and a copper tube were used to shield the high tension wire because it was more effective. An aluminum box was used to fit over the ignition coil. This box fit tightly to the engine block and was grounded there. All wires

emerged through rubber grommets set in the box. The wire braid was grounded inside the cover.

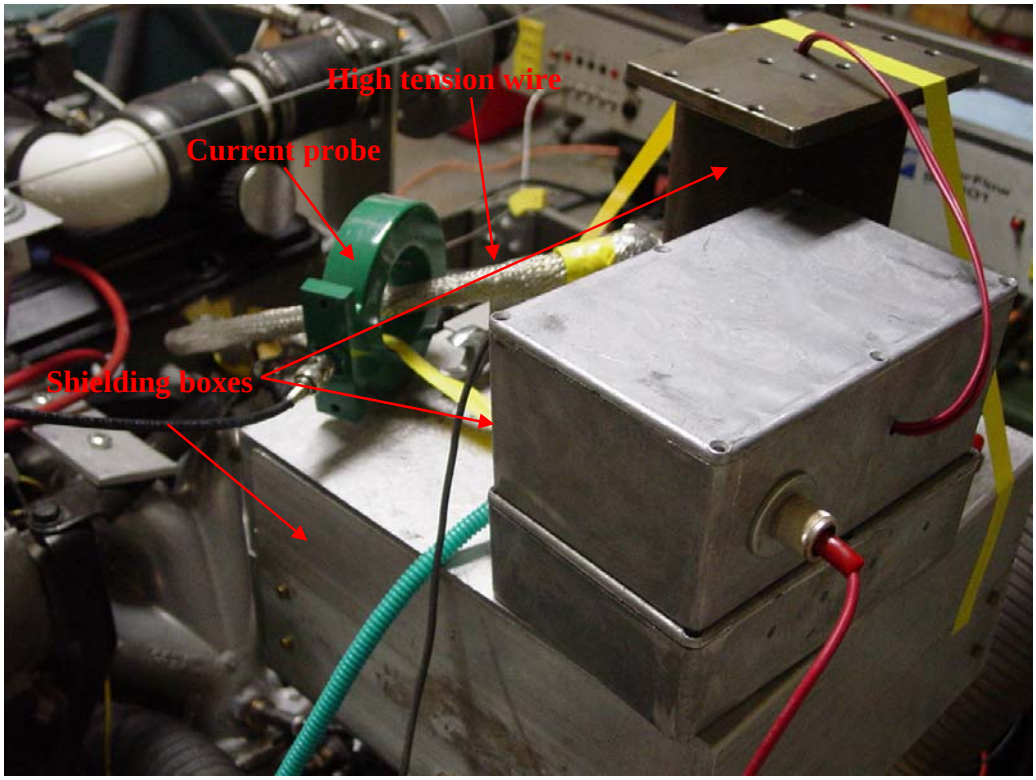

Figure 4.8. Railplug circuit and high tension wire shielding.

Low pass filters (LPF) were used for encoder signals just before the DSP connections to remove high frequency spikes. Those LPFs were designed by the author with C=104 pF and resistor less than 1 Ω.

4.6 **Engine-out emission measurements**

Engine-out emissions, such as NO_x, HC and CO, were measured from the engine-out raw exhausts (non-diluted). A non-sampling type Horiba MEXA-720 fast-response analyzer, as shown in Figure 4.9, was used to measure NO_x emission. A Horiba MEXA 554JU analyzer was used to measure HCs, CO, CO_2 and O_2. O_2 could also be measured from the wide range lambda sensor in addition to the 554JU.

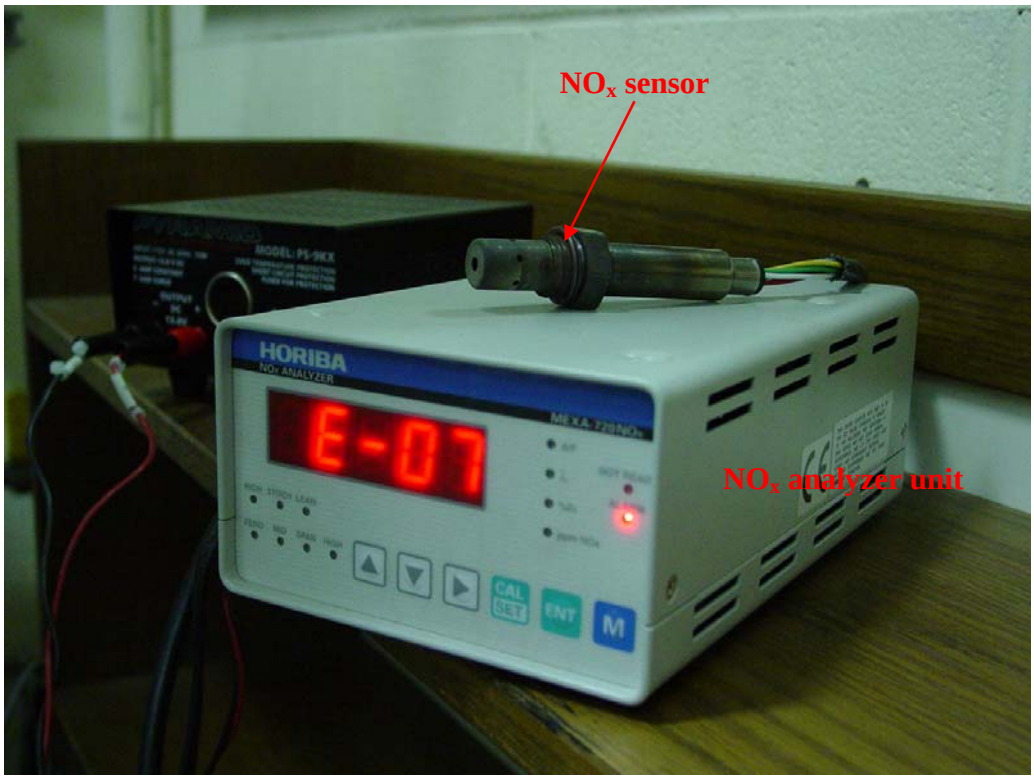

Figure 4.9. NO_x analyzer.

A Meriam Instrument Laminar Flow meter (Model 50MR2-2) was used to measure engine inlet air flow rate. So the fuel flow rate could be calculated from the Lambda value.

Chapter 5.0 Engine Tests and Results

It has been known for some decades that spark ignition internal combustion engines that apparently operate under steady-state conditions, do not maintain perfectly stable operation. A comparison between one cycle to another reveals random variations in the in-cylinder peak and Indicated Mean Effective Pressures (IMEP). This phenomenon is particularly noticeable in lean and highly diluted mixture. Previous studies have shown that if cyclic variation could have been eliminated, there would be a 10% increase in the power output for the same fuel consumption [69]. The cyclic variation also results in high levels of variation in the engine speed that is interpreted as poor drivability.

The cyclic variation can be quantified by the coefficient of variance (which from now on will be called the COV), which is usually attributed to the result of random fluctuations in equivalence ratio and flow field due to the turbulent nature of the flow in the cylinder. During early ignition kernel formation and development, any random convection of the spark kernel away from the electrodes or random heat transfer from the burning kernel to the spark electrodes can result in large variations of the entire combustion. This can be especially severe for lean burn engines due to the long ignition delay and slow flame propagation [69-72]. So cyclic variation (COV) has been widely used to evaluate igniter performance.

Base on Makekunas [73] and Heywood [74], COV can be characterized by the variations in different types of parameters. These parameters may be grouped into four categories: pressure related parameters, combustion related parameters,

flame front related parameters, and exhaust gas related parameters. From a practical point of view, the impact of the COV on the combustion process, and on vehicle drivability, its fuel consumption and its pollution, is of most interest. A measure of the COV, which may be obtained from pressure data, is the coefficient of variance in indicated mean effective pressure, which is usually expressed as COV of IMEP.

All the engine data in this dissertation were acquired at 1200 rpm and wide open throttle (WOT). The fuel was natural gas. The standard baseline railplug used to acquire most of the data presented was the magnet-enhanced railplug (Fig. 3.1) with the 4.5 Gauss magnet. The ignition timing was set to MBT (minimum advance for best torque) since the best combustion stability (minimum COV of IMEP) generally takes place at MBT spark timing [69]. This is also confirmed by Figure 5.1. The engine was run with a spark plug. The lowest COV of IMEP took place at the ignition timing at which IMEP was highest for a given mixture strength.

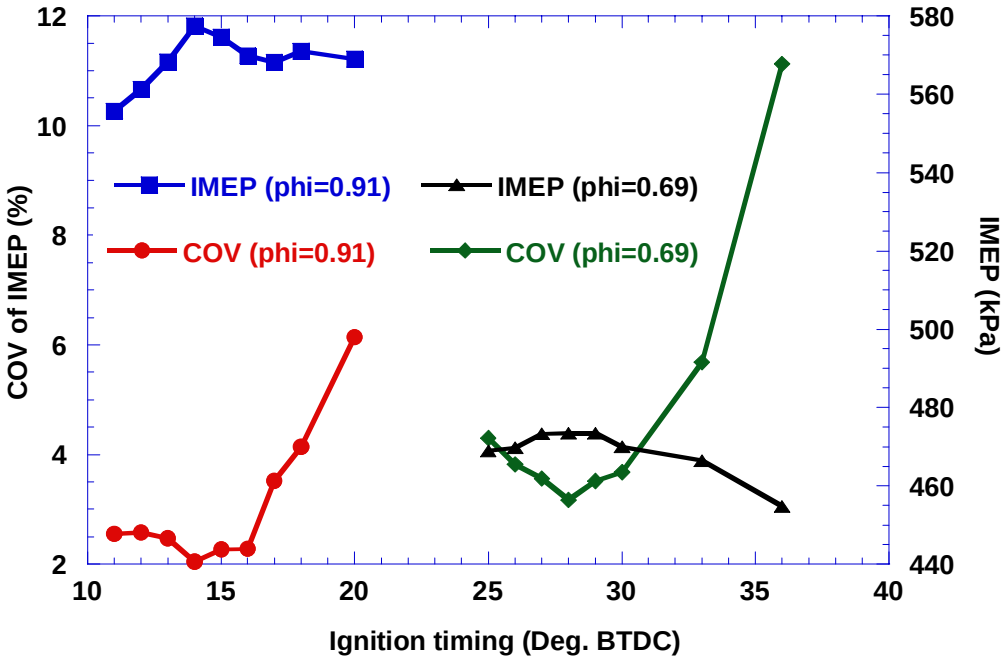

Figure 5.1. Effects of ignition timing on IMEP and COV of IMEP for different equivalence ratios, spark plug.

According to the definition of MBT, we can adjust the spark timing to obtain MBT by monitoring the torque value shown on the dynamometer display. This method, however, could not be used in this dissertation for the following reasons: first, only cylinder 4 was run with a railplug and other 3 cylinders were run with spark plugs; second, at very lean conditions, cylinder 4 ran different strength mixtures from the other 3 cylinders as described in the previous chapter; Third, this is a 1000 hp dyno, so we are at the low end of its range and the readout for torque is not very precise. Since we are just interested in cylinder 4 and it was instrumented to test its performance, we can observe the IMEP on the DSP to determine MBT. The principle behind this method is shown by the following formulas [75],

$$bp = \tau N / 9549.3 \tag{5.1}$$

$$imep = \frac{60000 ip \bullet x}{DN} = \frac{60000 bp \bullet x}{\eta_m DN} \tag{5.2}$$

Where bp is brake power, τ is torque, N is engine speed, and ip is indicating power. From expressions 5.1 and 5.2, the following expression can be get

$$imep = \frac{6.28 \tau x}{\eta_m D} \tag{5.3}$$

Where τ is torque, x is 2 for a 4-stroke piston engine, η_m is engine mechanical efficiency and D is engine displacement. Expression 5.3 shows that IMEP is proportional to engine torque.

Another widely used method to determine MBT is to observe the location of peak pressure (LPP). MBT timing was assumed to take occur at 15 to 17 degrees after TDC for gasoline engines. It should be noted that this method is not always accurate, especially for natural gas engines. Figure 5.2 shows that LPP is almost a linear function of the equivalence ratio. As mixtures get leaner, the location of peak pressure takes place earlier.

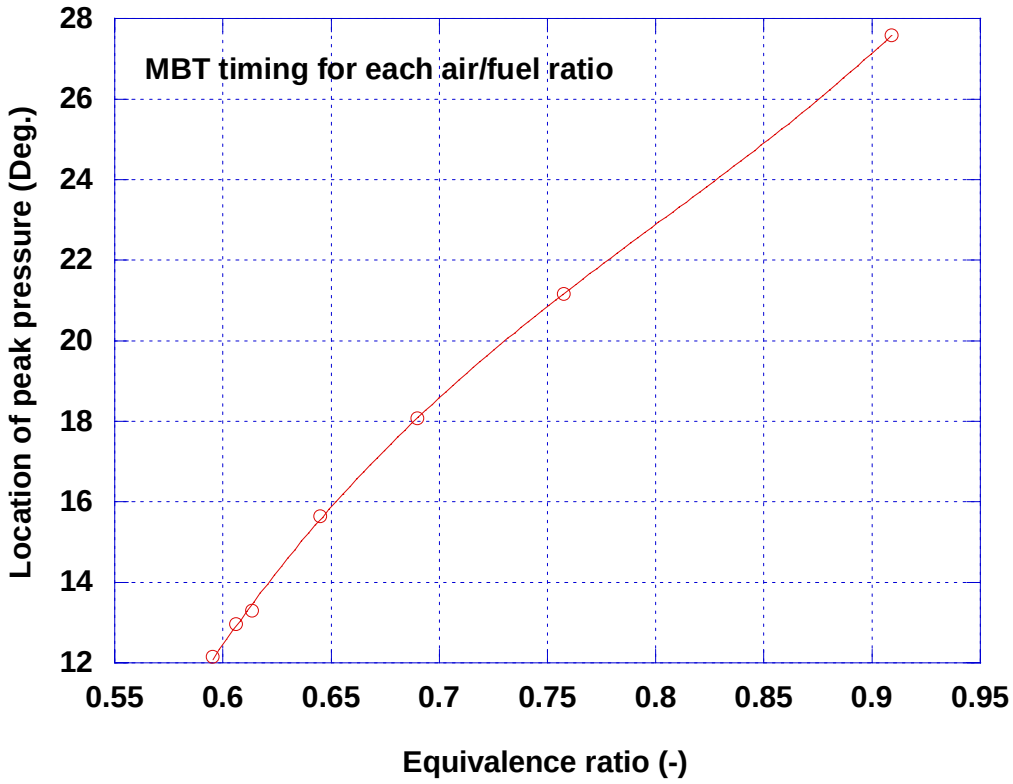

Figure 5.2. The effects of equivalence ratio on location of peak pressure, spark plug.

5.1 Comparison of the three ignition systems

Engine performance using the three igniters is compared and discussed in this section. The three igniters are a spark plug with an inductive circuit, a spark plug with a CDI circuit, and a parallel railplug.

Figure 5.3 shows the effects of the equivalence ratio on the COV of IMEP for three igniters: a conventional spark plug (Champion RF14LC) using both a

conventional inductive circuit with a Denso ignition coil and CDI circuit, and the magnet-enhanced parallel railplug. For equivalence ratios down to ~0.7, as usual the combustion stability is not affected by the type of igniter. The COV of IMEP

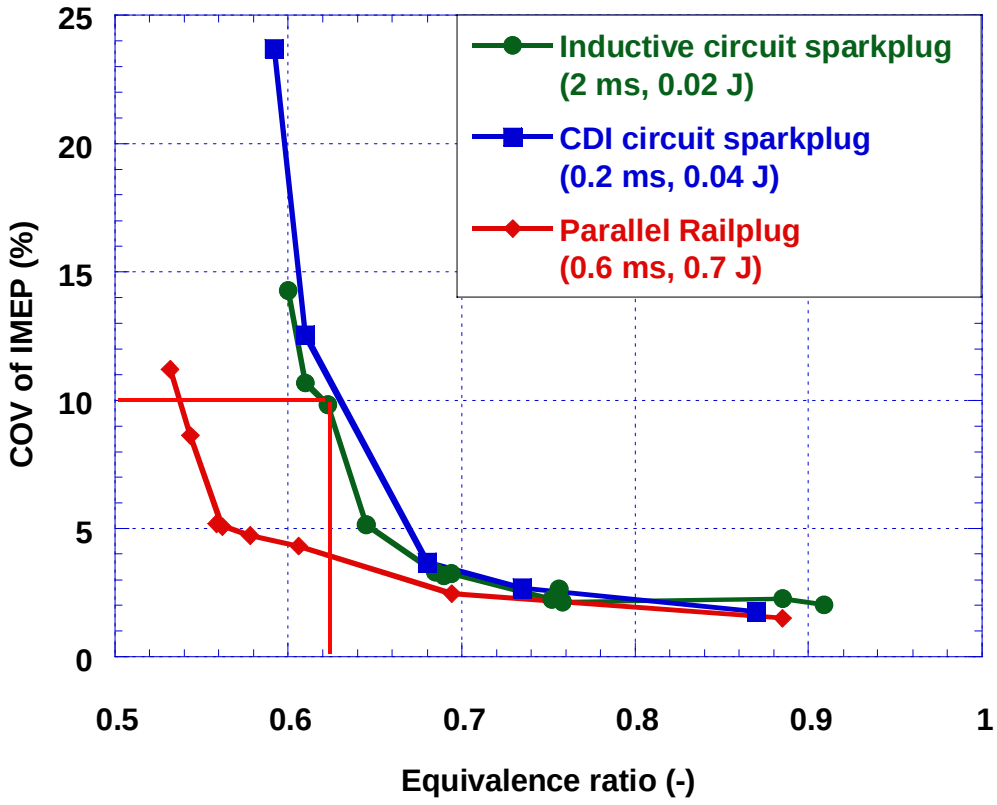

Figure 5.3. Comparison of engine performance using three igniters.

is so good (~2%) that little can be done to improve it. As the mixture gets leaner, the parallel railplug shows superior performance compared to spark plugs. The Lean Stability Limit (LSL) is defined as the equivalence ratio value at which the COV of IMEP reaches 10% as shown by Figure 5.3. The LSL of the inductive spark plug was $\varphi = 0.62$, whereas the parallel railplug extended the LSL to $\varphi = 0.535$. For light-duty SI engines, the baseline LSL for spark plugs is typical. As

one example, Edwards and coworkers [46] tested two spark plugs in a CFR engine operating on propane. At test conditions of 1000 rpm, 8:1 CR, MBT timing, and WOT, they found that the LSL of the Champion D-16 spark plug was $\varphi = 0.69$ while the Motorcraft λGP22 extended electrode spark plug (The discharge gap was 1.27 mm and the penetration of the electrodes into the mixtures 9.14 mm) produced a Lean Stability Limit of $\varphi = 0.64$. Similarly, using certification gasoline Zheng and coworkers [44] found a LSL of $\varphi = 0.66$ at 1300 rpm and 390 kPa IMEP using a Champion N12YC with a 0.9 mm (0.035") gap; they found a LSL of $\varphi = 0.62$ with a 1.8 mm (0.070") gap.

In order to check the reproducibility of the railplugs, four sets of tests were run on different days for the same parallel railplug. The results of reproducibility tests are shown in Figure 5.4. It can be seen that the results are quite reproducible.

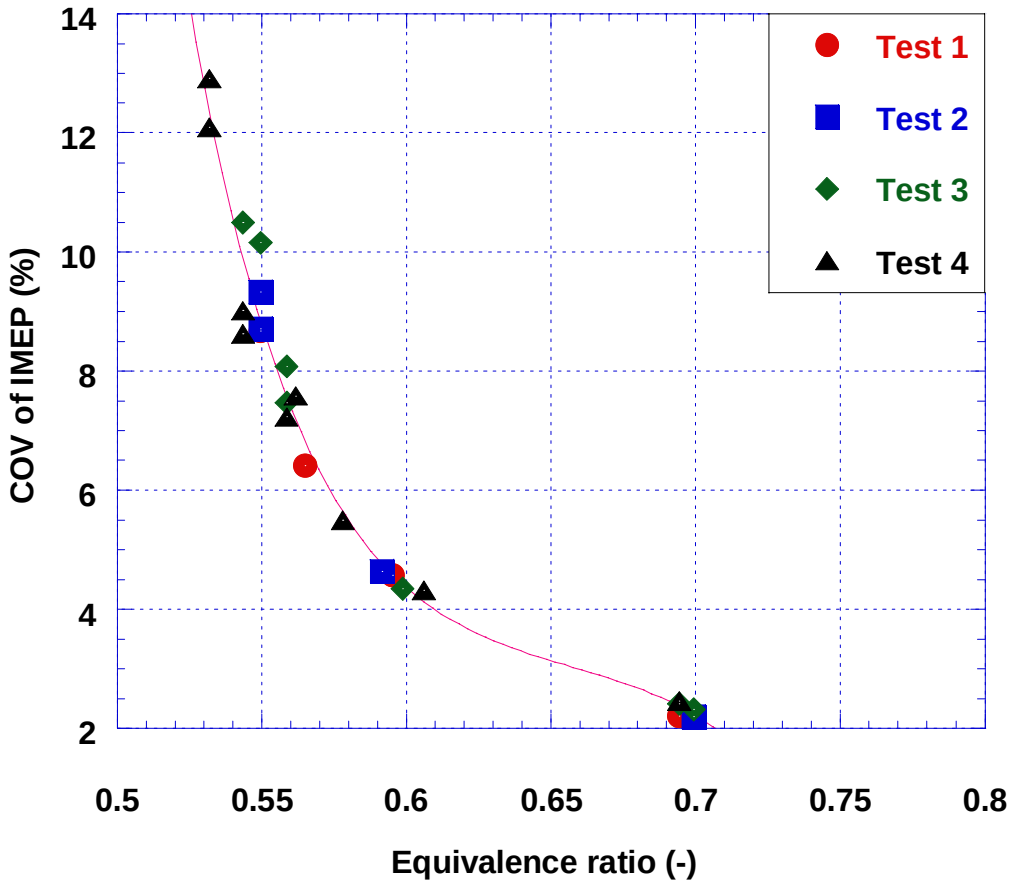

Figure 5.4. Railplug reproducibility tests.

Figure 5.5 provides the mass fraction burned information for two mixture strengths, φ=0.69 and φ=0.61, respectively, which is a histogram depicting three combustion phases. The three phases are: kernel formation (0-2% burned), early flame growth (0-10% burned), and fully developed flame propagation (10-90% burned). The duration of combustion is normally defined as the crank angle interval for 0-90% burned. Compared to the inductive spark plug, the CDI spark plug slightly decreased the duration of kernel formation and the 0-10% mass burned duration, had no effect on the duration of combustion. As described in

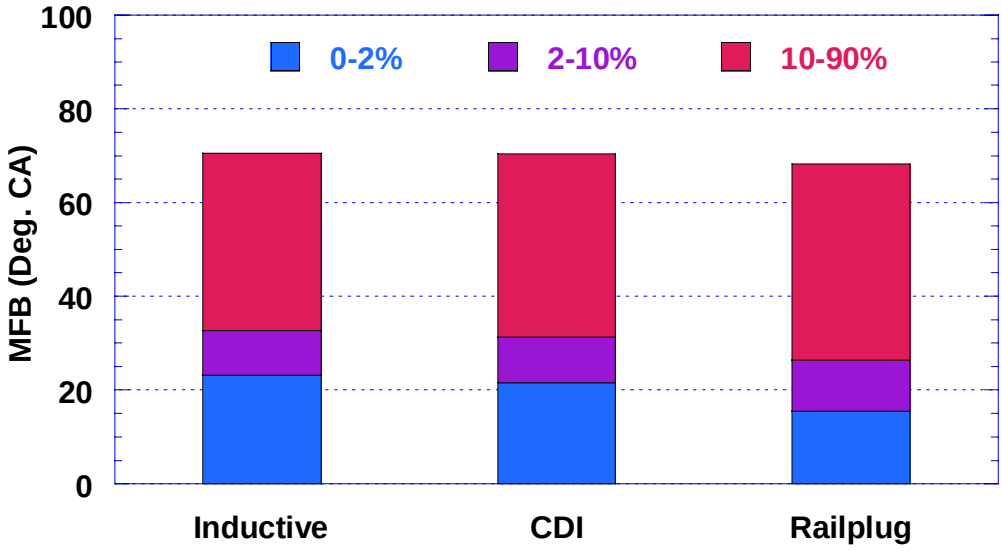

a: φ = 0.69

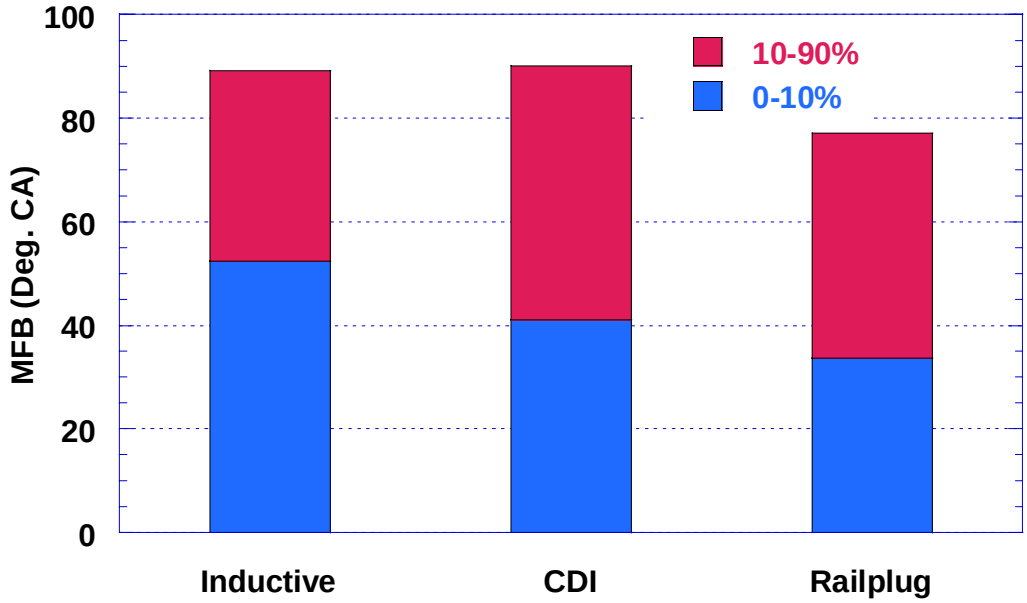

b: φ = 0.61

Figure 5.5. Comparison of mass burning rates of three igniters for two mixture strengths.

prior chapters, a railplug has a very fast plasma movement. So it generates a relatively large mass of plasma since the arc sweeps down the rails, ionizing essentially all of the gas in its path. The fast plasma movement also yields fast turbulent flame propagation. As shown in Figure 5.5, the railplug greatly decreases the duration of kernel formation, 0-10% mass burned duration and the duration of combustion. This trend becomes more obvious as mixtures become leaner. These trends are the result of the faster cylinder pressure rise during combustion for the railplug, as shown in Figure 5.6.

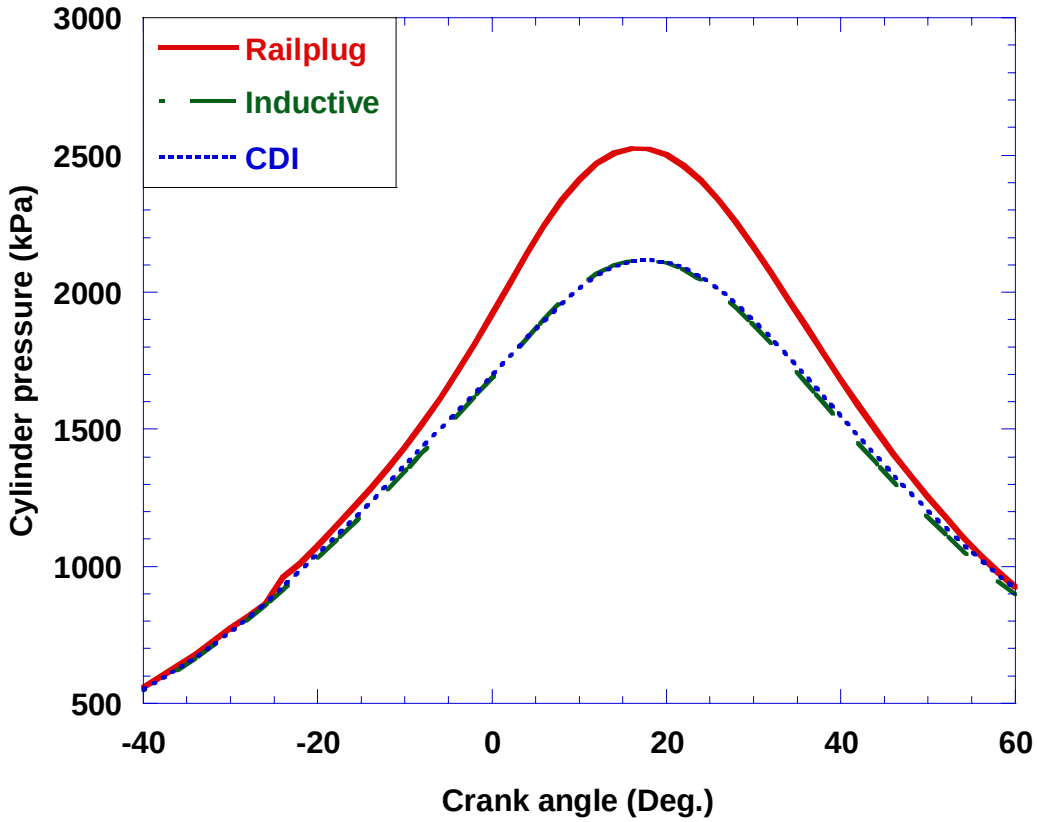

Figure 5.6. Comparison of the average cylinder pressure histories for the three igniters, φ = 0.61.

Figure 5.7 shows that MBT timing can be significantly retarded for railplugs compared to spark plugs since the engine has faster burning rates and shorter combustion duration with railplugs.

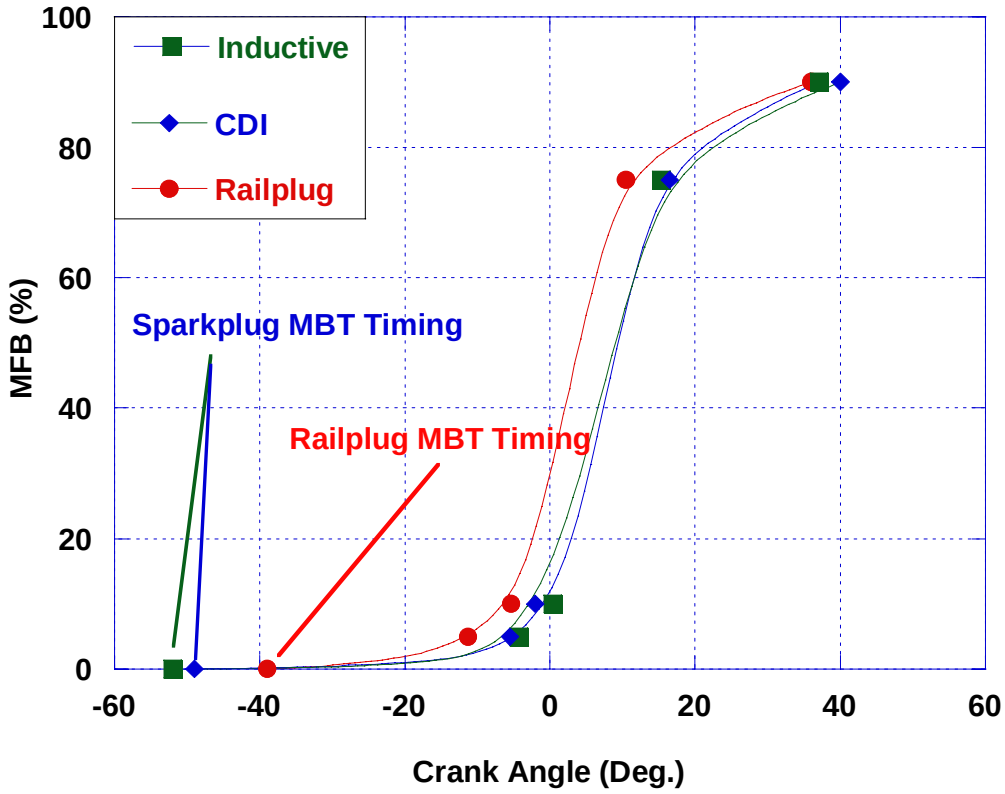

Figure 5.7. Comparison of the MBT timing of the three igniters, φ = 0.61.

Let's go back to Figure 5.3 before we move on to the next topic. Figure 5.3 shows that the CDI spark plug doesn't have as good performance as the inductive spark plug. The CDI spark plug, however, has higher ignition energy than the inductive spark plug, actually, almost double the ignition energy, as discussed in Chapter 2. On the other hand, the CDI spark plug has very short spark duration (~1/10 as long as the inductive spark plug). Besides ignition

energy, spark duration might affect igniter performance also, which will be discussed in the next section.

5.2 Effects of spark duration on igniter performance

Figure 5.8-a shows the effects of the equivalence ratio, ignition energy, and spark duration on the COV of IMEP for a spark plug. A conventional spark plug (Champion RF14LC) with a 1.0 mm (0.040'') gap was tested with both a conventional inductive ignition system and with the higher energy from the railplug circuit. In order to study the effects of spark duration on engine performance, a conventional spark plug with the railplug circuit was tested because it is easy to change the spark duration. The spark plug, however, cannot survive the high ignition energy provided by the railplug circuit. So it was necessary to change the spark plug frequently. The LSL of the spark plug with a conventional ignition system was $\varphi = 0.62$, whereas the spark plug with delivered energy of 0.7 J/shot extended the LSL to φ = 0.59-0.60. Compared to the delivered energy of 0.02 J/shot, the spark plug with 0.7 J/shot extended the LSL, but not significantly. The overall ignition performance for lean mixtures improved as the spark duration increased.

Figure 5.8-b shows the effects of spark duration on COV of IMEP for a railplug. It shares very similar trends with the spark plug, e.g., the overall ignition performance improved as the spark duration increased. Compared to Figure 5.8-A, for the same discharge energy (0.7 J/shot) and the same spark duration as the spark plug, the railplug extended the LSL from φ=0.59 to 0.535. The high-speed arc motion results in a fast burning rate and the ability to burn leaner mixtures than might ordinarily be possible.

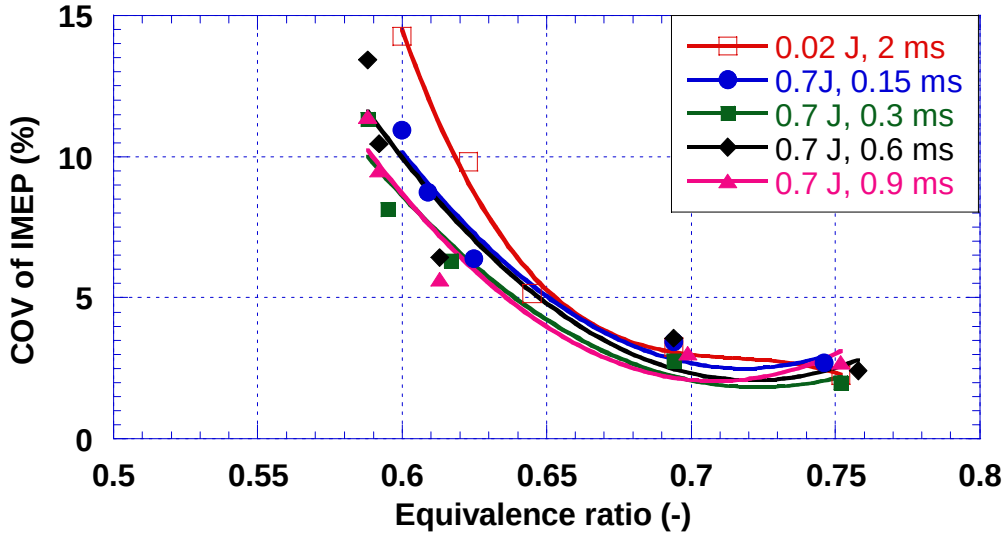

a: Spark plug

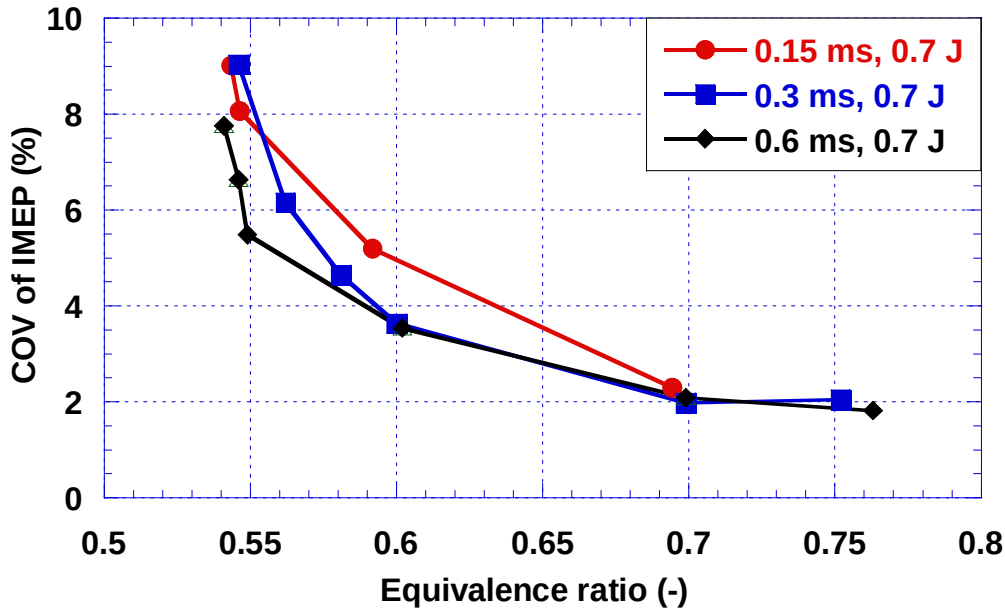

b: Rail plug

Figure 5.8. Effects of spark duration and spark discharge energy on combustion stability for both spark plug and railplug.

For this natural gas engine, especially at very lean conditions, relatively longer spark duration provided a big ignition window that improved the mixture cycle to cycle variation. For railplugs, a longer discharge duration also benefits plasma motion as discussed previously in Chapter 3.

5.3 Geometry design to improve railplug performance

The comparison of engine performance using both the parallel railplug and a coaxial railplug is shown in Figure 5.9. Compared to the coaxial railplug, the parallel railplug can significantly extend engine LSL because parallel railplugs have a higher inductance gradient as discussed in Chapter 3. So the plasma travel velocity of a parallel railplug is higher than that of a coaxial railplug for the same discharge current. It is noted that the parallel railplug has a lower COV of IMEP with less energy delivered, which means the parallel railplug has the potential for good durability since the erosion rate is directly related to the discharge energy. However, it should be realized that the coaxial railplug that the author tested was not optimized since this dissertation was focusing on parallel railplug development because of its intrinsic advantages compared to coaxial railplugs.

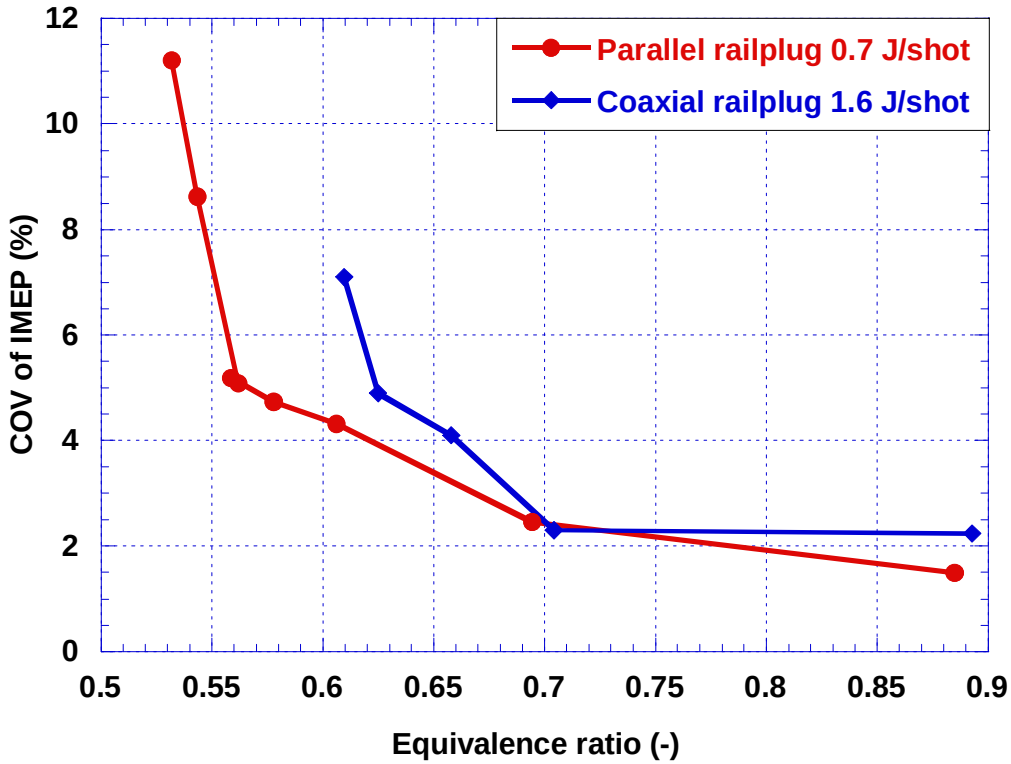

Figure 5.9. Comparison of performance of a parallel railplug and a coaxial railplug.

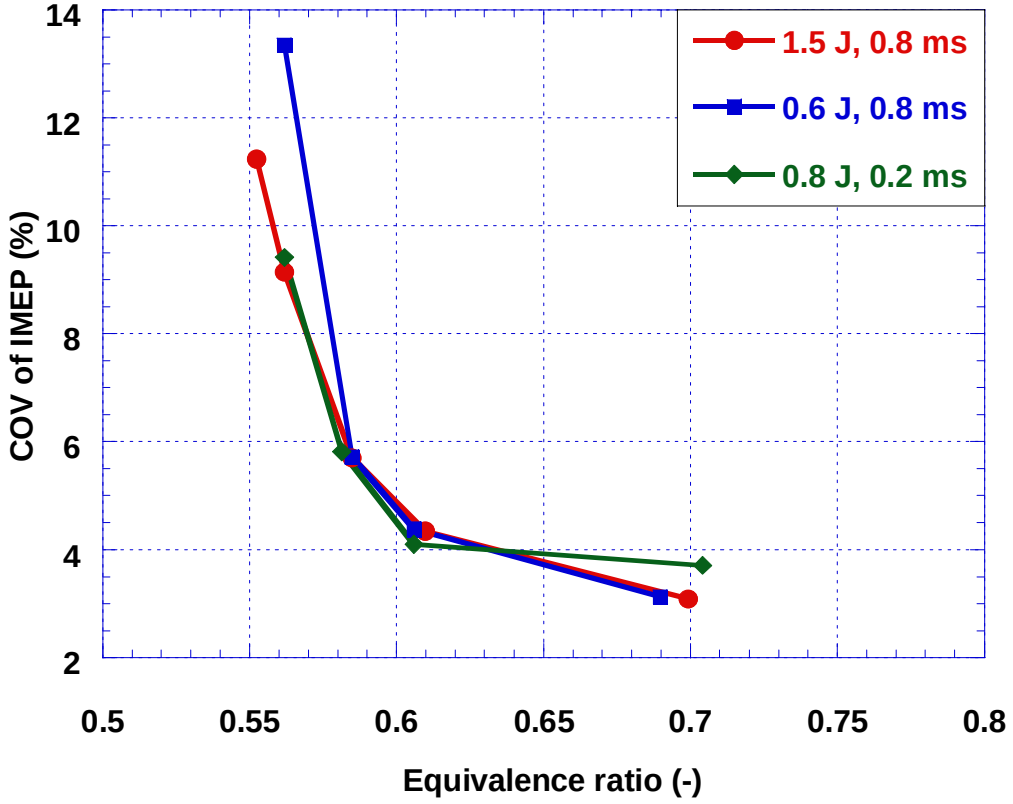

Figure 5.10. The effects of discharge energy and spark duration on COV of IMEP, open rails railplug.

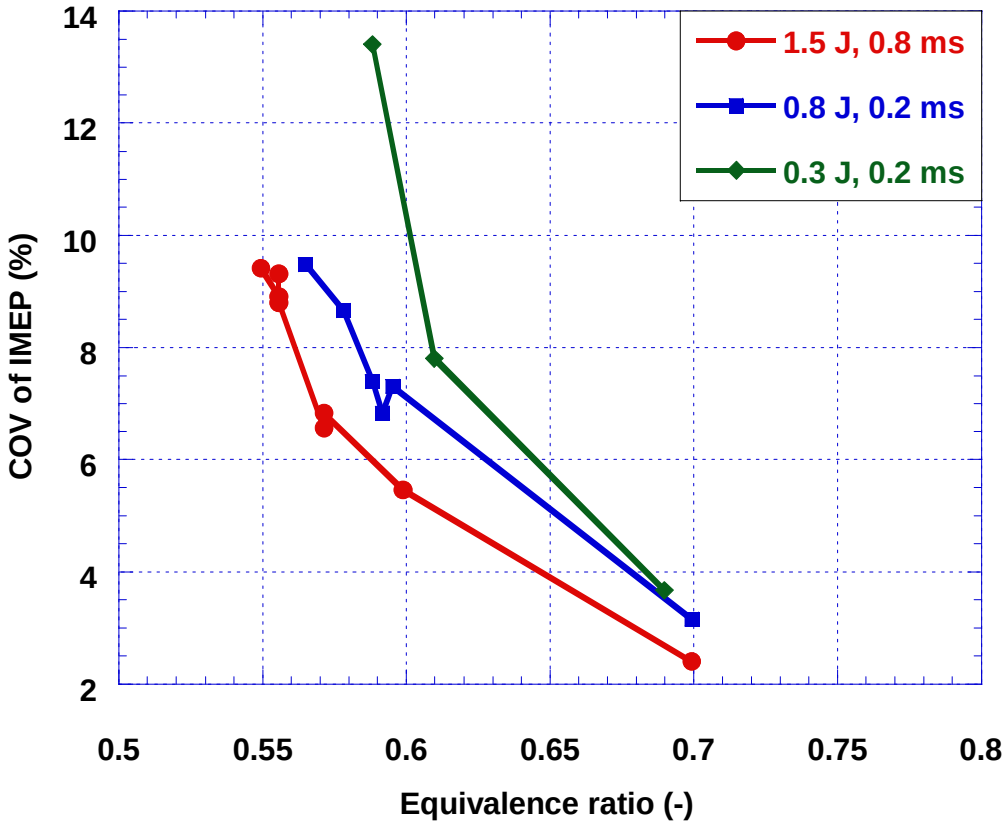

Figure 5.11. The effects of discharge energy and spark duration on COV of IMEP, partially enclosed railplug.

Figures 5.10 and 5.11 show the effects of discharge energy and spark duration on COV of IMEP for the two non-magnet enhanced railplugs, an open rail railplug and a partially enclosed railplug (Fig. 3.1). The overall trend is that the railplug performance determined by COV improved as the discharge energy increased. The effects of the discharge duration on COV are not so clear, however. One of the reasons is that there exists a trade-off between the discharge duration and current. For the same discharge energy, as the duration increases (which might benefit the arc motion) the current decreases; this decreases the arc

movement speed since the Lorentz force decreases as shown in Chapter 3. So the railplug geometric designs need to match the circuit designs. This will be explored in detail in future work.

The comparison of the open rail railplug and the partially enclosed railplug is shown in Figure 5.12. For the same spark energy and the same spark duration, the partially enclosed railplug had better performance because this design can improve plasma travel as discussed in Chapter 3.

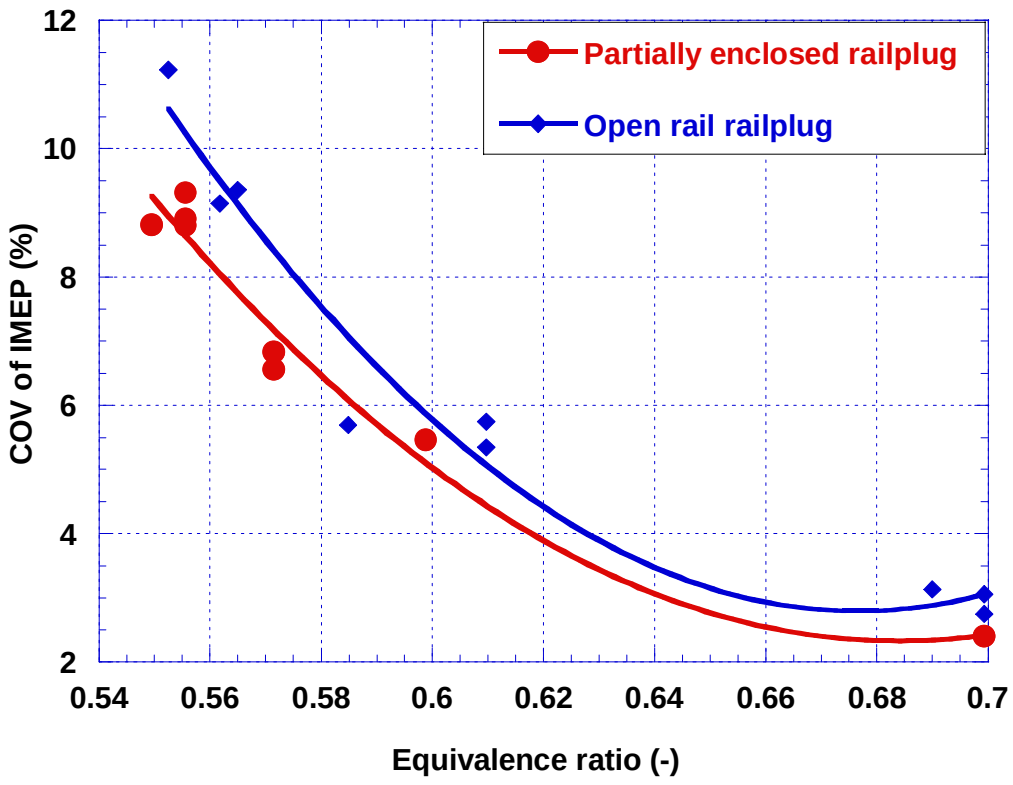

Figure 5.12. Comparison of performance of an open rail railplug and a partially enclosed railplug. Delivered energy 1.5 J/shot and spark duration 0.8 ms.

5.4 Parameter study to optimize railplug designs

It can be seen from the prior discussion that for a railplug, high speed plasma movement not only improves its ability to ignite leaner mixtures but also improves its durability. Since durability is a concern for railplug development, any approach that can improve the durability is always welcome. The effects of design parameters, such as local magnetic strength, ignition energy and electrode diameter, are discussed in this section.

The discussion from Chapter 3 shows that the Lorentz force is proportional to the strength of local magnetic field or the current for a given railplug. It is desired to use relatively small ignition energy and/or discharge current because railplug durability increases almost exponentially as the delivered energy decreases [44]. However, a smaller delivered energy or smaller discharge current means a smaller local self-induced magnetic strength and therefore smaller Lorentz force, which results in shorter plasma travel. The result is a decrease in ignitability. The durability may be adversely affected, as well, since although there is less energy to cause erosion, there will also be less arc movement. . In order to solve this dilemma, we can use a small permanent magnet to enhance plasma travel. The effects of the strength of the permanent magnet on plasma travel were discussed in Chapter 3. Figure 5.13 shows the effects of this magnet on engine COV. Magnet enhanced railplugs extended the LSL to about $\varphi = 0.53$ compared to $\varphi = 0.56$ for the non-magnet railplug. Engine performance was not particularly sensitive to the strength of the permanent magnets. The reason might be that a stronger magnet can increase plasma travel velocity as shown in Chapter 3; but it also increases heat loss because of its bigger volume. The mass fractional burning rates are shown in Figure 5.14.

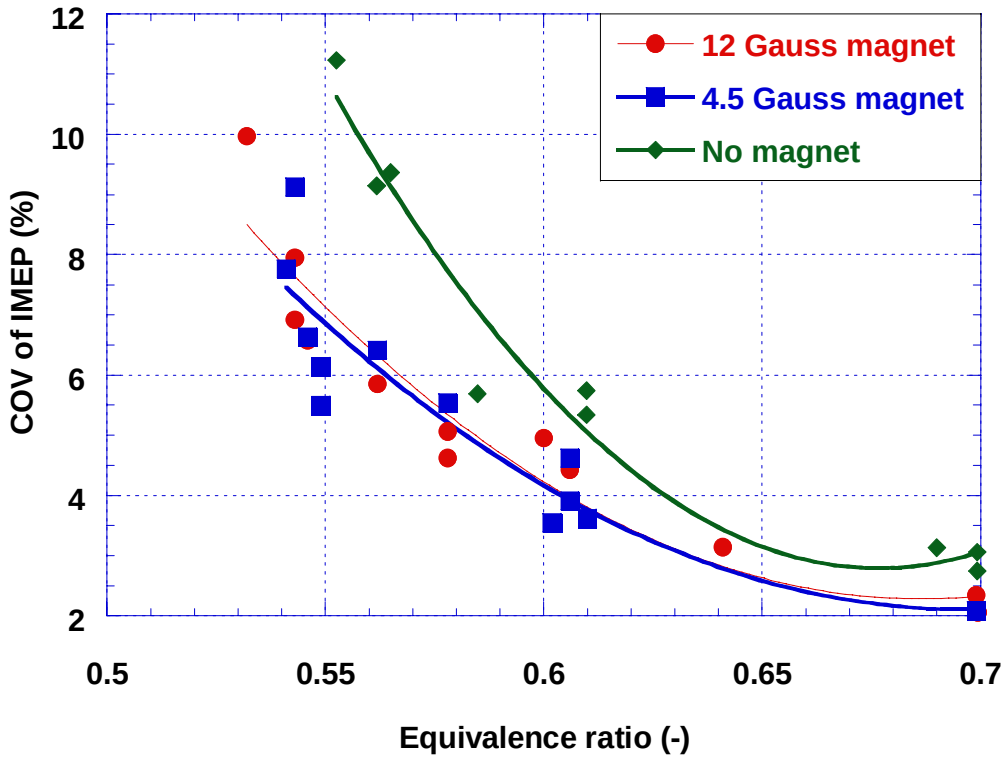

Figure 5.13. Effects of strength of permanent magnet on railplug performance; Delivered energy 0.7 J/shot, spark duration 0.6 ms, open rail railplugs.

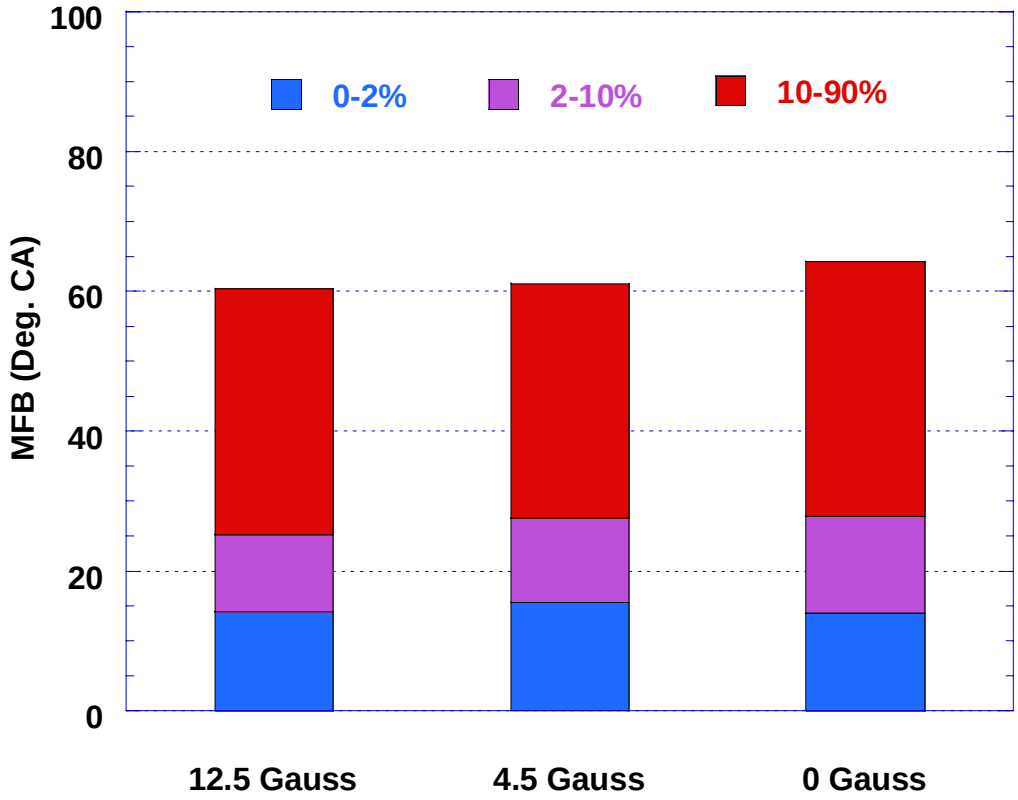

Figure 5.14. Effects of strength of permanent magnet on railplug performance; Delivered energy 0.7 J/shot, spark duration 0.6 ms, φ = 0.61.

Figure 5.15 shows the effects of ignition energy on the performance of a magnet enhanced railplug. For the magnet enhanced railplug, its performance is not as sensitive to the ignition energy as the non-magnet railplug as shown by Figures 5.10 and 5.11. The ignition energy can be as low as 150 mJ/shot, which is a typical ignition energy value for commercial CDI ignition systems used on large-bore natural gas engines.

The effects of electrode diameter on railplug performance are shown in Figure 5.16. As electrode diameter increases beyond a critical value, it greatly

affects the ability of rail plug to ignite lean mixtures . The railplugs with smaller electrodes had better ignition performance because small electrodes enhance plasma movement as discussed in Chapter 3. Small electrodes also decrease the flame kernel heat loss to the electrodes and improve the ignitability [16, 17]. Optimizing the cross-sectional size of the rails requires consideration of competing factors, however. Small electrodes absorb less heat from the mixture in the cylinder through convection heat transfer. They also dissipate less heat by conduction. Heat transfer analysis in next chapter will clarify the tradeoffs involved.

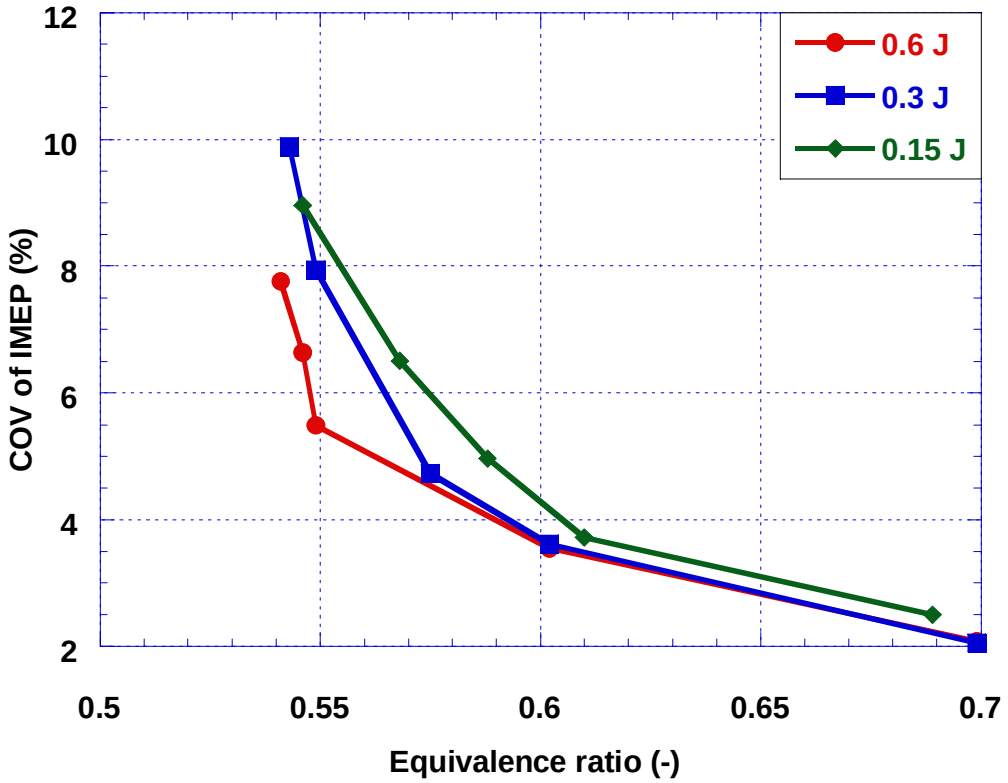

Figure 5.15. The effects of discharge energy on railplug performance; Magnet enhanced railplug.

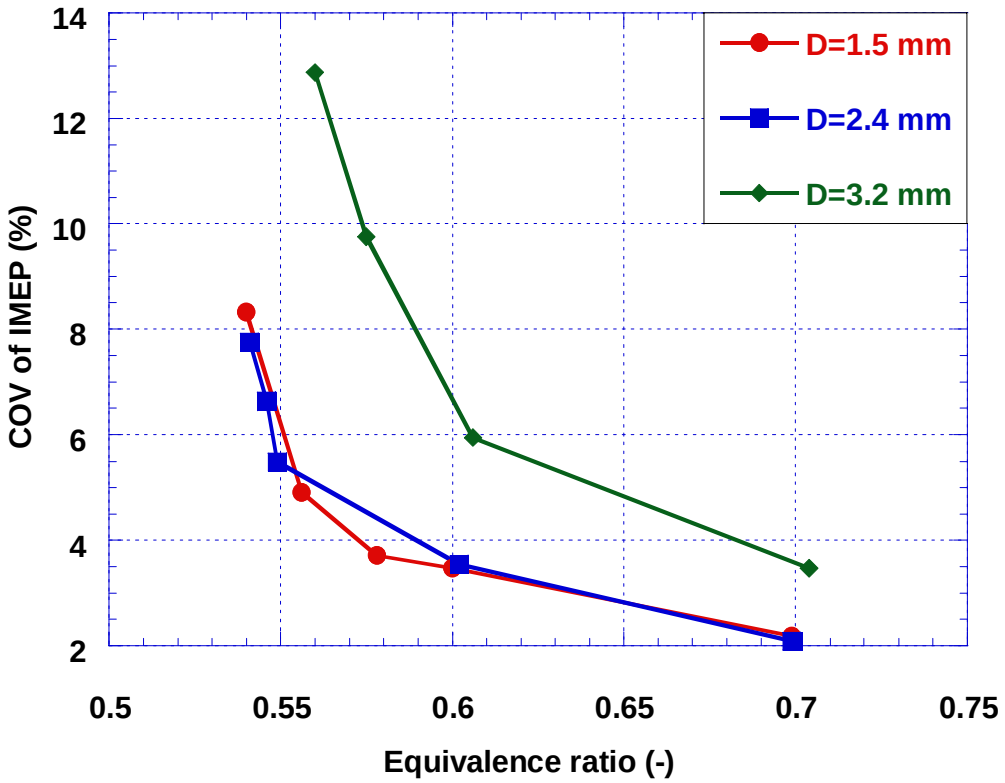

Figure 5.16. Effects of electrode size on railplug performance; Magnet enhanced railplugs; Discharge energy 0.7 J/shot and spark duration 0.6 ms.

5.5 Engine-out emission measurements

Engine-out emissions, such as NO_x, HC and CO, were measured for the engine operation with both spark plugs and railplugs. It was found that engine-out NO_x was a strong function of the ignition timing. Figure 5.17 shows that the NO_x concentration in the exhaust decreases almost linearly with a slope of 1 as the ignition timing is retarded. Engine-out HCs and CO don't change significantly as

ignition timing changes. So for the purpose of comparison, all emissions were measured at MBT ignition timing.

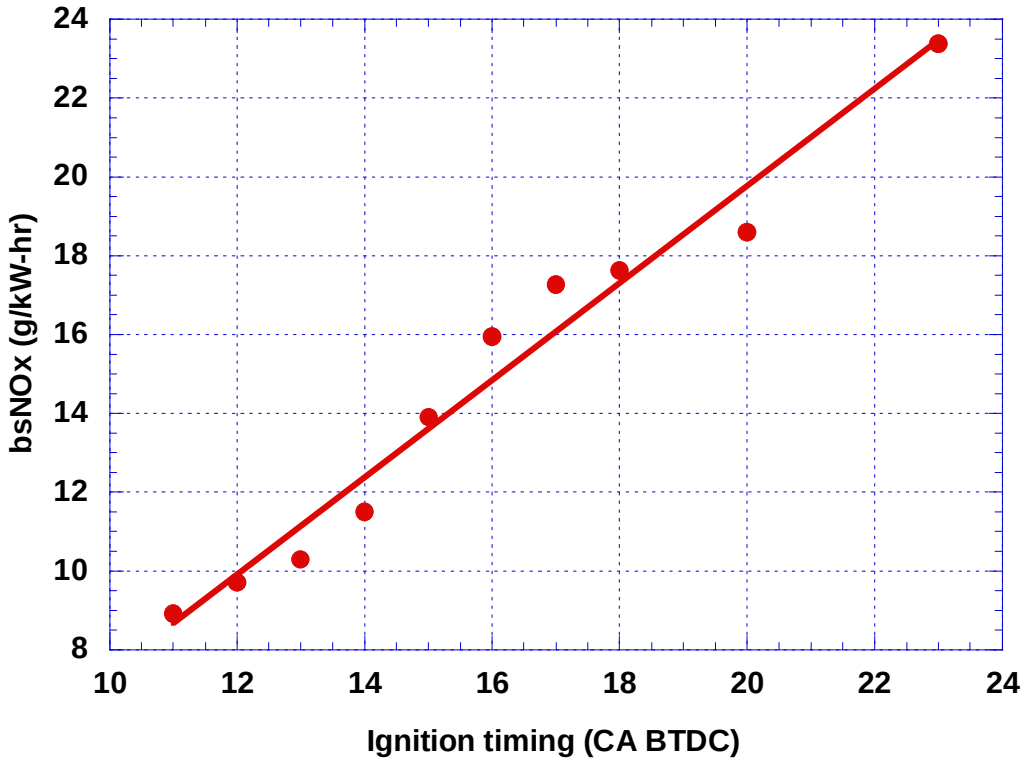

Figure 5.17. Effects of ignition timing on engine-out NO_x emissions, spark plug, $\varphi = 0.91$.

Figure 5.18 shows the effects of equivalence ratio on engine-out NO_x emissions for engine operation with both spark plugs and railplugs. The amount of NO_x emission decreases as the mixtures get leaner because the NO_x formation rate depends on in-cylinder temperature exponentially. Considering the LSL of the spark plug and railplug, the specific NO_x emissions can be reduced from 1.43 g/kW-hr for spark plugs down to 0.78 g/kW-hr using railplugs. However, as

mixtures get leaner, engine-out HC and CO emissions increase as shown in Figure 5.19 and 5.20.

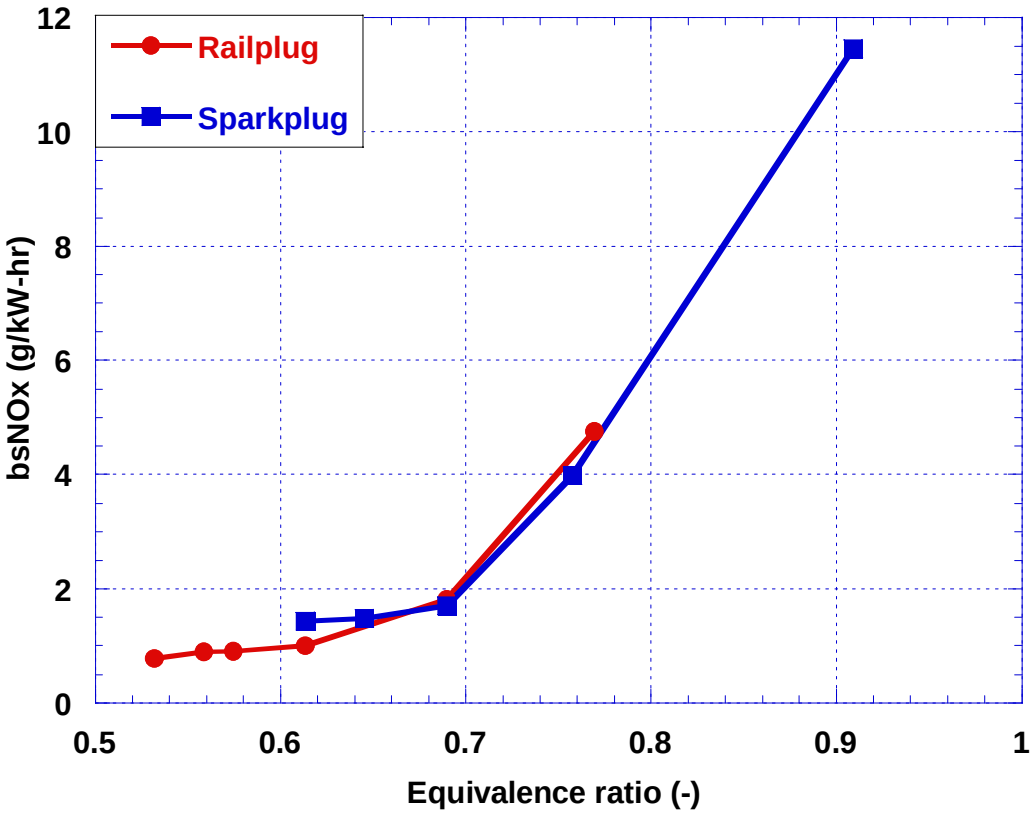

Figure 5.18. The effects of equivalence ratio on engine-out NO_x emissions, MBT timing.

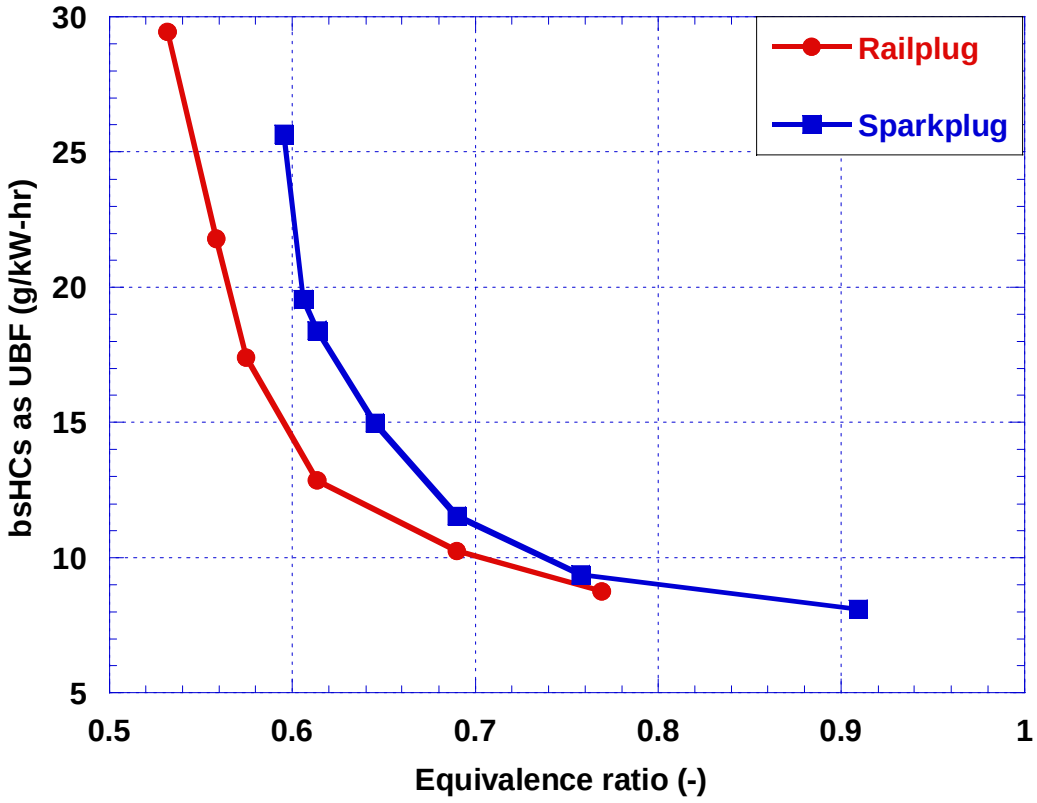

Figure 5.19. The effects of equivalence ratio on engine-out HC emissions.

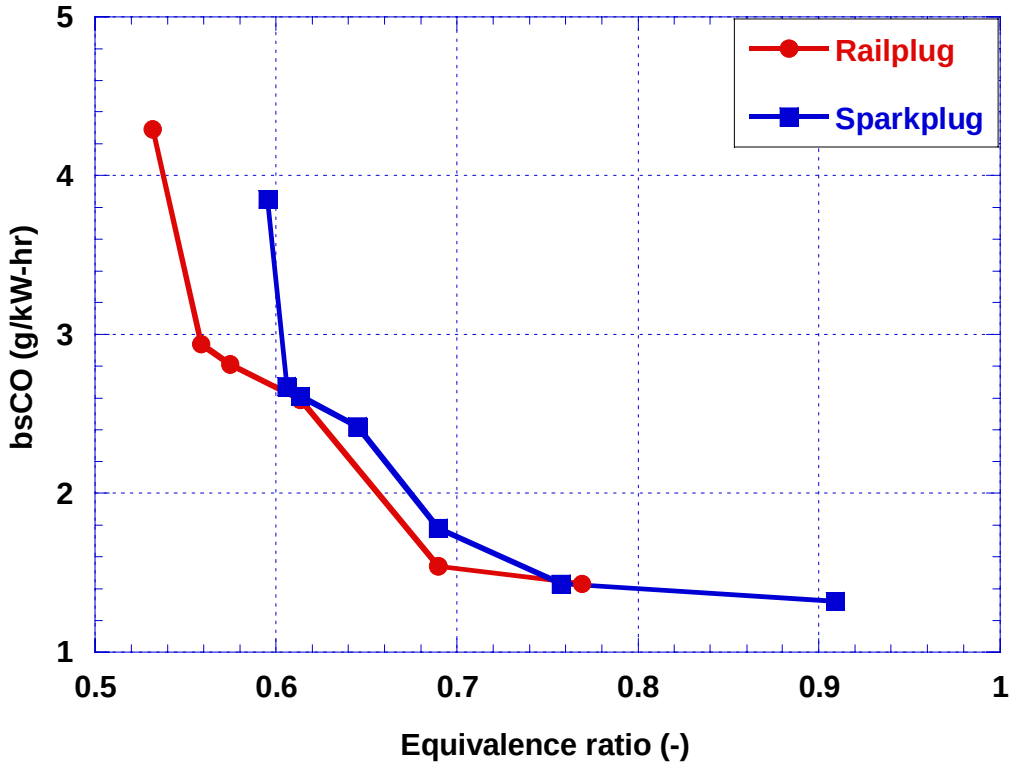

Figure 5.20. The effects of equivalence ratio on engine-out CO emissions.

5.6 Chapter summary

Three ignition systems, such as inductive ignition, capacitor discharge ignition and railplug ignition that includes both parallel railplug and coaxial railplug, were tested in a natural gas engine. The effects of discharge energy and duration on both spark plug and railplug performance were also investigated. The effects of some railplug design parameters on engine performance were also investigated. Engine-out emissions using both spark plugs and railplugs were measured.

Railplugs can increase the lean mixture burning rate and extend the lean stability limit for natural gas engines relative to a spark plug. The engine tests show that the LSL can be extended from a fuel/air equivalence ratio of $\varphi = 0.62$ (0.02 J) or $\varphi=0.59$ (0.7 J) for spark plugs used in a natural gas engines down to $\varphi = 0.53$ (0.7 J) using a railplug.

Engine results showed that spark plugs with high energy cannot extend the lean stability limit significantly. Spark duration affects the ignitability of both spark plugs and railplugs for lean mixtures.

The parallel railplug tested had better performance than the coaxial railplug. With less energy delivered, the parallel railplug yielded a better LSL than the coaxial railplug that was tested. This means that parallel railplugs potentially have better durability than coaxial railplugs.

A permanent magnet can be used to aid the plasma movement. The engine tests showed that the magnet-enhanced railplug had the best performance of the three railplugs tested. It improved both the railplug performance and durability. The LSL was extended to $\varphi = 0.54$ with delivered energy 0.15 J, a typical discharge energy for commercial capacitor discharge ignition systems.

Engine-out emission measurements show that engine operation with a railplug can decrease engine-out NO_x emissions compared to the engine with a spark plug. However, engine-out HC and CO increases as mixtures get very lean.

Smaller cross-sectional area electrodes have the potential to improve ignitability. In order to manage the electrode heat loading to prevent high rail temperatures and the potential for pre-ignition, suitable analysis is required to optimize the size, which is the topic of the next chapter.

Chapter 6.0 Railplug Temperature Measurements and Heat Transfer Analysis

Another issue that needs to be considered for railplug design is the thermal load of the railplug electrodes. For large-bore natural gas engines, in-cylinder pressures and mixture temperatures can be very high at the time of ignition (42 bars and 973 K) due to the high boost pressure. Hot spots may exist on the electrodes of the igniter, causing pre-ignition problems. High electrode temperatures can also reduce railplug durability. The wear of spark plug electrodes is classified as "sparking wear" caused by spark discharge, and "oxidation wear" caused by high electrode temperature [16]. Wear caused by spark discharge is attributed to arc discharge and glow discharge. During an arc discharge phase, the electrodes are heated to a few thousand degrees Centigrade locally and wear because the material melts and is ejected from the surface. Compared with the arc phase, electrodes experience lower wear rates during the glow phase [51]. Therefore, it is necessary to use a material with a higher melting point to improve the resistance to spark wear. To reduce electrode oxidation wear, besides using materials resistant to oxidation, it is necessary to decrease the electrode thermal load as much as possible.

In this study, the electrode temperature was measured in both a constant volume bomb and in an operating natural gas engine. A heat transfer model was developed to aid railplug design. The heat transfer analysis will be discussed in the latter part of this chapter.

6.1 Railplug and spark plug temperature measurements

The temperatures of some railplug electrodes both in a constant volume bomb and in an operating engine were measured. The temperature of a spark plug in an operating engine was also measured for comparison. Omega type K thermocouple probes were used. AWG 30 thermocouple wires were used to measure the temperature of the electrodes, and AWG 35 thermocouple wires were used to measure the mean gas temperature in an operating engine combustion chamber. A Tektronix oscilloscope Model 1012 was used to acquire the thermocouple voltage readings and then the voltage readings were converted to temperature.

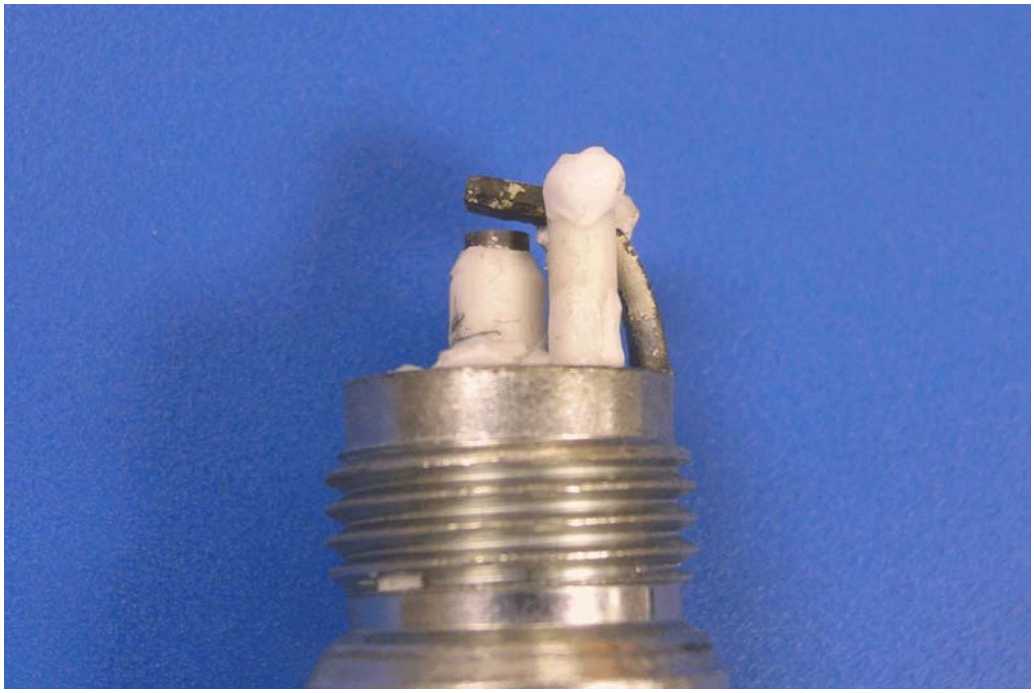

Figure 6.1. A spark plug with a thermocouple instrumented.

In order to measure electrode temperature in an operating engine, a spark plug and a railplug with thermocouple instrumented were fabricated as shown in Figure 6.1. A double-bore ceramic tube was used to wire the thermocouple. The joint of the thermocouple was buried on the measured surface of the electrode. For the spark plug, the measured electrode is the cathode because of its long extrusion to the combustion chamber and thus the high temperature.

The temperature of a railplug fired at room temperature with 1 J/shot and 10 Hz firing frequency is shown in Figure 6.2. The rail temperatures were measured at two locations: at the gap and at the end of the rail where the electrical lead attached to the rail. The gap end temperature was about 23 $^{\circ}$C higher than the lead end (listed in Figure 6.2 as the anode bottom) temperature. In the absence of a model it is hard to interpret this result. The results could be interpreted such that both the plasma heating and Joule heating (e.g., I^2R) are important to the electrode temperature rise or that one mechanism dominates and conduction along the electrode maintains the temperature considerably above the ambient temperature.

Figure 6.3 shows the effects of discharge energy and firing frequency on the railplug electrode temperature. This was also fired at room temperature. The electrode temperature increases linearly as frequency increases. The discharge energy affects the slope of the curves. This will be discussed in detail in the next section.

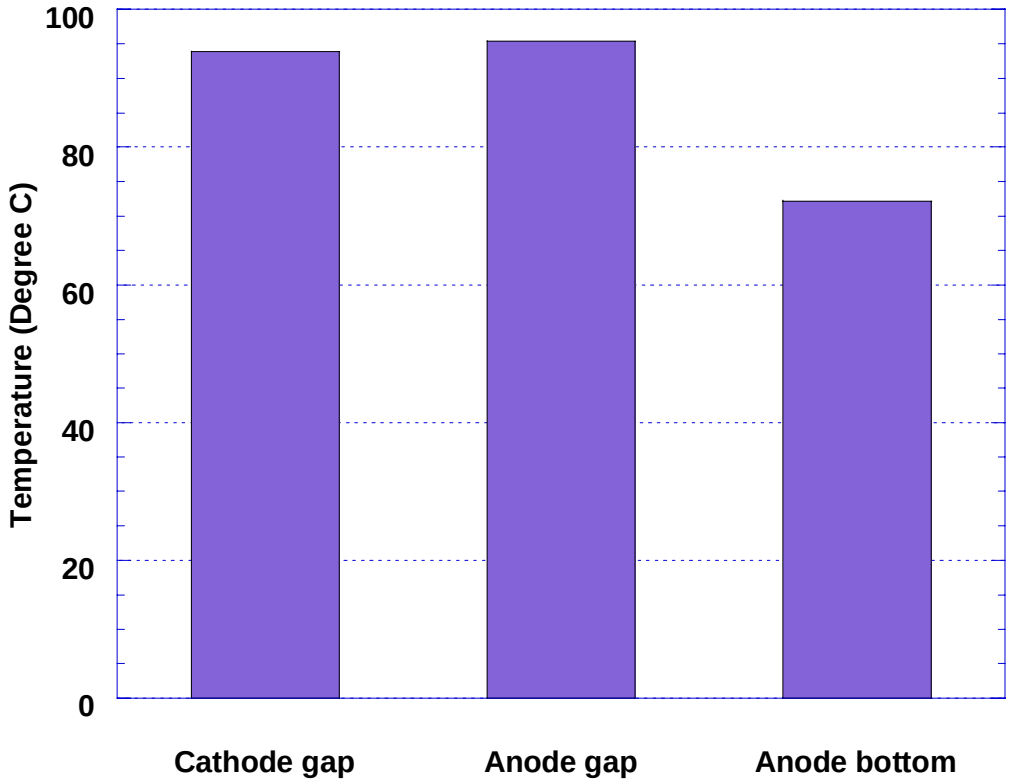

Figure 6.2. The effects of plasma heating and Joule heating on the electrode temperature, railplug fired at room temperature with 1 J/shot and frequency of 10Hz.

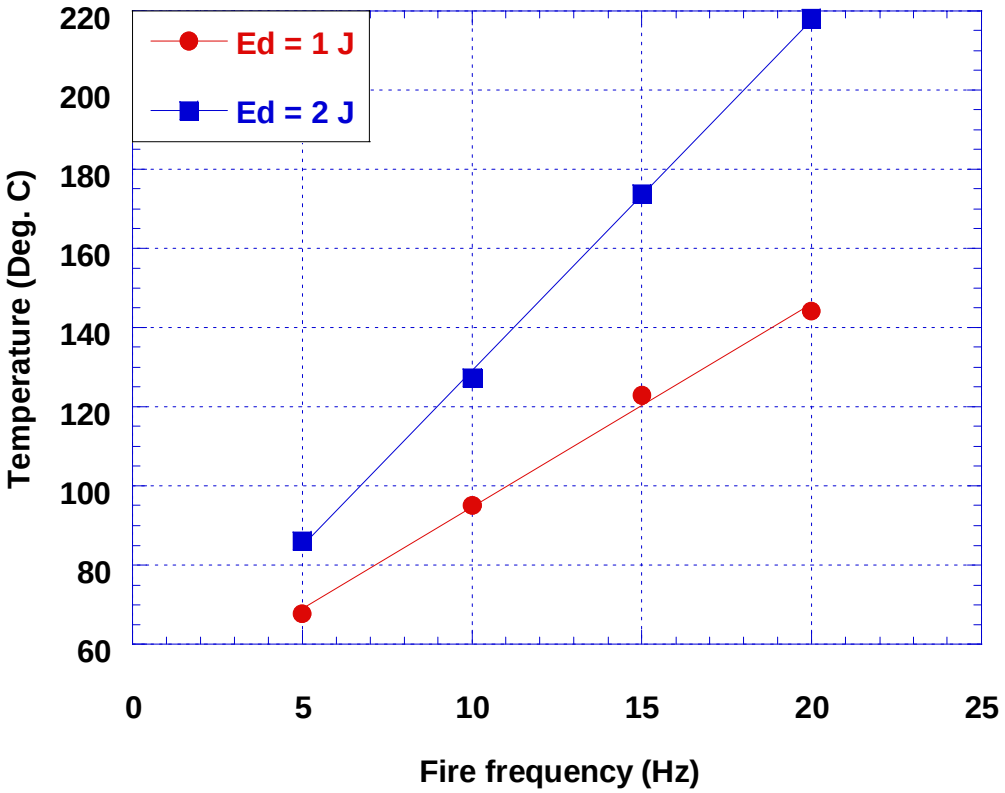

Figure 6.3. The effects of discharge energy and firing frequency on the electrode temperature, railplug fired at room temperature 295 K.

The railplug and spark plug temperatures in an operating engine are shown in Figure 6.4. Compared to Figure 6.3, railplug temperature does not change much as discharge energy changes. One of the reasons is that the heat transfer rate in an engine is higher than at room condition so that the in-cylinder combustion gas heat transfer dominates the temperature rise. As engine speed increases the electrode temperature increases due to higher rates of heat transfer from combustion gases to the electrode. From Figure 6.4 it cannot be concluded that the spark plug has a higher temperature than the railplug, however. The spark plug temperature was measured at a point 9 mm from the spark plug base, while

the railplug measurement point was 7.5 mm from the railplug base. A large temperature gradient existed along the electrode. As it was measured, the temperature at the electrode tip was about 710 °C at the condition 1200 rpm, WOT, and φ=0.87.

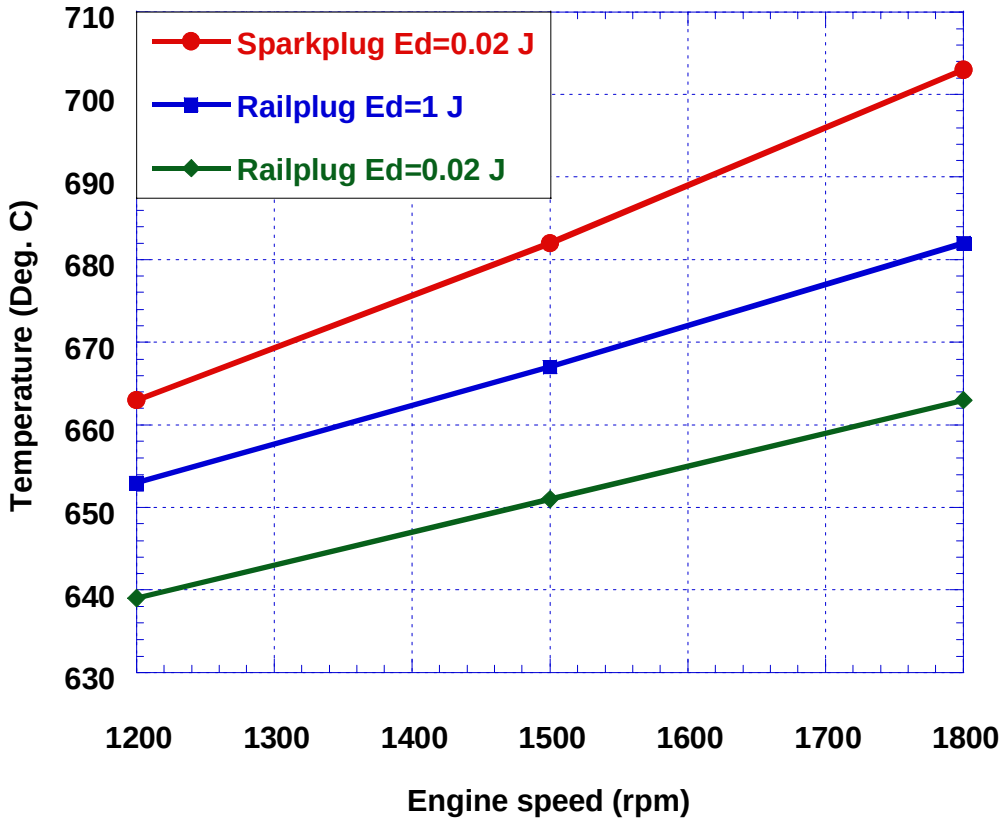

Figure 6.4. The effects of discharge energy and firing frequency on the electrode temperature, railplug and spark plug in an operating engine, WOT, φ=0.87.

Figure 6.5 shows the effects of equivalence ratio on the spark plug temperature. As the mixture got leaner, the spark plug temperature decreased because the combustion temperatures were lower.

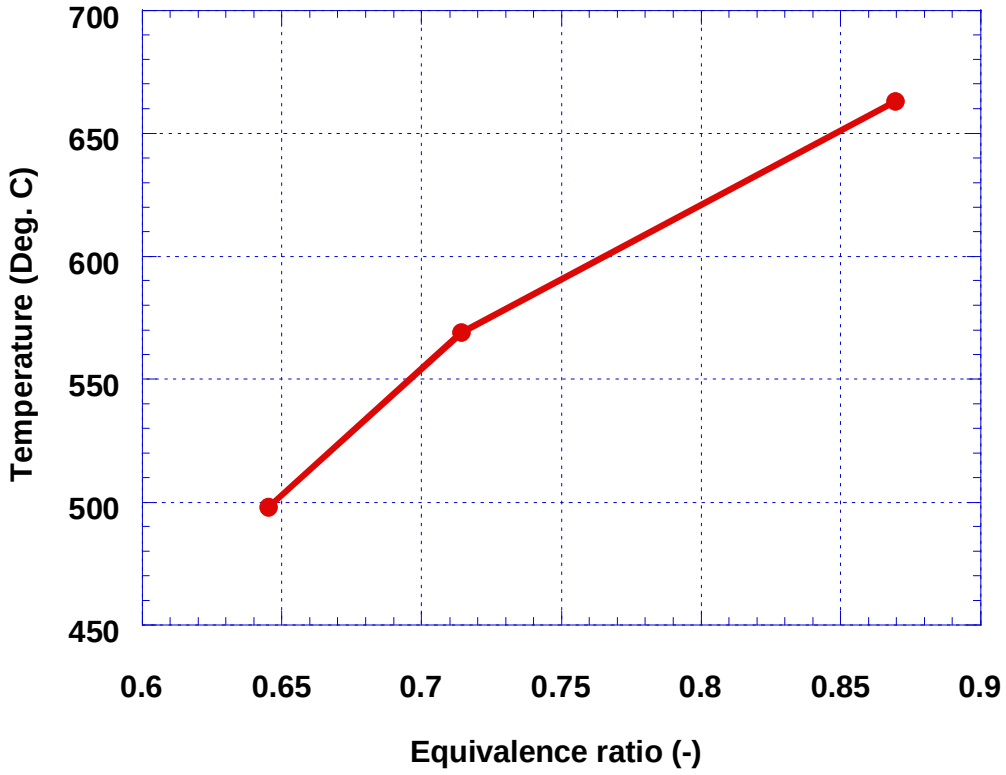

Figure 6.5. The effects of equivalence ration on the spark plug temperature, WOT, 1200 rpm.

6.2 Railplug and spark plug heat transfer analysis

Many possible electrode designs can be conceived. The common features, whether a railplug electrode or a spark plug electrode is that the length, diameter, energy deposition per shot, frequency of operation, and engine operating conditions will influence the thermal characteristics of the electrode. While detailed computational tools can be used to determine the thermal response for

any given electrode, the overall functional variation and interdependence of the various parameters is best examined using analytic tools. As such, we will show using simple analytical tools, the thermal response of an electrode to the operating characteristics discussed previously.

The electrode for both spark plug and railplug geometries is approximated by a cylindrical fin attached to a base of temperature, T_B. The fin approximation is valid for small Biot number (Bi<<1) and a large length to diameter ratio (L/D>>1). These limiting values are satisfied for the conditions of interest in this work

$$\frac{\partial T}{\partial t} = \alpha \frac{\partial^2 T}{\partial x^2} - \frac{hP}{\rho cA}(T - T_\infty(t)) + \frac{Q''P}{\rho cA} + \frac{S'''}{\rho c} \tag{6.1}$$

The last two terms are heat transfer from the plasma and heat transfer by Joule heating of the electrode. The magnitudes of these terms were assessed using combustion bomb experiments which were compared to modeled results.

The above equation is nondimensionalized to more clearly evaluate the relative magnitudes of the terms. We nondimensionalize time, t, by a characteristic time, t_C, which we will specify later, the axial length, x, is nondimensionalized by the true length, L, of the electrode, and temperature, T, is specified as $\theta = \frac{T - \bar{T}_\infty}{T_B - \bar{T}_\infty}$. In terms of the new variables, τ, z, θ for time, space, and temperature, we find that

$$\frac{\partial\theta}{\partial\tau} = Fo\frac{\partial^2\theta}{\partial z^2} - 4BiFo(L/D)\left[\theta + \frac{\bar{T}_\infty - T_\infty(t)}{T_B - \bar{T}_\infty}\right] + \frac{Q''t_C}{\rho cD(T_B - \bar{T}_\infty)} + \frac{S'''t_C}{\rho c(T_B - \bar{T}_\infty)} \tag{6.2}$$

where Fo is the Fourier number.

For analysis of the engine heat transfer problem, we can assume that the free stream temperature has a sinusoidal variation, $T_\infty(t) = \bar{T}_\infty + \Lambda\sin(\omega t_C\tau)$. We defined the nondimensional temperature, θ, as $\theta(t) = \mathrm{Im}(\phi(z)\exp(i\omega t_C\tau))$. In terms of the structure function φ(z) we solved the following ordinary differential equation.

$$Fo\frac{d^2\phi}{dz^2} - \left[4BiFo(L/D) + i\omega t_C\right]\phi = \frac{4BiFo(L/D)\Lambda}{T_B - \bar{T}_\infty} + \frac{Q''t_C}{\rho cD(T_B - \bar{T}_\infty)} + \frac{S'''t_C}{\rho c(T_B - \bar{T}_\infty)} \tag{6.3}$$

Prior to solving this we should examine the magnitudes of the plasma heating and Joule heating terms. We consider the simpler problem of electrode heat transfer in a constant volume bomb to sort out these effects.

For the bomb analysis we examine the temperature distribution in the pin fin electrode in a large time limit (i.e., for large Fo) corresponding to steady state temperature values. The Joule heating source term is defined in terms of the resistance, current, and electrode diameter, $S''' = \rho_E\bar{I}^2/A^2$. We can specify the average value of the current over the forcing period in terms of the energy of a

spark event. The energy, E_d, can be written as $E_d = \int_0^{t_s} R_{EQ} I^2 dt = \overline{R_{EQ} I_s^2} t_s$, where R_{EQ} is an equivalent resistance for the spark system. The current shown in the E_d expression is an average value over the spark event and must be normalized by the period to yield an appropriate value for the stead state operation. For steady state we have that $\overline{I}^2 = I_S^2 t_S f$ and that the Joule heating source terms is:

$$S''' = \frac{\rho_E E_d f}{R_{EQ} A^2} \tag{6.4}$$

While we do not know the exact magnitude of R_{EQ}, we have estimates of its magnitude. For a 1 mm spark gap and at room temperature and 1 atm, R_{EQ} is around 50 kΩ [62]. Numerically, the Joule heating volumetric source term is approximately

$$S''' = 0.11 E_d f \tag{6.5}$$

The average arc heat flux is determined in a similar manner. We know that a fraction χ of the total energy of the spark event is deposited onto the electrode as a heat transfer over every spark event. We determine an average heat flux using the frequency of sparking as

$$Q'' = \chi E_d f / PL \tag{6.6}$$

and is numerically

$$Q'' = 7960\chi E_d f \tag{6.7}$$

We note that both the Joule heating and the surface heating terms vary linearly with the frequency and with the deposited energy. This is consistent with Figure 6.2 where we see a near doubling in the temperature slope as the deposited energy is doubled. For the 1 J energy deposition, we have a slope of 5 ^{o}C/Hz and for the 2 J deposition, the slope is 9 ^{o}C/Hz. For a semi-infinite electrode we get the simple limiting case that

$$T = T_\infty + \left(7960\chi + 0.11D\right)\frac{E_d f}{h} \tag{6.8}$$

The efficiency factor associated with plasma heating would have to be smaller than 10^{-7} before the effects of Joule heating were of comparable magnitude as the plasma heating effects. This suggests that the plasma heating is the dominant effect. For natural convection and weak forced convection flows in the bomb tests, a reasonable estimate for h is 10 W/(m^{2}K). Matching the slopes with the experimental results shown in Figure 6.2, we find that the heat transfer efficiency factor, χ, is 0.6%. This result can be used to analyze the engine data.

Knowing the magnitude of the source terms, we can return to the engine electrode analysis. We see that the source terms have a relatively minor effect on the variation of the electrode temperature, given that the average engine heat transfer coefficient is much larger (i.e., by an order of magnitude) than that in the bomb. As such, the primary effect on the electrode temperature is heat transfer by the average gas temperature. That is, the thermal time constant for the electrode is much larger than the characteristic times in the engine. A steady fin analysis

where the fluid temperature is the average gas temperature is sufficient to predict the electrode temperature distribution. This is most clearly seen by examining the limiting case for an adiabatic tip fin with the previously stated sinusoidal free-stream temperature variation. In the limit of long length, we get a simple solution at the fin tip that looks like:

$$\theta = \frac{T - \bar{T}_\infty}{T_B - \bar{T}_\infty} = -\frac{H}{\sqrt{4Bi(L/D)}} \frac{\sin(\omega t_C \tau + \psi)}{\left(1 + \left(\frac{\omega t_C}{4Bi(L/D)}\right)^2\right)^{1/2}} \tag{6.9}$$

where

$$H = \frac{4Bi(L/D)\Lambda}{T_B - \bar{T}_\infty} + \frac{Q'' t_C}{Fo\rho cD(T_B - \bar{T}_\infty)} + \frac{S''' t_C}{Fo\rho c(T_B - \bar{T}_\infty)}$$

and

$$\psi = \arctan\left(\frac{-\omega t_C}{4Bi(L/D)}\right)$$

which is a phase lag between the electrode temperature and the gas temperature.

$$T = \bar{T}_\infty - \frac{\sqrt{4Bi(L/D)}\Lambda \sin(\omega t_C \tau + \psi)}{\left(1 + \left(\frac{\omega t_C}{4Bi(L/D)}\right)^2\right)^{1/2}} \tag{6.10}$$

Focusing on this particular engine electrode we find that Bi (L/D) <<1 and choose ωt_C to be approximately unity. We thus get a strong damping of the temperature

oscillations, Λ. The tip temperature is essentially the average gas temperature. While this problem reduces to a simple answer for the choice of parameters examined, we were able to quantitatively evaluate the relative effects of the parameters of interest in generating the solution. For different parameter cases, the methodology described may shed light on less obvious results.

Based on previous analysis, we can approximate the electrode temperature distributions. The electrode for both spark plug and railplug geometries is approximated by a cylindrical pin fin attached to a plug base of temperature, T_B. For simplicity, assuming steady heat transfer and neglecting source terms for Joule heating and plasma heating because they are small compared to combustion heat transfer, the conduction loss balances the convective heating.

$$\alpha \frac{\partial^2 T}{\partial^2 x} = \frac{hP}{\rho CA}\left(T - T_\infty\right) \tag{6.11}$$

where, A_C is the cross-sectional area and P is the perimeter of the electrode. Using insulated tip boundary condition yields the solution,

$$T^* = \frac{T - T_\infty}{T_B - T_\infty} = \frac{\cosh \beta (L - x)}{\cosh \beta L} \tag{6.12}$$

where, T_∞ is the in-cylinder gas temperature and T_B is the temperature of the plug base; $\beta = \left(\frac{h\ P}{kA}\right)^{1/2}$. h can be obtained from Eichelberg's formula [77],

$$h = 7.67(C_m)^{1/3}(pT)^{1/2}, \quad \text{W/(m}^2\text{.K)} \tag{6.13}$$

where, C_m is the mean-piston-speed, m/s; p is the pressure, MPa.

The non-dimensional temperature T^* is shown in Figure 6.6. As the electrode size becomes smaller, the tip temperature increases. The extreme case that the tip temperature equals the mean gas temperature should be avoided.

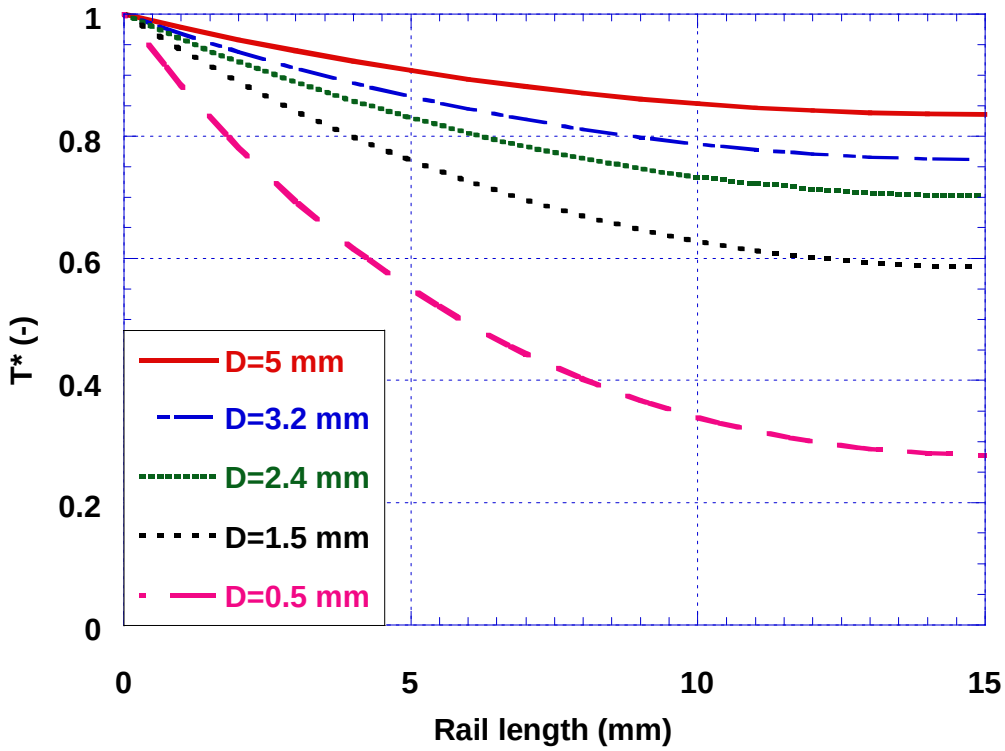

Figure 6.6. Electrode temperature distributions.

Chapter 7.0 Summary, Conclusions and Recommendations for Future Research

While large-bore natural gas engines continue to evolve, utilizing leaner mixture combustion and developing higher BMEP with the aim of reducing emissions and fuel consumption, one aspect that requires further advancement is the understanding and improvement of the ignition process. It was thus decided to study the fundamentals of and limitations of existing ignition systems. Based upon these studies the investigation began into a high energy igniter, the railplug, for large-bore natural gas engines.

7.1 Summary and conclusions

There are three primary topics discussed in this dissertation. Those topics include: the experimental investigation of the discharge characteristics of three different ignition systems; the design, fabrication and testing of a railplug system in both a combustion bomb and in an operating engine; and spark plug and railplug temperature measurements with an associated electrode heat transfer analysis. They are summarized in this section and some conclusions are drawn base on the discussion in the previous chapters.

7.1.1 The characteristics of the three ignition systems

The performance characteristics of three ignition systems were investigated experimentally outside of an engine. Those ignition systems are inductive ignition, capacitor discharge ignition (CDI), and railplug ignition.

Inductive ignition discharge has 4 phases: Pre-breakdown, breakdown, arc and glow. Since the breakdown phase is very short, most of the discharge energy is deposited during arc and glow. The arc phase has a higher discharge efficiency compared to the glow phase. It is, however, responsible for most of the electrode erosion, and therefore is a limiting factor for the life of spark plugs.

The spark discharge can be affected by many factors. The time at which the arc to glow transitions occurs can vary greatly. It was also observed that this transition does not occur at a fixed current level as many researchers assumed, rather, it can take place over a range of current values.

A spark plug's internal resistance and gap size greatly affect the delivered discharge energy. The delivered energy decreases as spark plug resistance increases because the spark duration decreases. The delivered energy increases as spark gap increases because both arc and glow voltages increase.

Compared to inductive ignition, both CDI and railplug ignition have shorter spark durations. They also don't have a glow phase. Their delivered energy, however, is higher than the inductive ignition because of the higher discharge current.

7.1.2 Railplug development

High speed photography was used to study the effect of the various design and operating parameters on railplug performance. Some of the parameters considered include railplug geometry, the diameter of the rails, and the amount of inductance in the railplug circuit, and the effect of using an external permanent magnet to enhance the Lorentz forces on the arc.

Three ignition systems, including inductive ignition, capacitor discharge ignition and railplug ignition with both parallel and coaxial railplugs, were tested in a natural gas engine. The effects of discharge energy and duration on both spark plug and railplug performance were also investigated. The effects of some railplug design parameters on engine performance were also investigated. Engine-out emissions using both spark plugs and railplugs were measured.

Railplugs can increase the lean mixture burning rate and extend the lean stability limit for natural gas engines relative to a spark plug. The engine tests show that the LSL can be extended from a fuel/air equivalence ratio of $\varphi = 0.62$ (0.02 J) or $\varphi=0.59$ (0.7 J) for spark plugs used in a natural gas engines down to $\varphi = 0.53$ (0.7 J) using a railplug.

Engine results showed that spark plugs with high energy cannot extend the lean stability limit significantly. Spark duration affects the ignitability of both spark plugs and railplugs for lean mixtures. For the same spark energy 0.7 J, spark plug extends the LSL from $\varphi=0.60$ with 0.15 ms spark duration down to $\varphi=0.585$ with 0.9 ms spark duration.

The parallel railplug tested had better performance than the coaxial railplug. With spark energy 0.7 J delivered, the parallel railplug yielded a LSL of φ=0.54, whereas for the coaxial railplug that the author tested, the LSL is $\varphi \approx 0.57$ using 1.6 J delivered energy. This means that parallel railplugs potentially have better durability than coaxial railplugs.

A permanent magnet can be used to aid the plasma movement. The engine tests showed that the magnet-enhanced railplug had the best performance of the three railplugs tested. It improved both the railplug performance and durability. The LSL was extended to $\varphi = 0.535$ with delivered energy 0.15 J, a typical discharge energy for commercial capacitor discharge ignition systems With the same delivered energy and the same spark duration, The LSL of a non-magnet rail plug is φ=0.55.

Engine-out emission measurements show that engine operation with a railplug can decrease engine-out NO_x emissions to 0.78 g/kW-hr compared to 1.43 g/kW-hr for the engine with a spark plug. However, engine-out HC and CO increases as mixtures get very lean.

Smaller cross-sectional area electrodes have the potential to improve ignitability due to the higher inductance gradient thus the larger Lorentz force and less heat transfer loss.

7.1.3 Plug temperature measurements and heat transfer analysis

The electrode temperatures of both a railplug and a spark plug were measured in a combustion bomb and in an operating engine. A heat transfer model was proposed to analyze and optimize the railplug designs for the purpose of better managing the electrode heat loading to prevent high rail temperatures and the potential for pre-ignition. Management of electrode heat loading can also benefit railplug durability. The results show that a railplug does not have a higher heat loading than a spark plug even though the railplug might have significantly higher discharge energy. The geometric design parameters, such as electrode diameter and electrode protrusion, greatly affect the electrode temperature.

7.2 Recommendations for future work

The study in this dissertation has shown that a railplug is a very promising igniter for lean burn engines, especially for large-bore natural gas engines. The design optimization lead to the conclusion that design factors such as using parallel railplugs and magnet-enhanced railplugs, can significantly improve the performance and durability of a rail plug. The durability, however, is still a concern, especially for high load large-bore natural gas engines. Quantification of erosion needs to be done that can give insight into how circuit parameters and railplug geometry parameters affect the durability of railplugs.

The lean-burn mechanism for operating engines needs to be studied further. It is known that for an operating engine, burning mixtures that are too lean leads to misfire even though the deposited ignition energy is much larger than the theoretical minimum ignition energy for the mixture. Is it flame propagation limitation because the flame propagation speed is too slow resulting

in partial burning and/or the intrinsic flammability limitation hard to form effective ignition kernel? We can probably answer this question by engine tests. The engine data acquisition system can record the misfire rate by pre-setting the IMEP threshold function in software. We can set the IMEP threshold to 2%, 10% or 50% of the average IMEP value and measure the misfire rates of both spark plugs and railplugs with different spark energies. Extensive engine tests plus statistical analysis can help us to better understand the lean-burn limitations, which would support the design of more effective igniters for lean-burn engines.

References

1. U.S. DOE, EIA (2001), Annual Energy Review 2001, Table 1.3.

2. Nichols, R.J. (1993), "The Challenges of Change in the Auto Industry: why Alternative Fuels?" ICE-Vol. 20, Alternative Fuels, Engine Performance and Emissions, ASME 1993.

3. Heisler, H. (1995), Advanced Engine Technology. SAE International Inc..

4. DOE Advanced Reciprocating Engines Program, 2001, "Distributed Energy Resources, Advanced Reciprocating Engines Systems (ARES) Program," http://www.eere.energy.gov/de/pdfs/reciprocating.pdf

5. Callahan, T.J. (2003), "Survey of Gas Engine Performance and Future Trends", Proceedings of the ASME ICE Division 2003 Spring Technical Conference, ICES2003-628.

6. Lewis, B. and von Elbe, G. (1987), Combustion, Flames, and Explosions of Gases, 3rd ed., Academic Press, New York.

7. Williams, F.A. (1985), Combustion Theory, 2nd ed., Benjamin-Cummins, Menlo Park, CA.

8. Ronney, P.D. (1994), "Laser versus Conventional Ignition of Flames", *Optical Engineering* **33**(2):510-521.

9. Joulin, G. (1985), "Point-Source Initiation of Lean Spherical Flame of light Reactants: an Asymptotic Theory", Combust. Sci. Tech. 43, 99-113.

10. Ballal, D.R., and Lefebvre, A.H. (1974), "Influence of Flow Parameters on Minimum Ignition Energy and Quenching Distance", 15th Symposium (International) on Combustion, the Combustion Institute, Pittsburgh, pp. 1473-1481.

11. Sloane, H.M. (1990), "Energy Requirements for Spherical Ignition in Methane – Air Mixtures at Different Equivalence Ratio", Combust. Sci. and Tech. Vol. 73, pp. 351-365.

12. Anderson, R.W., and Lim, M.T. (1985), "Investigation of Misfire in a Fast Burn Spark Ignition Engine", *Combustion Science and Technology*, 43, pp. 183-196.

13. Anderson, R.W. (1987), "The Effect of Ignition System Power on Fast Burn Engine Combustion", SAE Paper 870549.

14. Herweg, R. and Ziegler, G.F.W. (1990), "Flame Kernel Formation in a Spark-Ignition Engine", International Symposium COMODIA 90: 173-178.

15. Douaud, A., G. de Soete, and Henault, C. (1983), "Experimental Analysis of the Initiation and Development of Part-Load Combustion in Spark Ignition Engines", SAE Paper 830338.

16. Hori, T., Shibata, M., Okabe, S., and Hashizume, K. (2003), “Super Ignition Spark Plug with Fine Center & Ground Electrodes”, SAE Paper 2003-01-0404.

17. Nakamura, N., Kobayashi, T., Hanaoka, M., and Takagi, N. (1983), “A New Platinum Tipped Spark Plug Extends the Lean Misfire Limit and Useful Life”, SAE Paper 830480.

18. Maly, R., Saggau, B., Wagner, E.P., and Ziegler E. (1983), “Prospects of Ignition Enhancement”, SAE Paper 830478.

19. Ziegler, G.F.W., Wagner, E.P., Saggau, B., Maly, R., and Herden W. (1984), “ Influence of a Breakdown Ignition System on Performance and Emission Characteristics”, SAE Paper 840992.

20. Anderson, R.W., and Asik, J.R.(1985), “Lean Air-Fuel Ignition System Comparison in a Fast_Burn Engine”, SAE Paper 850076.

21. Pischinger, S.. and Heywood J.B. (1988),”A Study of Flame Development and Engine Performance with Breakdown Ignition Systems in a Visualization Engine”, SAE Paper 880518.

22. Cho, Y.S., Santavicca, D.A. and Sonntag R.M. (1992), “The Effect of Spark Power on Spark-Ignited Flame Kernel Growth”, SAE Paper 922168.

23. Chiriac, R., Radu, R., and Apostolescu, N. (2001), “A Study of Ignition Discharge Parameters Effect on Homogeneous Mixtures Combustion in Engine”, SAE Paper 2001-01-1953.

24. Grupp, D.J., and Martin, J.K. (2002), “Ignition System Characteristics and Effects on Combustion for a Two-Stroke Engine”, SAE Paper 2002-01-0644.

25. Ishii, K., Niu, K., Tsukamoto, T., and Ujiie, Y. (1990), “Analysis of Ignition Mechanism of Combustible Mixtures by Short Duration Sparks”, International Symposium COMODIA 90: 153-158.

26. Karim, G.A., Al-Himyary, T.J., and Dale, J.D. (1989), “An Examination of the Combustion Processes of a Methane Fuelled Engine When Employing Plasma Jet Ignition”, SAE Paper 891639.

27. Wagner, R.M., Andriulli, J.B., Edwards, K.D., Theiss, T.J., and Whealton, J.H. (2003), “Lean Limit Extension Through Rotating Arc Spark Plugs (RASP) and Adaptive Controls”, 2nd Distributed Energy Peer Review, December 2-4, 2003, Washington, DC.

28. Lim, M.T., Anderson, R.W., and Appci, V. S. (1987), “Prediction of Spark Kernel Development in Constant Volume Combustion”, Combustion and Flame, 69: 303-316.

29. Frendi, A. and Sibulkin, M. (1990), “Dependence of Minimum Ignition Energy on Igniiton Parameters”, Combust. Sci. and Tech., Vol. 73, pp. 385-413.

30. Bondre, S., Nguyen, K., and Phuoc, T. (2004), “Effects of Pressure and Equivalence Ratio on Minimum Ignition Energy of Methane-Air Mixtures”, Proceeding of the 2004 Technical Meeting of the Central States Section of The Combustion institute.

31. Phuoc, T., and White F.P. (1999), “Laser-Induced Spark Ignition of CH_4/Air Mixture”, *Combustion and Flame* **119**:203-216.

32. Ma, J.X., Alexander, D.R., and Poulain, D.E. (1998), “Laser Spark Ignition Combustion Characteristics of Methane-Air Mixtures”, Combustion and Flame 112:492-506.

33. McMillian, M.H.,Woodruff S.D., Ontko J., Richardson S.W., and McIntyre, D.L. (2002), “Laser-Spark Ignition for Natural Gas Fueled Reciprocating Engines”, Natural Gas Technologies Conference and Exhibition, Sept. 30.

34. McMillian, M.H., Woodruff S.D., Richardson S.W., and McIntyre, D.L. (2004), “Laser Spark Ignition: Laser Development and Engine Testing”, Proceedings of the ASME ICE Division 2004 Fall Technical Conference, ICEF2004-917.

35. Biruduganti, M.S., Gupta, S.B., Bihari, B., Klett, G., and Sekar, R. (2004), “Performance Analysis of a Natural Gas Generator Using Laser Ignition”, Proceedings of the ASME ICE Division 2004 Fall Technical Conference, ICEF2004-983.

36. Graf, J., Weinrotter, M., Kopecek, H., and Wintner, E. (2004), “Laser Ignition, Optics and Contamination of optics in an I. C. Engine”, Proceedings of the ASME ICE Division 2004 Fall Technical Conference, ICEF2004-833.

37. Saito, H., Sakurai, T., Sakonji, T., Hirashima, T., and Kanno K. (2001), “Study on Lean Burn Gas Engine Using Pilot Oil as the Ignition Source”, SAE Paper 2001-01-0143.

38. Gong, W., Bell, S.R., Micklow, G.J., Fiveland, S.B., and Willi, M.L. (2002), “Using Pilot Diesel Injection in a Natural Gas Fueled HCCI Engine”, SAE Paper 2002-01-2866.

39. Chrisman, B.M. and Callahan, T.J. (1998), Investigation of Micro Pilot Combustion in a Stationary Gas Engine”, Proceedings of the ASME ICE Division 1998 Spring Technical Conference, 98-ICE-106.

40. Harden, B., Matthews, R.D., Nichols, S.P., and Weldon, W.F. (1991), "A miniature railgun engine ignitor," US Patent Number 5,076,223.

41. Hall, M.J., Tajima, H., Matthews, R.D., Koeroghlian, M.M., Weldon, W.F., and Nichols, S.P. (1991), “Initial Studies of a New Type of Ignitor: the Railplug”, SAE Paper 912319.

42. Matthews, R.D., Hall, M.J., Faidley, R.W., Chiu, J.P., Zhao, X.W., Annezer, I., Koenig, M.H., Harber, J.F., Darden, M.H., Weldon, W.F., and Nichols, S.P. (1992), “Further Analysis of Railplugs as A New Type of Ignitor”, SAE Paper 922167.

43. Chiu, J.P., Darden, M.H., Matthews, R.D., Childs, H.E., Faidley, R.W., Zheng, J., Weigand, G., Weldon, W.F., and Nichols, S.P. (1994), “Examination of the Factors that Influence the Durability of Railplugs”, SAE Paper 940201.

44. Zheng, J., Capiaux, S., Chiu, J.P., Matthews, R.D., Faidley, R.W., Darden, M.H., Weldon, W.F., and Nichols, S.P. (1993), “Effects of Railplugs on the Dilution Tolerance of a Spark Ignition Engine”, SAE Paper 931800.

45. Dale, J.D. and Oppenheim, A.K. (1981), “Enhanced Ignition for I. C. Engines with Premixed Gases”, SAE Paper 810146.

46. Edwards, C.F., Oppenheim, A.K., and Dale, J.D. (1983), “A Comparative Study of Plasma Ignition Systems”, SAE Paper 830479.

47. Kupe, J., Wilhelmi, H., and Adams, W. (1987), “Operational Characteristics of a Lean Burn SI-Engine: Comparison between Plasma-Jet and Conventional Ignition System”, SAE Paper 870608.

48. Karim, G.A., Al-Himyary, T.J., and Dale, J.D. (1989), "An Examination of the Combustion Processes of a Methane Fuelled Engine When Employing Plasma Jet Ignition", SAE Paper 891639.

49. Modien, R.M., Checkel, M.D., and Dale, J.D. (1991), "The Effect of Enhanced Ignition Systems on Early Flame Development in Quiescent and Turbulent Conditions", SAE Paper 910564.

50. Hari, S., Lee, M. J., Hall, M.J., Ezekoye, O.A., and Matthews, R.D. (2005), "Analysis of Factors that Affect the Performance of Railplugs", SAE Paper 2005-01-0252.

51. Maly, R. (1984), "Spark Ignition: Its Physics and Effect on the Internal Combustion Engine", in Fuel Economy in Road Vehicles Powered by Spark Ignition Engines, Chapter 3, pp. 91-148, Editors: J.C. Hilliard and G.S. Springer., Plenum Press, New York.

52. Sze, S.M. (1969), Physics of Semiconductor Devices, Chapter 5, John Wiley and Sons Inc..

53. Meek, J.M., and J.D. Craggs (1953), Electrical Breakdown of Gases, Chapter 12, Oxford at the Clarendon Press.

54. Kim, J., and R.W. Anderson (1995), "Spark Anemometry of Bulk Gas Velocity at the Plug Gap of a Firing Engine", SAE Paper 952459.

55. Abd-Alla, T., G.R. Pucher, M.F. Bardon, and D.P. Gardiner (2003), "Effects of Spark Characteristics on Engine Combustion with Gasoline and Propane", SAE Paper 2003-01-3264.

56. Raizer, Y.P. (1997), Gas Discharge Physics, 2nd edition. Springer-Verlag, Germany.

57. Pashley, N., R. Stone, and G. Roberts (2000), "Ignition System Measurement Techniques and Correlations for Breakdown and Arc Voltages and Currents", SAE Paper 2000-01-0245.

58. Cobine, J.D. (1941), Gaseous Conductors, Theory and Engineering Applications, 5th edition, McGraw-Hill Book Company, New York.

59. Seers, P. (2003), "Spark Ignition: An Experimental and Numerical Investigation", PhD Dissertation, The University of Texas at Austin.

60. Gao, H., Matthews, R.D., Hall, M.J., and Hari, S. (2004), "From Spark Plugs to Railplugs – The Characteristics of A New Ignition System", SAE Paper 2004-01-2978.

61. Naidis, G.V. (1999), "Simulation of Streamer-to-Spark Transition in Short Non-Uniform Air Gaps." Journal of Physics D: Applied Physics, Vol. 32, pp. 2649-2654.

62. Lee, M.J., Hall, M.J., Ezekoye, O.A., and Matthews, R.D. (2005), "Voltage, Current, and Energy Deposition Characteristics of Spark Ignition Systems", SAE Paper 2005-01-0231.

63. Bengisu (Ed.), M. (2001), Engineering Ceramics, Springer-Verlag, Germany.

64. Harper, C.A. (2001), Handbook of Ceramics, Glasses, and Diamonds, McGraw-Hill.

65. Gao, H., Matthews, R.D., Hari, S., and Hall, M.J. (2004), "Use of Railplug to Extend the Lean Limit of Natural Gas Engines", Proceeding of the ASME ICE Division 2004 Fall Technical Conference, ICEF 2004-881.

66. Mardiguian, M. (1992), Controlled Radiated Emissions by Design, Van Nostrand Reinhold, New York.

67. Morison, R. (1992), Noise and other interfering signals, Wiley, New York.

68. White, D.R.J. and Mardiguian, M. (1988), Electromagnetic shielding, Gainesville, Va.

69. Ozdor, N., Dulger, M., and Sher, E. (1994), "Cyclic Variability in Spark Ignition Engines A Literature Survey", SAE Paper 940987.

70. Ramesh, A., Tazerout, M., and Le Corre, O. (2003), "An Experimental Study of Cyclic Variation in a Lean Burn Natural Gas Fuelled Spark

Ignition Engine", Proceeding of the ASME ICE Division 2003 Fall Technical Conference, ICEF 2003-772.

71. Fujikawa, T., Nomura, Y., Hattori, Y., Kobayashi, T., and Kanda, M. (2003), "Analysis of Cycle-by-Cycle Variation in a Direct Injection Gasoline Engine Using a Laser-Induced Fluorescence Technique", Int. J. Engine Res., Vol.4 No2.

72. Scholl, D. and Russ, S. (1999), "Air-Fuel Ratio Dependence of Random and Deterministic Cyclic Variability in a Spark-Ignited Engine", SAE Paper 1999-01-3513.

73. Matekunas, F.A. (1983), "Modes and Measures of Cyclic Combustion Variability", SAE Paper 830337.

74. Heywood, J.B. (1988), Internal Combustion Engine Fundamentals, McGraw-Hill Book Co.

75. Matthews, R.D. (2005), Internal Combustion Engines and Automotive Engineering, Test books for The University of Texas at Austin.

76. Ko, Y. and Anderson, R.W. (1989), "Electrode Heat Transfer During Spark Ignition", SAE Paper 892083.

77. Borman, G., and Nishiwaki, K. (1987), "Internal Combustion Engine Heat Transfer", Prog. Energy Combust. Sci., Vol. 13, pp. 1-46.

VITA

Hongxun Gao was born in Henan Province, China on February 9, 1966, the son of Xiu'e Wang and Jinzhu Gao. He entered Tianjin University in Tianjin, China in 1984. He received the degree of Bachelor of Engineering in 1988. He entered the graduate school of Tianjin University during the fall of the same year. In 1991 he received the degree of Master of Engineering from Tianjin University and began to work as a full time engine researcher in the campus. He decided to continue his Ph.D. study after he had been working for five years. He first entered University of California, San Diego in the fall of 1996 and then transferred to The University of Texas at Austin to pursue his Ph.D. degree a year later.

Permanent address: Nan-Shi-San, Chaoyang, Mengjin County, Henan Province, China

This dissertation was typed by the author.